AD-A056 574 PRATT AND WHITNEY AIRCRAFT GROUP EAST HARTFORD CT MAT--ETC F/G 11/6
DEGRADATION OF COATING ALLOYS IN SIMULATED MARINE ENVIRONMENTS.(U)
JUN 78 R H BARKALOW, F S PETTIT N00173-76-C-0146
UNCLASSIFIED PWA-FR-10225 NL

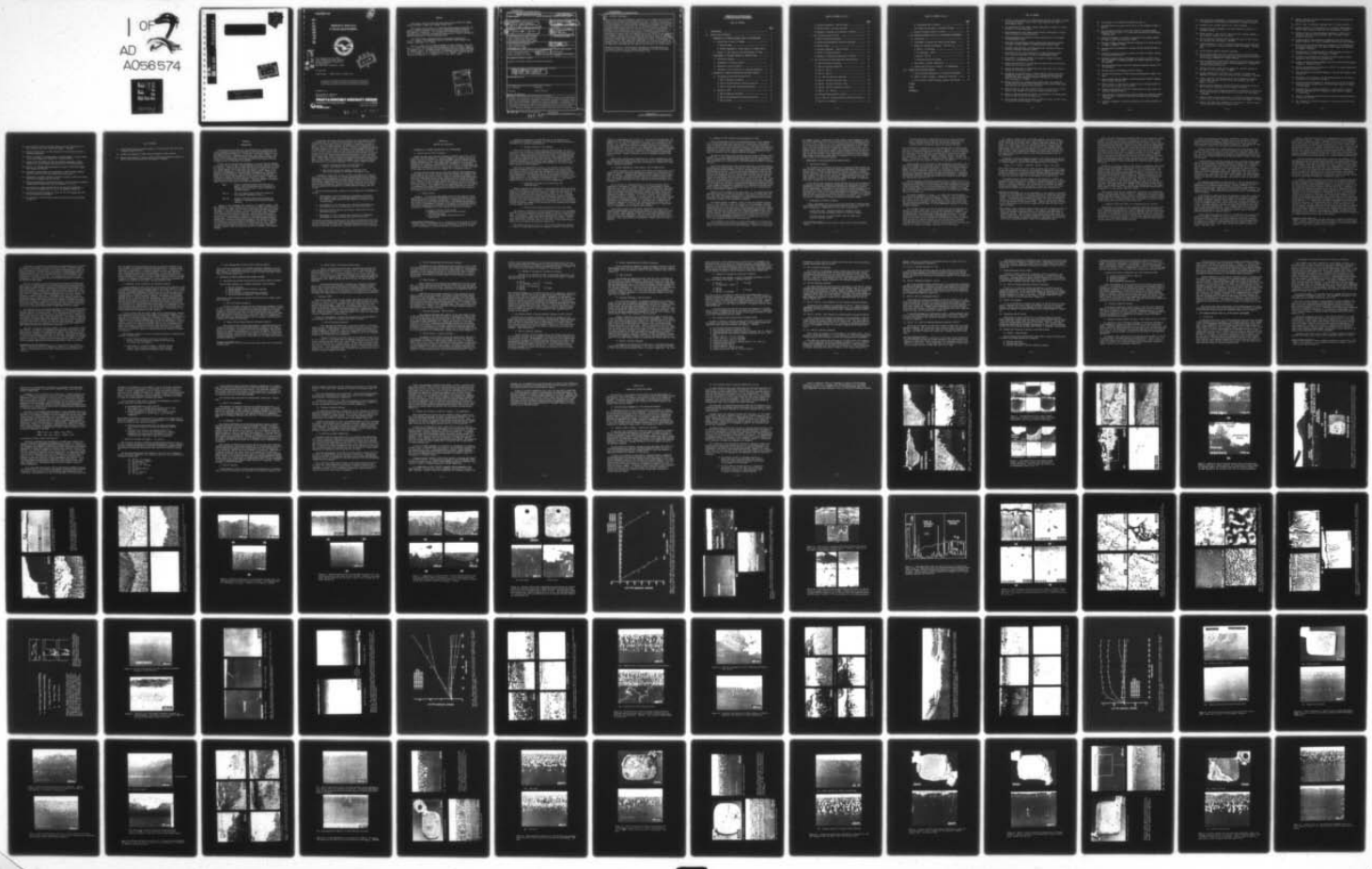

# DEGRADATION OF COATING ALLOYS IN SIMULATED MARINE ENVIRONMENTS



R.H. Barkalow and F.S. Pettit
Pratt & Whitney Aircraft Division
United Technologies Corporation
400 Main Street
East Hartford, Connecticut 06108

15 June 1978

Final Report: 1 March 1976 to 1 March 1978

Approved for public release; distribution unlimited

Prepared for:

Naval Research Laboratory
Washington, DC 20375

**PRATT & WHITNEY AIRCRAFT GROUP**
Government Products Division
UNITED TECHNOLOGIES

P. O. Box 2691
West Palm Beach, Florida 33402

Report No. FR-10225



Printed in the United States of America

# PREFACE

This report covers the work performed under Contract N00173-76-C-1046 during the period 1 March 1976 through 1 March 1978.

The Program was conducted by the Materials Engineering and Research Laboratory of Pratt & Whitney Aircraft Group, Commercial Products Division, East Hartford, Connecticut. Its purpose was to investigate the role of chlorides in hot corrosion of marine gas turbines and to develop coatings for improved resistance to chloride-induced attack.

The contract was accomplished under the technical direction of Dr. R. L. Jones of the Chemistry Division, Code 6130, Naval Research Laboratory, Washington, D.C., 20375.

Dr. F. S. Pettit was the Program Manager at Pratt & Whitney. The late Dr. E. J. Felten was the principal investigator during the initial stages of the program; Dr. R. H. Barkalow became associated with the program following Dr. Felten's death. The authors wish to acknowledge helpful discussions with Dr. G. W. Goward, Mr. J. A. Goebel and Mr. C. S. Giggins. Technical assistance was provided by T. J. Radzavich, C. V. Prue, and S. Russo.

UNCLASSIFIED

SECURITY CLASSIFICATION OF THIS PAGE (When Data Entered)

## REPORT DOCUMENTATION PAGE

READ INSTRUCTIONS BEFORE COMPLETING FORM

1. REPORT NUMBER

2. GOVT ACCESSION NO.

3. RECIPIENT'S CATALOG NUMBER

4. TITLE (and Subtitle)

(6) DEGRADATION OF COATING ALLOYS IN SIMULATED MARINE ENVIRONMENTS

5. TYPE OF REPORT & PERIOD COVERED

(9) Final Technical Report, 1 Mar 76 - 1 Mar 78

6. PERFORMING ORG. REPORT NUMBER

FR-10225

7. AUTHOR(s)

(10) R. H. Barkalow and F. S. Pettit

8. CONTRACT OR GRANT NUMBER(s)

(15) N00173-76-C-0146

9. PERFORMING ORGANIZATION NAME AND ADDRESS

Pratt & Whitney Aircraft Division
United Technologies Corporation
East Hartford, Connecticut 06108

10. PROGRAM ELEMENT, PROJECT, TASK AREA & WORK UNIT NUMBERS

11. CONTROLLING OFFICE NAME AND ADDRESS

Naval Research Laboratory
4555 Overlook Avenue
Washington, DC 20375

(11) 12. REPORT DATE

15 June 1978

13. NUMBER OF PAGES

107

14. MONITORING AGENCY NAME & ADDRESS (if different from Controlling Office)

Naval Plant Representative Office
Pratt & Whitney Aircraft
West Palm Beach, FL 33402

(12) 43 p.

15. SECURITY CLASS. (of this report)

UNCLASSIFIED

15a. DECLASSIFICATION/DOWNGRADING SCHEDULE

16. DISTRIBUTION STATEMENT (of this Report)

Approved for public release; distribution unlimited

17. DISTRIBUTION STATEMENT (of the abstract entered in Block 20, if different from Report)

(14) PWA-FR-10225

18. SUPPLEMENTARY NOTES

19. KEY WORDS (Continue on reverse side if necessary and identify by block number)

Hot Corrosion
Chlorides
Coatings
Sulfur Trioxide
Marine Environments

20. ABSTRACT (Continue on reverse side if necessary and identify by block number)

Chloride- and $SO_3$ induced hot corrosion of state-of-the-art and developmental coatings were studied in a program of laboratory hot corrosion testing correlated with metallographic examination of service hardware. Laboratory furnace tests showed that CoCrAlY coatings are highly susceptible to degradation by chloride-containing salt deposits; the mechanism of attack involves dealloying of aluminum via formation of an interconnected network of coarse and fine pores. Sputtered platinum overlayers are an effective means of retarding the

Over

DD FORM 1 JAN 73 1473 EDITION OF 1 NOV 65 IS OBSOLETE

UNCLASSIFIED

SECURITY CLASSIFICATION OF THIS PAGE (When Data Entered)

410 765

20. Abstract (continued)

onset of this type of degradation, especially at low temperatures where dissolution of the overlayer by interdiffusion is slow. In spite of this demonstrated potential for chloride-induced degradation, dissimilar microstructures of test specimens and service hardware (primarily the presence of a zone of internal attack in test specimens but not in engine-run parts) indicates that chloride alone cannot account for the severity of the marine environment. Emphasis on the program was then shifted to examination of $SO_3$ effects. It was shown that the microstructural features of service hardware could be reproduced in furnace tests with $Na_2SO_4$ deposits and $SO_3$ in the gas. Substantial attack of various types of coatings was produced at 649°C and 0.04 atm $SO_3$ pressure, although the nodular morphology and thin $\beta$-depleted zone usually observed in engine parts were better reproduced at 760°C. The mechanism of $SO_3$ attack is not fully understood; undoubtedly it involves acid fluxing of alumina scales, but other steps in the process must still be defined in order to explain the microstructure and element distribution at the attack front.

Coatings resistant to chloride-induced degradation unfortunately are not necessarily resistant to $SO_3$ effects; new approaches to alloy development will be required in designing for resistance to $SO_3$.

# DEGRADATION OF COATING ALLOYS IN SIMULATED MARINE ENVIRONMENTS

TABLE OF CONTENTS

TABLE OF CONTENTS (Cont'd)

TABLE OF CONTENTS (Cont'd)

## LIST OF FIGURES

64. Hot corrosion observed with same material and test conditions as in Fig. 63 except that salt deposit was $Na_2SO_4$ - 50% NaCl.

65. Microstructural effect of 649°C exposure of CoCrAlY-coated IN 738 in various environments.

66. Surface structure of polished wafers of single-crystal $\alpha$-$Al_2O_3$ coated with 1 mg/cm$^2$ $Na_2SO_4$ and exposed for 4 hours at 649°C.

67. Attack of PWA 68 CoCrAlY and PWA 273 diffusion aluminide at 649°C produced by 1 mg/cm$^2$ $Na_2SO_4$ salt deposit and 0.04 atm $SO_3$ pressure.

68. PWA 68 + Pt overlayer coating exposed 100 hours at 649°C with $Na_2SO_4$ salt deposit and $SO_3$ gas.

69. Secondary electron images of Pt underlayer + PWA 68 CoCrAlY coating after 100 hours at 649°C with $Na_2SO_4$ salt and $SO_3$ gas.

70. Degradation of Ni-base diffusion aluminide coatings in 649°C hot corrosion test with $Na_2SO_4$ salt and $SO_3$ gas.

71. SEM photomicrographs of sputtered platinum + PWA 273 diffusion aluminide coating tested concurrently with the specimens of Fig. 70.

72. Hot corrosion of CoCrAlY-coated IN 738 and bulk PVD Co-25Cr-6Al in 899°C test with $Na_2SO_4$ salt and $SO_3$ in the gaseous environment.

73. CoCrAlY-coated IN 738 exposed 40 hours at 760°C with $Na_2SO_4$ salt and $SO_3$ in the gaseous environment.

74. Pt underlayer + PWA 68 CoCrAlY tested concurrently with the specimen of Fig. 73.

LIST OF TABLES

# SECTION I

## INTRODUCTION

Field experience has shown that sulfate-induced hot corrosion of gas turbine hardware is generally more severe in marine environments than for non-marine operating conditions. The problem is obviously related to sulfate deposition due to ingestion of sea salt. Less clear, however, is why these sulfate deposits are so effective in degrading marine turbines, especially at low temperatures and on coating alloys which appear resistant to $Na_2SO_4$ attack in non-marine environments.

At the time this program was formulated, it was felt that the presence of chlorides in sea salt was a likely explanation for the severity of marine hot corroion. Chloride ions had been detected in salts dissolved from vanes of a marine engine[1], and it was known that chloride in $Na_2SO_4$ could cause more severe degradation of some alloys than $Na_2SO_4$ alone[2]. Hence it was proposed to investigate the chloride effect by comparing hot corrosion degradation induced by $Na_2SO_4$ - NaCl mixtures with that of chloride-free $Na_2SO_4$ and to assess the significance of the chloride factor in marine hot corrosion by comparing the microstructural features of $Na_2SO_4$ - NaCl test specimens with those of service hardware. A one-year program to accomplish these objectives consisted of the following three Tasks:

Task I - Develop a testing procedure involving use of $Na_2SO_4$ - NaCl salt mixtures which simulates the microstructural features of service exposure in shipboard engines.

Task II - Test and compare state-of-the-art coatings by the procedure determined in Task I.

Task III - Attempt to develop coatings with improved resistance to degradation by chloride-containing deposits.

Coating of test specimens with a deposit of ~1 mg/cm$^2$ of $Na_2SO_4$ - 50% NaCl followed by cyclic oxidation in air at 649 and 899°C (1200 and 1650°F) was found to be a useful and convenient experimental procedure for studying the effect of chloride on $Na_2SO_4$ - induced hot corrosion and comparing the resistance of various alloys to chloride. CoCrAlY-type alloys, currently a bill-of-material coating for blades and vanes of marine gas turbines, were found to be particularly susceptible to degradation by chloride-containing melts. Microstructural features of the test specimens included a tendency for localized pitting attack similar to that observed in engine-run hardware; as in service produced degradation, the pit was filled with Al- and Cr-rich oxides and mounds of CoO formed above the pits. However the structure and element distribution of the attack front differed in important respects from that typically observed in hardware from shipboard engines.

Concurrently with these results, studies at the Naval Research Laboratory[3] showed that hot corrosion microstructures very similar to those encountered in marine service could be developed by depositing mixtures of $Na_2SO_4$ - $CoSO_4$ on CoCrAlY specimens and heating in air to temperatures in the range of 649 to 760°C (1200 to 1400°F). Similar microstructural features were also observed at the Naval Ship Research and Development Laboratory[4] in a 704°C (1300°F) ducted burner rig test using fuel doped with 1% sulfur. In view of such results, and since the microstructures developed in the laboratory test using chloride were different from service, it was concluded that chloride alone could not account for the severity of marine hot corrosion. Further work on this program was therefore redirected to consider the effect of $SO_3$ content of the gaseous environment on hot corrosion behavior. The objectives of a six-month extension to the original program included:

- Develop a testing procedure involving $Na_2SO_4$ or $Na_2SO_4$ - NaCl deposits and $SO_3$ in the gas
- Test various alloys and coatings, especially those found to be resistant to chlorides, with $Na_2SO_4$ - $SO_3$

A laboratory furnace test at 649° to 760°C with $Na_2SO_4$ salt deposits and ~ 0.05 atm $SO_3$ pressure in the furnace atmosphere was found to produce substantial coating degradation in short exposure times (100 hours or less); metallographic examination and microprobe analysis showed that the microstructure and element distribution at the attack front were very similar to those of service hardware. Several coatings were evaluated in this test; all were significantly degraded by the short exposure to $Na_2SO_4$ salt and $SO_3$ gas.

In the following sections, results of this program will be presented as follows:

1. Metallography of service hardware to characterize the initial and advanced stages of coating degradation and provide a basis for comparison with microstructural features of laboratory hot corrosion tests.
2. Development of a hot corrosion test utilizing sulfate-chloride salt mixtures and cyclic oxidation in air at 649 and 899°C.
3. Testing of state-of-the-art and modified compositions with sulfate chloride salts.
4. Development of a hot corrosion test utilizing $SO_3$ atmosphere; performance of various coatings and alloys in this test.

Conclusions are based on correlation of the service evaluation and data from the hot corrosion experiments, primarily the similarity (or lack of it) between the microstructural features of degraded engine hardware and those developed in specimens corroded under controlled conditions in the laboratory.

## SECTION II

## RESULTS AND DISCUSSION

### 1. EXAMINATION OF TURBINE HARDWARE FROM GTV ASIAFREIGHTER

#### a. Initial Work at Start of Program

Blades and vanes were obtained from Engine P-686570 after 4801 hours of operation on GTV Asiafreighter. The major segment of operating time on the engine (1100 hours) was at a low shaft horsepower where the maximum radial average temperature of the first stage blades is expected to be in the neighborhood of 675°C (1247°F). The highest SHP corresponds to a blade metal temperature of approximately 860°C (1562°F) for 50 hours. Corresponding vane temperatures are known to vary much more widely, since the hot and cold spots of the burner can profiles are not averaged out by component rotation.

Sections from two blades and two vanes were examined metallographically. It was observed that the hot corrosion attack was always more severe on the concave than on the convex surfaces. Often the coating was completely consumed over large areas of the concave surface, while the convex showed numerous sites of localized attack but the coating was still present and protective. However, the less severely degraded sections of the concave surface showed localized attack and penetration of the coating similar to features on the convex surface. This suggests that the degradation mode on both surfaces is fundamentally the same, with the convex surface exhibiting the initial stages of the same mechanism responsible for destruction of the coating on the concave face of the airfoil.

##### 1) Nodular Attack

Figures 1 - 3 include photomicrographs and X-ray area scans at various magnifications which show the characteristic form of the localized nodular attack believed to be primarily responsible for degradation and failure of the coating on both the blades and the vanes. The information presented in this series of photographs is intended to illustrate the following features which are of significance in deducing the mechanism of attack* and in comparing service degradation with that produced in laboratory specimens;

a) general condition of the coating
b) composition of the oxides in the protrusion and overlying mound
c) structure and element distribution at the attack front

*Determination of the mechanism of hot corrosion is not an objective of this program, except to the extent that an understanding of mechanism is essential to development of testing procedures and interpretation of results.

Although interpretation of these features is not unequivocal or straightforward, important inferences can be drawn and either supported or discounted by subsequent experimentation.

a) General Condition of the Coating

Except for the areas of highly localized nodular attack, the microstructure of the coating and the coating/substrate interdiffusion zones illustrated in Figure 1 are indistinguishable from those of as-processed hardware. This observation restricts the thermal history of the affected zone to a range of time-at-temperature which did not cause significant dilution of the coating chemistry by long range diffusion. Thus the scale/metal interface advanced at a rate which is rapid compared to diffusion of Co, Cr, and Al in the coating and the propagation mechanism did not involve long range diffusion of these elements.

Note that the temperature of attack is not defined by the absence of noticeable alteration of the coating microstructure; the nodular attack could have occurred at relatively low temperatures or very rapidly during high temperature excursions which were too short to alter the general coating microstructure. The operating history of the engine would favor the former possibility, and subsequent experimentation should be useful in determining whether or not the features illustrated in Figs. 1 - 3 are better reproduced in hot corrosion tests at low or high temperatures.

b) Composition of Oxides in the Protrusions and Overlying Mounds

Figure 2 presents low magnification x-ray area scans showing the entire depth of a protrusion and oxide mound. It is evident that the volume of the protrusion is primarily $Cr_2O_3$ with relatively little CoO; conversely the oxide mound contains CoO but very little $Cr_2O_3$ (Figs. 2b, 2c). Aluminum oxide is present in both the protrusion and the mound; aluminum enrichment delineates the attack front in some areas and several lines of Al concentration in the protrusion presumably mark prior locations of the scale/metal interface (Fig. 2d). Sulfur appears to be concentrated at the attack front, although the entire boundary of the protrusion is not uniformly well defined in X-ray images (Figure 2e).

c) Structure and Element Distribution at the Attack Front

The presence or absence of a diffusion-affected zone at the scale/metal interface is of critical importance with respect to the hot corrosion mechanism. As apparent in Figure 1, however, the microstructure of the attack front is not uniform. Some areas are characterized by a thin but unequivocally recognizable $\beta$-depleted zone (e.g. the right half of Figs. 1b, 1c); others show a type of in-situ attack of the $\beta$-CoAl, leaving non-continuous areas of $\alpha$-Co in contact with the scale (Figure 1d).

The distribution of Cr, Co, Al, S, and O at the scale/metal interface is shown by the high magnification X-ray images in Figure 3 (the area ill-

ustrated is approximately that of Fig. 1d). The scan for chromium (Fig. 3b) suggests that the $\alpha$-Co phase immediately in contact with the scale may be depleted in Cr, but there is otherwise no indication of a Cr gradient in the coating. The scale/metal interface is sharply defined by Co depletion in the protrusion (Fig. 3c) as well as by Al enrichment (Fig. 3d); however, the entire periphery of the protrusion is not marked by Al enrichment as prominent as that in the area of Fig. 3d. Sulphur is likewise non-uniformly concentrated in the scale at the attack front (Fig. 3e), apparently in areas also rich in aluminum. Oxygen is present up to the scale/metal interface (Figure 3f).

Small sulfide precipitates, apparently CrS, could be detected by careful probing near the attack front (i.e. within ~ 20 $\mu$m), although massive ingress of sulfur and subsequent oxidation of sulfides was clearly not a significant degradation mechanism.

2) Surface Degradation, Leader Defects, and Cut-Edge Attack

A second morphology of the attack front observed in several areas of the blades was the type of surface degradation and shallow pit formation illustrated in Figure 4. Characteristic features were an external scale of $Al_2O_3$ (Fig. 4a, 4b) and a prominent $\beta$-denuded zone at the surface and around the pit. The denuded zone was laced with a network of corrosion product, and sulfur was readily detectable on the surface and around the periphery of the pit (Fig. 4c).

Also of concern in characterization of the service hardware was an assessment of the effect of coating quality (i.e. the presence of leader defects) on hot corrosion behavior. Oxidized leader-type defects were sometimes associated with coating protrusions as shown in Figure 5a, although it cannot be concluded from such observations whether the leader defects promoted nodular attack or whether the presence of the protrusion resulted in opening and oxidation of leaders. It is clear, however, that leaders are not a prerequisite for initiation of nodular attack, as shown by the frequent observation of coating protrusions in the absence of any recognizable coating defect (e.g. the area of Figure 1). Also there was no indication of significant preferential attack of the coating/substrate interface due to oxidation of leaders. It is thus felt that leaders were not a significant factor in degradation of the hardware being examined.

Lastly the so-called cut edge effect illustrated in Figure 5b is a uniquely distinguishable failure mode encountered in both overlay and aluminide coatings[5]. Rapid edgewise consumption of the coating emanates from a local site of coating penetration, with the exposed edge characterized by massive sulfides and preferential consumption of the coating rather than the substrate. This type of attack in a laboratory furnace coupon is shown in Figure 6.

b. Analysis of Salt Deposits and Metallography of Vanes

After approximately one year of experimental effort on this program, a set of nozzle guide vanes were obtained from P-686570 in a scheduled hot section inspection after 2770 hours service. Salt deposits and surface scale, including pink crystals observed on many of the vanes, were removed by scraping, and a soluble salt analysis was performed by washing the vane surfaces with a stream of water from a squeeze bottle and analyzing the wash water for dissolved ions by standard chemical techniques.

XRD results and soluble salt analysis data are listed in Tables I and II respectively. Of most significance in these tables are the x-ray identification of a sodium-cobalt double sulfate $Na_2Co(SO_4)_2$ and the presence of Co ions (presumably due to dissolution of the sodium-cobalt sulfate) in the wash solution.

One of the CoCrAlY-coated vanes on which $Na_2Co(SO_4)_2$ had been detected was prepared for metallographic examination by dry cutting and dry polishing; optical and SEM photomicrographs of typical features near the leading edge are presented in Figure 7. The coating on the leading edge itself was completely consumed and the substrate was attacked; however, the coating microstructure was unaffected up to the attack front and there was no diffusion zone at the scale/metal interface (Figure 7a). A thin $\beta$-denuded zone was present in other regions of the attack front (arrow in Fig. 7b); Fig. 7b also shows the Co-containing sulfate salt on the surface of the vane. High magnification study of a shallow but well developed protrusion showed continuous $\alpha$-Co in contact with the scale, although the thickness and morphology of the $\alpha$ layer suggested preferential consumption of $\beta$ (leaving $\alpha$-Co at the attack front) rather than formation of additional areas of $\alpha$ via a diffusion-controlled transformation (Figure 7c).

Figure 8 is X-ray images of the area of Fig. 7c. As observed on blades examined previously, the bulk of the nodule was Cr and Al oxides (Figs. 8a, 8b). The attack front was characterized by concentration of sulfur in the scale (Fig. 8c) with minimal incidence of sulfide precipitation or internal oxidation in advance of the scale/metal interface.

Of further interest in Figures 7 and 8 is that the corrosion products include a zone (brackets in Fig. 7c) adjacent to the scale/metal interface which is richer in Cr, Al, and S and leaner in Co (Fig. 8) than the oxides comprising the bulk of the protrusion. The boundary of this zone is usually not well defined, even in high resolution SEM photomicrographs where a ghost image of the coating microstructure and a layered appearance of the scale are very evident. The implication of this sulfur-rich zone adjacent to the metal is that the propagation mechanism involves formation at the attack front of an aluminum-chromium oxysulfide (i.e. a phase rich in Al, Cr, S, and O) and subsequent oxidation of the oxysulfide.

Also informative with respect to sulfur enrichment at the attack front and its implication about the attack mechanism is comparison of sulfur X-ray images of dry polished and wet polished specimens. Figure 8 (dry polished),

for example, shows a uniform sulfur content clearly above background in the bulk of the protrusion and further concentration of sulfur immediately behind the attack front. Figs. 2e, 3e, and 4c (wet polished) show concentration of sulfur at the attack front, but it is questionable whether or not the remainder of the scale is emitting above-background characteristic X-rays. Presumably the dry polished scale is soaked with residual sulfate salt and thus appears clearly on sulfur X-ray images. Wet polishing dissolves the salt but does not prevent delineation of the scale/metal interface by sulfur enrichment at the attack front. Hence there must be an insoluble sulfur-containing phase formed at the attack front which is responsible for the sulfur concentration shown in wet polished specimens.

## 2. DEVELOPMENT OF CHLORIDE-INDUCED HOT CORROSION TEST

### a. Introductory Remarks

Any program of hot corrosion testing must compromise between realism and cost, the cost factor involving both facilities requirements and testing time. Nothing short of formidably expensive engine testing can hope to duplicate service conditions. The closest approach to service conditions is probably a type of burner rig test, but this too is relatively expensive and it is sometimes difficult to control test conditions. Laboratory furnace testing is least realistic in terms of reproducing the engine environment but generally convenient, inexpensive, and easily controllable.

It was decided that laboratory furnace testing would be most suitable for performing the necessary background experiments and determining the relative resistance of various state-of-the-art and modified coatings to chloride-induced degradation. Considered in conjunction with the metallographic analysis of service hardware described in the preceeding section and extensive experience with a test of this type using deposits of 100% $Na_2SO_4$, the results were expected to be useful in defining the effect of chloride on hot corrosion behavior and determining whether or not chlorides are likely to be a significant factor in degradation of turbine hardware in shipboard engines.

### b. Development of Testing Procedure

Initial experiments were run on bulk alloys fabricated by electron beam vapor deposition to produce microstructures similar to those of overlay coatings on superalloys. Compositions of the alloys evaluated were:

Co-25Cr-6Al-0.5Y* - selected because its oxidation and hot corrosion had been thoroughly studied in a previous program.

Co-33Cr-14Al-0.3Y - a second CoCrAlY alloy of higher chromium and aluminum content.

*Alloy and salt compositions are given in weight percent unless otherwise noted.

Co-19Cr-12.5Al-0.5Y, Ni-18Cr-23Co-12.5Al-0.5Y, and Ni-17Cr-12Al-0.5Y - compositions of state-of-the-art CoCrAlY, NiCoCrAlY, and NiCrAlY coatings (PWA 68, PWA 270, and PWA 267 respectively) currently used in industrial, marine and aircraft turbines.

Salt was applied by spraying warm (~ 250°C) specimens with an aqueous salt solution to produce a deposit of approximately 1 mg/cm$^2$. Cyclic conditions were used to accelerate degradation by scale spallation; the cycle consisted of 50 minutes in the hot zone plus 10 minutes in the cold zone of a static air tube furnace. Specimens were washed, examined, weighed, and recoated with fresh salt every 20 hours. Deposits of $Na_2SO_4$, $Na_2SO_4$ - 1% NaCl, and $Na_2SO_4$ - 10% NaCl were utilized. Tests were run for times up to 500 hours at temperatures of 899, 760, and 649°C (1650, 1400, and 1200°F).

Weight changes of all specimens in these experiments were small; $\Delta M/A$ vs. time data indicated the alloys were still in the initiation stage after 500 hours and no effect of chloride was evident. Results of visual and metallographic examination were more informative. As observed by others, it was evident on visual inspection during test that the presence of NaCl in the deposit was causing the $Al_2O_3$ scales to spall more extensively. Subsequent metallography confirmed that NaCl had increased the severity of degradation, although the effect was not striking and was less pronounced at the higher test temperatures than at 649°C.

Typical features of the surface microstructure of Co-25Cr-6Al-0.5Y produced at test temperatures of 649 and 899°C are shown in Figure 9 and 10; the degradation mode appears to involve dissolution and/or preferential oxidation of the β-CoAl phase. This type of microstructure was observed in all of the alloys examined (Figure 11), although Co-25Cr-6Al-0.5Y appeared to be generally more resistant to sulfate-chloride attack than the other alloys (compare Figure 11 and Figure 9c).

The results presented in Figure 9 - 11 showed that sulfate-chloride melts were more aggressive than 100% $Na_2SO_4$. However, it was suspected that the severity of the test was being decreased by loss of chloride from the salt deposit (due to the higher vapor pressure of NaCl), and a more severe test was considered necessary to shorten exposure times while better simulating the more advanced stages of coating degradation observed in the Asia-freighter hardware.

In an attempt to avoid the loss of chloride from the chloride-sulfate deposits, the use of NaCl vapor in the furnace atmosphere was examined. It was reasoned that the chloride vapor might fix the activity of NaCl in the condensed deposit, thus increasing the average aggressiveness of the melt during the 20 hour intervals between replenishment of the salt. The NaCl vapor was introduced in a concentration of approximately 300 ppm by passing slowly flowing air over NaCl crystals at 760°C as described by Jones[6,7]. Specimens were coated with chloride-sulfate mixtures and heated in the chloride-containing air at 899°C. After 20 hours, however, it was found that there was no visually discernable salt deposit on the specimens.

To isolate a possible effect of the NaCl vapor on loss of the salt deposit, platinum coupons were coated with 100% $Na_2SO_4$ and exposed at 899°C in air containing 300 ppm NaCl vapor. These coupons were observed to lose weight at a linear rate of about 0.4 $mg/cm^2/hr$ or about 8 $mg/cm^2$ after 20 hours (vs. a total weight loss of about 0.08 $mg/cm^2$ for a sulfate-coated coupon heated for 20 hours in chloride-free air). It was therefore evident that the NaCl vapor was causing the $Na_2SO_4$ to be removed from specimen surfaces at 899°C. This condition was observed on using either dry air (i.e. air passed through anhydrous $CaSO_4$) or air saturated with water vapor at room temperature.

Subsequent to these experiments, Stearns et al[8] studied the interaction of NaCl and HCl vapors with condensed $Na_2SO_4$. They demonstrated the removal of condensed $Na_2SO_4$ by vaporous NaCl and proposed that it occurred by

$$Na_2SO_4\ (l) + 2\ HCl(g) \rightarrow 2NaCl(g) + H_2O(g) + SO_2(g) + 1/2\ O_2(g)$$

where HCl(g) forms from hydrolysis of NaCl by water vapor present in the gas. It was also shown that the rate of loss of $Na_2SO_4$ increased with water vapor content of the gas, but the authors pointed out that significant amounts of HCl would be produced by hydrolysis unless extraordinary measures were taken to reduce the moisture content of the environment to sub-ppm levels.*

Accelerated loss of the salt deposit by this reaction is probably responsible for the reduced attack of IN738 in chloride-containing vs. chloride-free air as shown in Figure 12. This alloy is known to degrade via a basic fluxing - sulfidation mechanism, and the severity of such attack increases with increasing amounts of the salt deposit. Hence the loss of the liquid sulfate due to the NaCl vapor decreased the amount of hot corrosion.**

---

*The loss of the sulfate salt in the experiments of this program is therefore attributed to the inability of the $CaSO_4$ (Drierite) to reduce the water vapor content of the furnace gas to a sufficienty low level to prevent hydrolysis of NaCl. If hydrolysis were negligible, sulfate could still be removed by a reaction of the form $Na_2SO_4(l) + Cl_2 \rightarrow 2NaCl + SO_2 + O_2$ which would proceed to the right because of the absence of $SO_2$. However, the reaction involving $Cl_2$ has significance only in very dry gases and even then the rate is probably very small.

**This example does not indicate that chloride vapor will decrease the rate of attack of any alloy coated with $Na_2SO_4$. For example, more spallation of $Al_2O_3$ from CoCrAlY is encountered in cyclic oxidation when NaCl vapor is present in the gas. Thus in a cyclic hot corrosion test using a thin deposit of $Na_2SO_4$ salt, the increased degradation resulting from poorer scale adhesion may outweight the beneficial effect of less $Na_2SO_4$ and the net result could be an adverse effect of NaCl on the degradation rate.

Since the use of flowing air with NaCl vapor did not produce the desired increase in severity of the test by retaining the chloride content of the deposit, work was directed towards characterizing the rate of loss of the chloride component and studying the attack of alloys by NaCl - $Na_2SO_4$ deposits containing more than 10% NaCl. Results of this work showed that negligible loss of chloride would occur at 649°C during the 20 hour cycles between application of fresh salt but virtually all of the chloride would vaporize from the deposit in 20 hours at 899°C. In spite of this loss at 899°C, it was known from previous tests that the transient presence of chloride applied every 20 hours was sufficient to influence the severity of hot corrosion. Hence it was decided to continue the procedure of cyclic testing with reapplication of fresh salt every 20 hours, but to test at 649°C where both $Na_2SO_4$ and NaCl remain present in the condensed phase and at 899°C where the initial concentration of chloride decreases to a very low level during the test cycle.

The effect of chloride content of the deposit was determined from weight change data and metallographic observations of 649°C and 899°C cyclic hot corrosion tests with deposits containing 0, 5, 10, 50, and 90% NaCl. The results showed that severity of hot corrosion attack of CoCrAlY alloys increased substantially with increasing NaCl content of the deposit (e.g. the 899°C data for Co-25Cr-6Al-0.5Y in Figure 13). Equally significant is the consistency of the data in Figure 13 with the concept of an initiation and propagation stage in hot corrosion attack and the effect of chloride in shortening the length of the initiation stage. Thus two of the samples plotted in Figure 13 did not reach the propagation stage during the 300 hour test time. The sample tested with 50% NaCl showed the same initial weight change as with $Na_2SO_4$ and $Na_2SO_4$ - 10% NaCl but suffered onset of the propagation stage in ~260 hours.[2] The sample exposed to 90% NaCl showed onset of propagation in a much shorter time (< 20 hours).

The chloride effect is also dramatically illustrated in the photomicrographs of CoCrAlY-coated IN738 in Figure 14. Exposure for 500 hours at 899°C produced negligible attack under a deposit of 100% $Na_2SO_4$ but almost complete $\beta$-dissolution and internal oxidation of the coating under a deposit of $Na_2SO_4$-5% NaCl (Fig. 14b). A higher concentration of chloride in the deposit (90%) caused coating failure in only 40 hours (Fig. 14c).

c. Mechanism of Chloride Effect in Sulfate-Induced Hot Corrosion

Established at this point was that chloride-containing melts were capable of producing more degradation of CoCrAlY-type alloys than 100% $Na_2SO_4$. Still considered desirable prior to start of coatings evaluation was a better definition of the mechanism of the chloride effect and its role in the overall process of sulfate hot corrosion. Toward these objectives, several experiments were run on a bulk alloy of PVD (physical vapor deposited) Co-25Cr-6Al-0.5Y and the specimens examined in detail by conventional metallography, scanning microscopy, and microprobe analysis.

Figure 15 shows the microstructural degradation produced by cyclic hot corrosion testing with $Na_2SO_4$ - 90% NaCl for 100 hours at 899°C; the boxed areas in 15a are shown at higher magnification in 15b and 15c and in the X-ray area scans for aluminum and oxygen in Figure 16. The specimen had been dry polished to prevent loss of water soluble corrosion products.

SEM photomicrographs and corresponding X-ray area scans showed a relatively thick layer of Al-rich oxide scale adjacent to the alloy (Figs. 15a, 15b, 16a, 16b); the outer portion of the scale, which appears lighter gray in Fig. 15a due to higher average atomic number, is primarily $Cr_2O_3$, and Co was detected in the outermost regions of the external scale (Cr and Co area scans not presented).

A semiquantitative line trace through the zone of internal attack showed that the alloy was almost completely depleted of aluminum, and a steep gradient in the concentration of chromium was detected (Figure 17). Features in the zone of internal attack (e.g. areas like Fig. 15b and 15c) at first glance appeared to be particles but on close examination looked more like holes containing a nonmetallic phase. The nonmetallic phase in the zone adjacent to the scale contained aluminum and oxygen (Figs. 16a, 16b) and is presumably $Al_2O_3$. Deep within the attack zone, however, the holes contained aluminum but no oxygen (Figs. 16c, 16d). Spectrometer scans of these areas detected chlorine and sulfur (presumably from residual salt) but no sodium or chromium.

The important implication of these results is that the degradation sequence involves passage of several reaction fronts. Apparently the alloy is penetrated by the chloride-containing melt, resulting formation of an aluminum-rich phase which contains chlorine and possibly other elements but relatively little oxygen. This phase is subsequently oxidized to $Al_2O_3$. The remaining metal, by now substantially depleted in Al and Cr, suffers general surface oxidation.

In an attempt to learn more about the nonmetallic phase that appeared to be forming as the initial attack front advanced into the alloy, a specimen was heated isothermally for 20 hours at 899°C in a crucible containing a thick melt of $Na_2SO_4$ - 90% NaCl. These conditions resulted in formation of a zone of internal attack with cavities filled with a nonmetallic corrosion product containing aluminum, chlorine, and oxygen (Figure 18) as well as Na, S, and Cr at lower concentrations. It is apparent from these results that liquid sulfate-chloride salts are capable of selectively leaching aluminum from CoCrAlY-type alloys via a mechanism which leaves voids or cavities partially filled with a corrosion product.

A third experiment involved coating of a Co-25Cr-6Al-0.5Y specimen with 1 $mg/cm^2$ of $Na_2SO_4$ - 90% NaCl and cyclic oxidation for 20 hours at 899°C. The specimen was then cooled in liquid nitrogen and fractured. Scanning microscopy of the fracture surface showed that the zone of internal attack is composed of a network of interconnected pores and channels (Figure 19). The pores were of various sizes, some comparatively large but others extremely fine (Fig. 19d).

Lastly, a short-time test was run to characterize the initial stages of void and pore formation. A specimen of Co-25Cr-6Al-0.5Y was metallographically polished, coated with $Na_2SO_4$ - 90% NaCl, and oxidized for 10 minutes at 899°C, after which the features of the oxidized surface were compared with the phase morphology in the original microstructure. As can be seen upon comparing Figures 20a and 20b, strongly preferential attack has occurred and the pattern of this attack is similar to that of the β-CoAl phase. Features of the oxidized surface are illustrated at higher magnification in Figures 20c and 20d. The general shape and distribution of the voids, particularly the numerous Y-shaped triple points in Fig. 20c, clearly defines a grain boundary-like network similar to the distribution of β in the CoCrAlY microstructure.

A section through the specimen shown in Figure 20 was examined on the scanning microscope after mounting and polishing. As expected from the surface appearance, the β phase was observed to have been preferentially removed, leaving numerous pores near the surface (Fig. 21a). Some of the pores were in direct contact with the β-phase (Fig. 21b), demonstrating a direct channel to the surface through which liquid salt could penetrate and attack the β particle.* Also, as inferred from the surface examination documented in Figure 20, the pores were similar but not identical in shape to the β-phase particles (Fig. 21c), indicating that the reaction by which the pores are formed also involves redistribution of cobalt and chromium from the α matrix as well as dealloying of aluminum by preferential attack of β.

A sequence of reactions which would account for the observed features of CoCrAlY alloys exposed to sulfate-chloride melts is presented in Figure 22. In order to permit a reaction between Al and Cl (i.e. to form the Al-rich chlorine-containing phases apparently present in the samples of Figs. 15 and 18), oxygen and sulfur must be removed from the liquid salt, supposedly by reaction with aluminum and chromium in the alloy as in reactions a) and b). The deposit thus becomes enriched in NaCl, promoting reaction with $Al_2O_3$ and oyxgen to form sodium aluminate and chlorine gas as in c). As shown schematically in the sketch of Figure 23, conditions for enrichment of the melt in NaCl and concentration of $Cl_2$ gas would be especially favorable at the base of a pore because interdiffusion and mixing of the liquid is restricted. Concentration of chlorine results in formation of an aluminum chloride phase as in reaction d). As oxygen from the surface environment subsequently penetrates into the alloy, the aluminum chloride is oxidized to $Al_2O_3$ and the chlorine is freed to react again with the alloy at the bottom of the pore. In this manner a randomly initiated site of pitting attack tends to propagate into a very deep, elongated pore, and a small amount of NaCl can produce a substantial effect because it is recycled by oxidation of aluminum chloride. The process is not completely self-sustaining, however, because some of the $Cl_2$ produced in reaction e) is lost to the environment and must be replaced by by further deposition of NaCl salt on the surface.

*Features such as that in Fig. 21b were difficult to locate on polished specimens. However, the fractured sample illustrated in Fig. 19 would suggest that continuous channels to the surface are common in the three-dimensional geometry of pores and β particles in the α matrix.

The ability of the pores to grow rapidly at temperatures as low as 649°C is believed to be related to surface diffusion effects. Strikingly similar pore structures have been observed at much lower temperatures as a result of aqueous corrosion[9]. In these cases, pore growth via preferential removal of an element was accounted for by surface diffusion of those elements not reacting with the liquid or by their solution in the liquid followed by precipitation on the sides of the pore. Such effects would account for the development of pores associated with the aluminum-rich phase in CoCrAlY but not having its exact shape.

The role of chromium in chloride-induced hot corrosion of CoCrAlY-type alloys is not as well understood as the observations and proposed mechanism which appear to satisfactorily account for the dealloying of aluminum by sulfate-chloride melts. In alloys containing no aluminum (binary Ni-20Cr and type 309 austenitic stainless steel), exposure to molten halide salts at 800-1000°C has been shown to generate an interconnected void network due to chromium loss[10].* Dealloying of chromium apparently does not occur, however, if aluminum is present in the alloy. Simultaneous line scans for Al and Cr through the zone of internal attack of CoCrAlY show a generally smooth chromium gradient rather than matrix depletion by formation of internal Cr-rich phases (e.g. Figure 17). Depletion of the Cr content of CoCrAlY thus appears to involve long range diffusion of Cr through the zone of internal attack to the Cr-rich scale, the process undoubtedly being accelerated by surface diffusion due to the porous network left by dealloying of the Al content.

The observed effects and proposed mechanism of attack by chloride-containing salt deposits fit well into known characteristics of sulfate-induced hot corrosion behavior of CoCrAlY alloys. It is well established that CoCrAlY is highly resistant to hot corrosion attack upon exposure in air to deposits of 100%-$Na_2SO_4$; protective $Al_2O_3$ scales are stable for long periods of time even under cyclic conditions where scale spallation may occur. Eventual depletion of aluminum and chromium results in formation of less protective reaction products and introduction of sulfur into the alloy from the $Na_2SO_4$. Subsequent degradation then occurs by oxidation of the sulfide phases and formation of more sulfides beneath the nonprotective oxide scale.

When NaCl is added to the $Na_2SO_4$ deposit, the $Al_2O_3$ scales tend to spall more readily. In addition, and probably more important, the chloride in the deposit causes aluminum to be preferentially removed from the alloy via the development of a network of interconnected channels. This dealloying effect of the chloride-containing liquid does not take place immediately but requires a period of time for enrichment of the liquid in NaCl and depletion of oxygen adjacent to the alloy. Thus an initially greater amount of NaCl in the deposit accelerates degradation because less enrichment of NaCl is required.

*Dealloying of Cr and internal oxidation of binary Ni-48Cr and Co-48Cr by $Na_2SO_4$ - 50% NaCl deposits was subsequently observed in independent experiments run simultaneously with the 899°C coatings evaluation reported in Section 3.

Also the length of the initiation stage would be expected to depend on aluminum content, since higher aluminum concentrations tend to inhibit oxygen depletion by development of a continuous barrier of $Al_2O_3$. Eventually, however, the increase in rate of aluminum depletion due to scale spallation and/or dealloying causes sulfur from the $Na_2SO_4$ to react with the alloy after a shorter period of time than that in the absence of chloride. In the extreme case where the deposit is primarily NaCl, the alloy will suffer rapid depletion of aluminum via development of a porous network and subsequent degradation by oxidation of the porous, aluminum-depleted alloy.

d. Selection of Test Conditions for Coatings Evaluation

It was recognized at this point that the microstructural features of service degradation differed in important respects from those induced by sulfate-chloride hot corrosion testing (compare Figs. 1 -5 vs. Figs. 9 - 11, 14, 15). The most significant difference was undoubtedly the zone of internal attack characteristic of laboratory test specimens and the absence of significant internal attack in service hardware. However, the potential for increased degradation due to chloride had been demonstrated, and any knowledge of the chloride effect would be of value in insuring that newly developed coatings were not surprisingly susceptible to chloride-induced attack. In addition the laboratory tests were reproducing at least some of the features of service hardware (e.g. cut-edge attack and the tendency for development of localized protrusions and oxide mounds). For these reasons and the fact that a better testing procedure was not evident at the time, it was decided to continue working with sulfate-chloride salt deposits.

It was concluded from the weight change data and metallographic observations presented in the previous section that a salt mixture of $Na_2SO_4$ - 50 wt% - NaCl would be most suitable for screening of coatings. This composition appeared to be sufficiently aggressive to provide for reasonable exposure times while still allowing differentiation of relative performance. More important, in spite of the fairly high NaCl content, the test results and proposed mechanism would support the argument that the test investigates the effect of chloride on sulfate-induced hot corrosion rather than a chloride effect which overwhelms the role of the sulfate. This point is important because it is known that deposits on engine hardware are primarily sulfates, not chlorides.

The essential features of the test procedure selected for evaluation and ranking of coatings were:

- Cyclic furnace oxidation, each cycle consisting of 50 minutes in the hot zone and 10 minutes in the cold zone of a static air tube furnace
- Salt deposit of 1 $mg/cm^2$ of $Na_2SO_4$ - 50% NaCl applied every 20 hours after water washing to remove previous deposit; weight change data obtained at each washing

- Test temperatures of 899 and 649°C (1650 and 1200°F)

Cyclic oxidation was employed to accelerate materials degradation by scale spallation. Two temperatures were used to investigate conditions where the NaCl component of the deposit vaporizes rapidly and where negligible vaporization of chloride takes place.

## 3. EVALUATION OF STATE-OF-THE-ART AND MODIFIED COATINGS

### a. Processing and Pre-test Microstructure of State-of-the-Art Coatings

The following coatings, all on IN738 substrates*, were evaluated

- PWA 273 aluminide
- LDC-2A platinum modified diffusion aluminide
- PWA 68 CoCrAlY
- PWA 68 CoCrAlY + sputtered platinum overlayer
- sputtered platinum underlayer + PWA 68 CoCrAlY

Processing of these coatings and pre-test microstructures of sample coupons were as follows:

#### 1) PWA 273 Diffusion Aluminide

The PWA 273 process includes two-pack aluminizing treatments (2 hours at 760°C, 3 hours at 1024°C) followed by a four-hour anneal at 1079°C (1975°F) in argon. Characteristic features of the coating microstructure on IN738 (Figure 24) include an outer layer of β-NiAl, usually with fine refractory metal precipitates (primarily α-Cr) if the surface aluminum content is toward the higher limits of the specification range (27 - 36%). An intermediate layer is β-NiAl with substrate carbides, and the innermost diffusion zone is a mixture of β and Cr-rich carbides.

#### 2) Howmet LDC-2A Platinum Modified Diffusion Aluminide

The coating process includes application of a platinum layer on the substrate followed by a pack aluminizing treatment (details of the Howmet process are not known, but similar structures and performance were obtained later in the program by sputtering of ~ 6 μm of Pt followed by the PWA 273 aluminizing cycle). The microstructure is similar to that of a conventional diffusion aluminide except that the outer layer is a mixture of β-NiAl and platinum aluminides, possibly with a thin outer zone of single phase platinum aluminide (Figure 25).

---

*Nominal composition: Ni-16.0Cr-8.5Co-3.4Al-3.4Ti-1.75Mo-2.6W-1.75Ta-0.85Nb-0.12Zr-0.012B

3) PWA 68 CoCrAlY and Platinum Modifications

PWA 68 is applied by electron beam vapor deposition followed by glass bead peening and annealing for 4 hours at 1079°C. The specified composition range is 15 - 24% Cr, 11.5 - 13.5% Al, 0.2 - 0.7% Y. The microstructure (Figure 26a) is a three-phase mixture of $\alpha$-Co, $\beta$-CoAl, and small amounts of yttride which are usually not discernable by optical metallography except at very high magnifications. Alloy content of the metallic phases is approximately 3% Al, 24% Cr and 28% Al, 8% Cr for the $\alpha$-Co and $\beta$-CoAl respectively.

The platinum-modified PWA 68 coatings are illustrated in Figures 26b and 26c and in the back scattered electron images of Figure 27 where atomic number contrast defines the platinum layers and adjacent diffusion zones as well as the $\alpha$-Co + $\beta$-CoAl structure of the unaffected PWA 68. The platinum layers were deposited by sputtering; in the case of the Pt underlayer, the sample was annealed one hour at 1079°C prior to deposition of the PWA 68.

b. Testing at 899°C

Duplicate specimens of each of the systems were tested to failure or exposed for a total of 500 hours. Weight change data were obtained, but proved of relatively little value in comparison with the information from visual inspection and metallography. Figure 28, for example, shows only that the CoCrAlY coatings are losing weight due to scale spallation after ~ 60 hours, while the aluminides continue to show weight gains for a significantly longer time. Beyond the time plotted, data were compromised by deterioration of the tabs holding the samples in the furnace and hence of no value as an indicator of rate of degradation or coating failure.

Visual and metallographic observations concerned with the performance of each coating in the 899°C hot corrosion test were as follows:

1) PWA 273 Diffusion Aluminide

Both specimens performed well in 500 hours at 899°C. Attack was highly uniform, and there was no visually definable coating failure in either of the specimens. Metallographic cross sections, although indicating substantial degradation (Figure 29), revealed no penetration into the substrate. In fact, a substantial amount of $\beta$-phase was evident in one of the specimens, indicating the coating was still protective.

Figure 29 includes x-ray area scans of the degraded coating for Al, Ti, Cr, O, and S. It is evident that the external scale is $Al_2O_3$; this scale is much thicker than that which would have formed in absence of the salt deposit and is spalling off in numerous areas. Oxides found within the coating are rich in Al and Ti, and chromium sulfides are also readily apparent (Figures 29b-29f). Such development of internal oxides in a coating still rich in aluminum (i.e. still containing $\beta$-NiAl) indicates the liquid salt must be dealloying localized regions of aluminum.

2) LDC-2A Platinum-Modified Diffusion Aluminide

Performance of this coating was obviously inferior to that of PWA 273, although both of the duplicate specimens were exposed 500 hours without conclusive indication of coating failure on visual inspection. Metallographic examination showed complete dissolution of the β-NiAl and uniform internal oxidation extending completely through the coating (Figure 30a). Attack of the substrate was detected on several planes of polish through the samples (Figure 30b).

3) PWA 68 CoCrAlY

Edge distress of both specimens was evident from the start of the test. An obvious edge failure was observed after 160 hours, and the sample was removed from test after 320 hours. Testing of the duplicate specimen was terminated after 220 hours due to edge deterioration and generally poor surface condition.

Edge failure and cut-edge consumption of the coating are illustrated in Figure 31a and protrusions of the type in Figure 31b were readily observable in both specimens. As on the PWA 273 coating, X-ray area scans (Figure 32) showed a relatively thick external scale of $Al_2O_3$. At locations where coating protrusions were developing, stringers of $Al_2O_3$ extended into the coating and the microstructure was depleted of β-CoAl. Chromium sulfide precipitates were evident in the Al-depleted areas. The mound of scale over the protrusion was composed of an outer zone of cobalt chromate spinel and well defined layers of $Cr_2O_3$ and $Al_2O_3$.

4) Platinum Underlayer + PWA 68 CoCrAlY

The duplicate specimens were exposed for the same length of time as the unmodified PWA 68 (320 and 200 hours); no difference in failure mode or extent of degradation was discernable from visual inspection during the test. Severe edge deterioration was observed in less than 200 hours as well as apparent coating penetration (i.e. large oxide mounds) in other areas after 200 to 300 hours. Subsequent metallography showed that the platinum underlayer was not effective in stopping a developing protrusion from penetrating into the substrate; in fact some indication of enhanced penetration of liquid salt along the platinum layer, perhaps due to poor adherence of the Pt to the substrate could be detected at coating failure sites (Figure 33).

5) PWA 68 CoCrAlY + Platinum Overlayer

Performance of the CoCrAlY coating was significantly improved by the platinum overlayer; both samples were exposed for 500 hours, although edge distress was evident in some locations after 300 hours. In spite of oxide mounds on the surface, metallographic examination showed no penetration of the coating except at edges of the coupons. Development of coating protrusions appeared to involve the same mechanism of aluminum dealloying and internal oxidation as in PWA 68 but the coating lifetime was extended by the necessity of first penetrating the platinum overlayer (Figure 34). Pene-

tration of the overlayer appears to involve partial dissolution of the continuous single phase zone characteristic of the as-deposited coating, leaving the surface still enriched in platinum but permitting the melt to dealloy the $\alpha$-Cr + $\beta$-CoAl structure beneath the remnants of the overlayer.

6) Ranking of Coatings and Discussion of Results

Ranking of the coatings in order of increasing resistance to the test conditions used (i.e. 899°C cyclic hot corrosion with $Na_2SO_4$ - 50% NaCl deposits) would be:

- PWA 68
- Pt underlayer + PWA 68

} ~ the same

- PWA 68 + Pt overlayer
- LDC-2A
- PWA 273

} ~ the same

The relative performance of the PWA 68 and PWA 273 was unexpected. Burner rig tests at 899°C (1650°F) with 30 ppm of ingested sea salt had shown PWA 68 to perform better than most aluminide coatings. Apparently the detrimental effect of chloride is much more pronounced on PWA 68 than on PWA 273, perhaps because of Ni-base vs. Co-base or because the two-phase $\alpha$ + $\beta$ structure of CoCrAlY is more susceptible to penetration and dealloying by chloride-containing melts than the single phase outer layer of $\beta$-NiAl on IN738/PWA 273. This ranking thus applies only to the case of $Na_2SO_4$ - 50% NaCl and would be expected to change with chloride content in the direction of improved ranking of the CoCrAlYs with respect to the aluminides at lower concentrations of chloride in the deposit.

c. Hot Corrosion Tests of State-of-the-Art Coatings at 649°C (1200°F)

Duplicate sets of samples were tested. One set was exposed for 1000 hours; the other was tested for various times depending on coating performance. Weight change data were obtained but showed only that $\Delta M/A$ values were very small and that the aluminides tended to gain weight at a slightly greater rate during the initial 300 hours of exposure (Figure 35). Visual and metallographic observations were much more useful in characterizing coating performance. These results were:

1) PWA 273 Diffusion Aluminide

Visual inspection of both samples during test revealed edge distress, but the extent of attack was not regarded as coating failure and general surface condition was good. Metallography of the 1000 hour coupon showed attack originating at the edge and spreading laterally (Figure 36a); however, there was negligible degradation of surface away from the edges (Figure 36b). The duplicate specimen was exposed for 2000 hours; visual inspection showed no indication of incipient failure (Figure 37a). Surface microstructure was noticeably degraded, but attack was uniform and confined to the 30 $\mu$m depth illustrated in Figure 37b.

2) LDC-2A Platinum-Modified Diffusion Aluminide

Visual observations suggested coating performance similar to PWA 273. Metallography after 1000 and 2000 hours showed the coating was still protective, although attack was generally greater and more irregular than on PWA 273 (Figure 38).

3) PWA 68 CoCrAlY

One specimen was removed from test after 260 hours to examine the initial stages of coating degradation. Extent of attack at this point was not severe; maximum depth of dealloying and internal oxidation in some areas near the edge was about 75 μm. The duplicate specimen developed surface pits and edge deterioration after 340 hours but the defects did not propagate at the low test temperature. A typical microstructure after 1000 hours exposure is illustrated in Figure 39. Most areas were dealloyed and internally oxidized to depths of about 25 to 50 μm, and there were numerous protrusions and areas of internal oxidation of the entire coating thickness (as in the right side of Figure 39).

4) Platinum Underlayer + PWA 68 CoCrAlY

As in the tests at 899°C, the platinum underlayer did not appear to affect the life time or degradation mechanism of the PWA 68 coating. Large mounds of oxide were observed at approximately the same time of exposure (320 to 380 hours), and post-test metallography after 1000 hours (Figure 40a) showed microstructural degradation apparently equivalent in nature and extent to that of the PWA 68 coating directly applied to the IN738 substrate. Testing of the duplicate specimen was terminated at 780 hours and a typical coating protrusion (Figure 40b) examined in the microprobe.

Figure 41 includes a back scattered electron image and X-ray area scans for oxygen, sulfur, and the major coating constituents. These photos, a line scan along the path shown in Figure 41a, and KEVEX spectra of selected points indicate the affected area consists of a front of $Al_2O_3$ particles, a zone of $Al_2O_3$ and CrS particles, and a mixture of Cr- and Al-rich oxides forming the volume of the protrusion. There is relatively little CoO (Figure 41d) except for the outer layer of the oxide mound. The line scan showed that the matrix solid solution in the zones of CrS and $Al_2O_3$ precipitation was almost completely dealloyed of aluminum and a gradient of Cr content existed through this zone. This shows that the chloride-containing melt is capable of dealloying the coating of chromium, as well as aluminum, although the aluminum is apparently attacked first and its concentration must be reduced to a low level before chromium is preferentially removed from the alloy.

5) PWA 68 + Platinum Overlayer

As expected from results of the 899°C test, the platinum overlayer significantly improved the performance of the PWA 68. The beneficial effect at 649°C was even more pronounced than at the higher temperature. One of the

samples developed a small greenish spot at 380 hours but it appeared to be very shallow and did not grow with continued exposure. Metallographic examination of this sample showed only superficial oxidation and possibly development of very small oxide stringers (arrow in Fig. 42a). After 2000 hours the coating on the duplicate specimen was still protective, although dealloying and internal oxidation could be observed in some areas (Figure 42b).

6) Ranking of Coatings and Discussion of Results

Ranking of the coatings in order of increasing resistance to 649°C cyclic hot corrosion with $Na_2SO_4$ - 50% NaCl would be:

- PWA 68
- Pt underlayer + PWA 68

} ~ the same

- LDC-2A
- PWA 273
- PWA 68 + Pt overlayer

} ~ the same

The relatively poor performance of PWA 68 and the ineffectiveness of the platinum underlayer is the same as observed at 899°C. LDC-2A is ranked next because the 1000 hour sample was more degraded than the 273 and 68 + Pt; the 2000 hour samples of LDC-2A and PWA 273 were essentially the same. Degradation of the PWA 68 + Pt overlayer was negligible after 1000 hours; of the three samples tested to 2000 hours, the PWA 68 + Pt appeared slightly better than the PWA 273.

The microstructural features (and hence the mechanism) of coating failure at 649°C appeared similar to that observed at 899°C; i.e. dealloying of the coating of aluminum by the chloride in the deposit followed by oxidation of the chromium and then the cobalt.

d. Hot Corrosion Tests Using Modified Coatings Systems

In order to attempt to develop coatings with better resistance to chloride effects than the state-of-the-art coatings, the following systems were subjected to the 899°C hot corrosion test ($Na_2SO_4$ - 50% NaCl);

- low aluminum diffusion aluminide (PWA 73)
- high aluminum diffusion aluminide (PWA 273)
- chromium-modified low aluminum diffusion aluminide (PWA 70 + PWA 273)
- platinum-modified high aluminum diffusion aluminide (6 μm Pt + PWA 273)
- CoCrAlY (PWA 68) + 6 μm Pt overlayer
- CoCrAlY (PWA 68) + 12 μm Pt overlayer)
- aluminized CoCrAlY (PWA 68 + PWA 273)
- platinum-modified aluminized CoCrAlY (PWA 68 + Pt - PWA 273)
- titanium-modified PWA 68
- titanium-modified PWA 273
- CoCrAlY (PWA 68 + nickel overlayer)
- preoxidized CoCrAlY (PWA 68, 1 hour at 1200°C)

Performance of these coatings is summarized in Table III; visual and metallographic observations were as follows:

(a) PWA 73 Diffusion Aluminide

In contrast to the favorable results obtained with PWA 273 on the IN738 substrate, the lower aluminum PWA 73 coating was rapidly attacked. Black oxide mounds were observed at 40 hours and corner failure at 100 hours (Figure 43a). The typical microstructure showed β dissolution and internal oxidation to a depth of ~ 50 μm (Figure 43b), and there were several areas of complete dealloying and internal oxidation of the coating (Figure 43c).

(b) PWA 273 Diffusion Aluminide

Two tests verified the relatively good performance of the PWA 273 coating, although greater microstructural degradation was observed than in the initially run tests on state-of-the-art coatings. Figure 44a shows complete dissolution of the β-NiAl, precipitation of CrS, and internal oxidation of the entire coating thickness after 1000 hours exposure. Testing of the second sample was terminated at 700 hours due to tab failure; the coating microstructure was again completely depleted of β-NiAl but not penetrated except for the tab failure (Figure 44b).

(c) PWA 70 + PWA 73 - Pack Chromize Plus Low Aluminum Diffusion Aluminide

Chromizing did not improve the performance of PWA 73. General surface degradation on visual inspection appeared more rapid, and coating microstructure after only 80 hours of exposure was almost completely devoid of β-NiAl (Figure 45).

(d) PWA 70 + PWA 273 - Pack Chromize Plus High Aluminum Diffusion Aluminide

Prior chromizing was markedly detrimental to the performance of PWA 273. Surface deterioration was evident from the start of the test, and a massive corner failure was observed after 80 hours (Figure 46a). The microstructure still contained β-NiAl (Figure 46b), but the extent of degradation after only 80 hours was comparable to that of the directly applied PWA 273 after 1000 hours.

(e) Pt + PWA 273 Diffusion Aluminide

This coating was intended to be equivalent to the Howmet LDC-2A. It was applied by vacuum sputtering of ~ 6 μm of platinum at a sputtering temperature of approximately 900°C followed by the PWA 273 aluminizing pack treatments.

The sample was exposed for 1000 hours in the 899°C cyclic hot corrosion test. Visual inspection indicated performance comparable to that of PWA 273. Subsequent metallography was puzzling and inconclusive. Small areas were essentially unaffected (e.g. the left side of Figure 47a), while others showed complete dealloying and internal oxidation of the coating (Figure 47b).

However, there was no indication of substrate attack on either visual inspection or metallographic examination.

(f) PWA 68 + Platinum Overlayer (~ 6 μm)

This specimen was nominally the same as that tested in the section on state-of-the-art coatings; it performed as expected from previous results. Testing was terminated because of tab failure and cut-edge attack at 720 hours*; the rest of the coating was significantly degraded but not penetrated (Figure 48).

(g) PWA 68 + Platinum Overlayer (~ 12 μm)

Due to the favorable results obtained with a 6 μm overlayer, additional specimens were prepared to determine if further improvement could be realized with thicker overlayers. Duplicate specimens showed apparently similar performance, however. Metallographic observations could have been interpreted as slightly less degradation at the same exposure times, but the effect was not of significant magnitude (Figure 49).

(h) PWA 68 + PWA 273 (Aluminized CoCrAlY)

Considering the favorable performance of PWA 273 on IN738, it was reasoned that resistance of CoCrAlY to sulfate-chloride attack might be improved by pack aluminizing. However, the specimen surface turned charcoal gray after only 40 hours and testing was discontinued after a massive edge failure at 80 hours (Figure 50). General surface degradation away from the edge failure was also extensive, including a thick external scale and a dealloyed layer with $Al_2O_3$ and CrS precipitates (Figure 50b).

A duplicate specimen also deteriorated rapidly, showing extensive spallation and non alumina-forming areas from the start of the test. After 200 hours the microstructure was completely dealloyed of the aluminum added by the PWA 273 treatment.

(i) PWA 68 + Pt + PWA 273 (Platinum-Modified Aluminized CoCrAlY)

Except for the massive cut edge attack shown in Figure 51a, the system appeared promising. The coating was still protective after 520 hours (Figure 51b). Although one side of the coupon was more severely degraded than the other, the depth of attack was uniform and no deeper than that illustrated.

---

*Cut edge degradation was not considered in evaluating coating performance, since all Ni-base coatings and Co-base coatings on Ni-base substrates are apparently susceptible. Where testing had to be terminated because of extensive cut edge attack, coating performance was assessed by surface condition and microstructure in areas away from the cut edge.

A duplicate specimen was exposed 940 hours before one side of the coupon was almost entirely consumed by cut-edge attack. Surprisingly the microstructure of this side was unaffected except for the cut-edge attack; the other surface was uniformly dealloyed and internally oxidized to a depth of ~ 80 μm (Figure 52).

(j) Titanium-Modified PWA 68 CoCrAlY

A modified CoCrAlY composition containing 3.1% Ti in addition to the specified Cr and Al contents of PWA 68 was applied by electron beam vapor deposition. Cut-edge attack was again observed (Figure 53a), but the amount of microstructural degradation away from the cut edge was much less than that of PWA 68 after comparable exposure times (Figure 53b).

(k) Ti + PWA 273 (Titanium-Modified Diffusion Aluminide)

A thin (~ 6 μm) layer of titanium was applied to an IN738 coupon by vacuum sputtering prior to PWA 273 aluminizing. The effect of the Ti was apparently beneficial. Visual observations showed no indication of incipient failure (except at the tab) in 1000 hours. Subsequent metallography showed internal oxidation to a depth of only about 20 μm and retention of large amounts of β-NiAl in the microstructure (Figure 54).

(l) PWA 68 + Ni Overlayer

A ~ 25 μm sputtered Ni overlayer was applied on PWA 68 CoCrAlY to determine if overlayers of a metal other than platinum could produce beneficial effects. Results were not encouraging; the nickel overlayer was rapidly oxidized and exerted no significant effect on the coating beneath it (Figure 55).

(m) Preoxidized PWA 68 CoCrAlY

Preoxidation (1 hour at 1200°C) did not produce beneficial effects. Visual inspection revealed that the $Al_2O_3$ scale spalled extensively and black oxide mounds were visible after the initial 20-hour exposure. Coating penetration at specimen edges was evident at 100 hours. Thick surface scale, substantial dealloying and internal precipitation of $Al_2O_3$ and CrS particles through the entire coating thickness were evident on subsequent metallography.

(n) Summary and Discussion of Results on Modified Systems

1) CoCrAlY - Type Coatings

The following process modifications were found to improve the resistance of CoCrAlY to sulfate-chloride hot corrosion:

- Platinum overlayers
- Alloying with titanium
- Platinum overlayers + PWA 273 diffusion aluminide

Consistently favorable results were obtained with platinum overlayers, although increasing the thickness of the overlayer from 6 to 12 μm did not effect a significant improvement in performance. The addition of 3.1% Ti to PWA 68 approximately doubled the time required to dealloy and internally oxidize the coating at 899°C. Performance of the 68 + Pt + PWA 273 was variable but unquestionally an improvement over conventionally processed PWA 68.

Coating modifications investigated and found ineffective were:

- Aluminized CoCrAlY (PWA 68 + PWA 273)
- Platinum underlayers
- Nickel overlayers
- High temperature preoxidation

Since the mechanism of chloride-induced attack involves dealloying of aluminum, it is puzzling why an increase in the surface aluminum content by aluminizing of CoCrAlY does not improve performance. The ineffectiveness of the platinum underlayer, at least against the initial stages of attack, is more easily understandable in view of the mechanism of chloride-induced attack. Overlayers of metal other than platinum do not appear promising; apparently the less noble metals will oxidize and spall off rapidly. Likewise a thicker scale formed by high temperature preoxidation also appears susceptible to penetration and spallation, offering no protection against the dealloying action of the sulfate-chloride melt.

2) Diffusion Aluminide Coatings

Sputtering of platinum or titanium prior to PWA 273 pack aluminizing appears to be beneficial, although the platinum effect is not as potent as that of the overlayer on PWA 68. Aluminide coatings applied by the single pack PWA 73 process did not perform as well as PWA 273. Chromizing prior to aluminizing appeared to be ineffective and perhaps slightly detrimental against chloride-induced attack.

e. Platinum Overlayer Effect on $Na_2SO_4$ - NaCl Induced Attack of CoCrAlY

To examine the role of platinum overlayers in inhibiting chloride-induced degradation, specimens of PWA 68 and PWA 68 + Pt were coated with $Na_2SO_4$ - 50% NaCl deposits and heated in air at 899°C for short periods. Surface condition was characterized with the scanning microscope after exposures of 10, 20, 60, and 120 minutes; the specimens were then run for 20 hours in the automatic cycling furnace (1 hr/cycle) and sectioned for metallographic examination.

As expected, scale spallation and surface pores were evident on the PWA 68 coating after very short exposure time (Figure 56a). After 1 hour, the pores were larger and much more numerous (Figure 56b). After a total exposure of 22 hours, the coating was dealloyed and internally oxidized to a depth of about 100 μm in some areas (Figure 56c).

Surface features and a cross section through the platinum overlayer after the same exposure times are presented in Figure 57. A grain boundary-like attack of the platinum aluminide phase is evident, but the depth of attack after 1 hour is not noticeably greater than after 20 minutes (Figure 57a, 57b). Metallography after 22 hours (Figure 57c) shows that the surface features are only superficial grooves causing no discernable degradation of the coating microstructure at the 500x magnification where substantial dealloying and internal oxidation of PWA 68 were readily observable.

Ultimate degradation of the platinum overlayer occurs by interdiffusion and possibly by aluminum depletion due to repeated formation and spallation of alumina scales. Some interdiffusion takes place during processing such that the overlayer contains sufficient cobalt and chromium to form small areas of $\alpha$-Co,Cr and sufficient aluminum to render it an alumina-former on high temperature exposure (Figure 58). Also a Pt-containing diffusion zone with a platinum aluminide phase (apparently the same as that in the overlayer) forms beneath the surface. As long as the Pt,Al phase in the overlayer remains continuous, the layer is protective, apparently because reaction of chlorine with aluminum in the platinum aluminide is not thermodynamically favorable. When the continuous overlayer is broken up by Al depletion, however, the chloride-containing melt is capable of dealloying the CoCrAlY structure in spite of the discontinuous Pt,Al phase in the remnants of the overlayer and diffusion zone (Figure 59). The overlayer is thus most effective at low temperatures where dissolution of the Pt,Al phase by interdiffusion is slowest.

Also evident from these observations is the ineffectiveness of a platinum underlayer because the chloride-containing melt can dealloy the coating of aluminum and chromium before the underlayer enters into the reaction.

## 4. HOT CORROSION TESTING USING $SO_3$ IN THE GASEOUS ENVIRONMENT

### a. Introduction

As mentioned previously, the CoCrAlY degradation microstructures developed in the laboratory tests using $Na_2SO_4$ - NaCl deposits were not a total reproduction of the degradation microstructures obtained from marine service hardware. Tests performed at the Naval Research Laboratory[3] using deposits of mixed sulfate salts (e.g. $CoSO_4$ - $Na_2SO_4$) heated in air at 649° - 760°C (1200-1400°F) and at the Naval Ship Research and Development Laboratory[4] using a ducted burner rig test at 704°C (1300°F) with 1% sulfur in the fuel produced degradation microstructures of CoCrAlY that were virtually identical to those generated in the field. Such results indicate that the $SO_3$ content of the gas may play a significant role in the development of the service related microstructures. Work was therefore performed to develop a test using $SO_3$ which hopefully would generate degradation microstructures more similar to those from the field, and which would then be used to evaluate various coatings previously tested in chloride-induced attack.

b. Development of Laboratory Furnace Test Using $SO_3$ and $Na_2SO_4$

A PWA 68/IN738 coupon was covered with a thick deposit of $Na_2SO_4$ - 50 mol% $CoSO_4$ (about 300 mg of the mixture per square centimeter) and heated in air for 41 hours at 760°C (1400°F); the specimen at that time contained numerous coating protrusions of the type and depth shown in Figure 60. Scanning microscopy of these protrusions shows a well defined ghost image of the coating microstructure (Figure 60a). Microprobe analysis shows a zone of sulfur enrichment outlining the area of nodular attack (Figure 60c), and cobalt, chromium and aluminum are distributed in the protrusion and oxide mound as illustrated in Figures 60d, e, and f. Higher magnification (Figure 61) shows evidence of preferential attack of β-CoAl, leaving a continuous layer of α-Co in contact with the scale. The sulfur is primarily in the scale, although small CrS precipitates can be detected in the α-Co layer. The X-ray image (Fig. 61c) suggests depletion of Cr from the metal immediately adjacent to the Cr-rich scale, although line traces did not show a detectable Cr gradient in advance of the scale/metal interface. The β-denuded zone and concentration of Al in the adjacent scale are strikingly evident in the X-ray image for aluminum (Fig. 61d).

The photomicrographs just discussed should be compared with those of service degradation in Figures 1-3 and 7-8. The fundamental similarity of the microstructure and element distribution are obvious.

The type of attack produced by thick deposits of mixed sulfates is believed to involve $SO_3$ produced by decomposition of the metal sulfate*. If such is the case, similar microstructural features should be produced by $Na_2SO_4$ deposits heated in a furnace atmosphere containing $SO_3$ in the gas. This type of experiment was run in a horizontal tube furnace where atmosphere control was achieved by flowing $SO_2$:$O_2$ gas mixtures at appropriate rates over a platinum catalyst to produce a known (assuming equilibrium) partial pressure of $SO_3$.

The initial experiment was run at a very high $SO_3$ pressure (~ 0.2 atm) to determine in a short testing time if attack would occur at a low temperature (649°C, 1200°F) where a thin $Na_2SO_4$ deposit heated in air is known to be innocuous. Both CoCrAlY (PWA 68) and a diffusion aluminide coating (PWA 273 on IN738) suffered significant microstructural degradation in 20 hours (Figure 62). Except for a tendency to general surface degradation rather than localized, nodular attack, the microstructure of the attack front in the CoCrAlY coating appeared very similar to those observed in the mixed sulfate experiment and in service hardware.

Subsequent tests were run at a lower $SO_3$ pressure obtained by passing a mixture of 95 vol% $O_2$ and 5 vol% $SO_2$ over a platinum catalyst at a total

*Hence a large quantity of salt is needed to maintain a supply of $SO_3$. The attack is not produced by a thin deposit heated in air because a thin deposit cannot supply enough $SO_3$.

flow rate of 11.5 liters/hour; equilibrium $SO_3$ pressures under these conditions are approximately 0.04 atm at 649°C (1200°F) and 0.01 atm at 899°C (1650°F) respectively.

Specimens of bulk Co-25Cr-6Al were coated with ~ 1 mg/cm$^2$ of $Na_2SO_4$ and $Na_2SO_4$ - 50% NaCl and exposed for 100 hours (5 cycles with washing and reapplication of fresh salt every 20 hours) at 649°C. The rate of attack was less at the lower $SO_3$ pressure, but the nature of the scale and the attack front was apparently the same. Also significant was the virtually identical degradation of the specimens coated with sulfate and sulfate-50% chloride (Figures 63, 64), the sulfate-chloride specimen exhibiting substantial scale formation but no evidence of the porous zone of internal attack characteristic of chloride-induced dealloying.

The lack of a discernable chloride effect in this experiment must be interpreted with caution, considering that the $SO_3$ pressure is still much higher than that in the combustion gases of a turbine engine and that the test conditions involved a continuous supply of $SO_3$ but deposition of the chloride-containing salt only once every 20 hours.[3] Thus the result does not rule out the possibility of a chloride effect at lower $SO_3$ pressures and continuous deposition of salt during operation of a marine engine. Demonstrated by the observation, however, is that effects of gaseous sulfur oxides are capable under certain conditions of completely overwhelming any influence of chloride in the condensed deposit, presumably due in part at least to removal of the chloride by reactions of the form

$$2NaCl + SO_2 + O_2 \rightarrow Na_2SO_4 + Cl_2, \text{ and/or}$$
$$2NaCl + SO_2 + H_2O + 1/2\ O_2 \rightarrow Na_2SO_4 + 2HCl$$

as discussed by McKee, Shores, and Luthra.[11]

Additional experiments were performed to isolate other variables potentially involved in low temperature degradation of CoCrAlY. To check the possibility of low temperature oxidation or sulfate-induced hot corrosion in air, specimens were exposed for 4000 hours at 649°C; there was no discernable degradation of either the uncoated or sulfate-coated material (Figure 65a). Exposure of an uncoated specimen for 60 hours to the $O_2$ - $SO_2$ - $SO_3$ gas mixture also produced no observable attack (Figure 65b), but significant degradation was encountered after only 20 hours exposure of a sulfate-coated specimen to the $SO_3$ - containing gas (Fig. 65c). Pink salt crystals, which appeared to have been liquid at the test temperature, were observed on the specimen surface and subsequently identified by XRD as $Na_2Co(SO_4)_2$. Post-test metallography showed numerous small pits with features of the scale/metal interface (i.e. preferential attack of β-CoAl) common to service-induced degradation.

It is clear from these results that the simultaneous presence of $Na_2SO_4$ salt deposits and $SO_3$ in the gaseous environment can produce substantial hot corrosion of CoCrAlY alloys at a low temperature where negligible attack would result from exposure to the salt in sulfur-free air or the $SO_3$-contain-

ing gases in the absence of a salt deposit. One of the factors undoubtedly involved in the attack mechanism is acid fluxing of the alumina scale on CoCrAlY, as shown by negligible attack of a salt-coated alumina tablet on heating in air vs. dramatic etching of the surface by $Na_2SO_4$ salt equilibrated with 0.04 atm $SO_3$ (Figure 66). Obviously, however, fluxing of the external scale is not the only important factor, especially at the base of an oxide pit where the oxygen pressure is probably very small.

It was decided at this point to evaluate the performance of various coatings under the following test conditions:

- Isothermal exposure at 649°C (1200°F)
- Salt deposit of ~ 1 mg/cm$^2$ $Na_2SO_4$ applied every 20 hours after water washing to remove previous deposit
- Gaseous atmosphere of 0.96 atm $O_2$, 0.04 atm $SO_3$ obtained by equilibration of a mixture of $SO_2$ - $O_2$ at the test temperature

The problem encountered in testing with an $SO_3$ pressure much higher than expected in an engine ($10^{-4}$ to $10^{-5}$ atm) were recognized, but several arguments could be advanced for the conditions selected:

- Conditions much more severe than the engine environment are obviously required to provide for reasonable testing times
- Microstructural features of specimens tested at $SO_3$ pressures of 0.2 and 0.04 atm were apparently identical, suggesting that the mechanism (although not the rate) of attack is the same over a range of $SO_3$ pressures

c. Testing of Coatings with $Na_2SO_4$ - 0.04 atm $SO_3$

PWA 68 CoCrAlY and PWA 273 diffusion aluminide were exposed 60 hours to the test conditions described in the preceeding paragraph. Visual inspection indicated significant degradation, although subsequent metallography showed less material consumption than inferred from the surface condition (Figure 67).

The following systems were then exposed for 100 hours in an attempt to produce more severe degradation in a slightly longer but still experimentally convenient testing time:

(a) PWA 68 + Pt overlayer
(b) Pt underlayer + PWA 68
(c) PWA 68 + PWA 273
(d) PWA 68 + Pt + PWA 273
(e) PWA 273
(f) Ti-modified PWA 273
(g) PWA 73
(h) PWA 70 + PWA 273
(i) Pt + PWA 273

Visual inspection again indicated substantial degradation of all specimens, although attack was generally very uniform and there was no incidence of localized coating penetration or edge failure. The aluminides appeared to have thinner scales and less evidence of scale spallation, but the magnitude of the effect would not be described as significantly better performance of the aluminide than the CoCrAlY-type coatings.

The specimens were sectioned for metallographic observation. Results were:

a) PWA 68 + Pt Overlayer

Unfortunately the platinum overlayer was ineffective against $SO_3$ - induced acid attack, in contrast to its very favorable resistance to sulfate-chloride salt mixtures. Visual inspection suggested degradation at the same rate as the unmodified PWA 68; post-test metallography showed complete oxidation of the overlayer (Figure 68a ) and numerous instances of penetration below the Pt-containing diffusion zone into the $\alpha + \beta$ microstructure (Figure 68b).

b) Pt Underlayer + PWA 68

The platinum underlayer was of particular interest because of service experience and burner rig test results from NAVSEC which were indicating superior performance over bill-of-material CoCrAlY. However, a difference between this system and PWA 68 or PWA 68 + Pt was not evident on visual inspection; after the initial 20 hour exposure cycle, the specimen surface was generally green in color and exhibited scale spallation. Post-test metallography (Figure 69) indicated less material consumption than the 68 + Pt overlayer sample tested concurrently, although the difference was probably within the range of experimental scatter and no difference in the microstructure of the attack front which would account for a different rate of degradation was discernable.

Even though the surface microstructure and attack front were indistinguishable from those of the directly applied PWA 68, microanalysis showed that the Pt underlayer had reduced the interdiffusion with the substrate which occurs during the 1079°C/4 hour heat treatment in processing. KEVEX spectra at various points near the attack front in the sample with the platinum underlayer contained no Ni peaks, while those from several CoCrAlY specimens tested earlier in the program included small but clearly recognizable amounts of Ni. While it is not yet clear if compositional differences due to reduced interdiffusion are a significant and reproducible effect, no other explanation for improved performance of engine tested vanes with Pt underlayer + CoCrAlY coatings is presently apparent.

c) PWA 68 + PWA 273

Visual inspection did not indicate improved performance due to aluminizing of CoCrAlY; pink crystals were observed on the surface and edges at the

20-hour inspection intervals, and the specimen was dark gray in color after 20 hours. Thick gray scale, spalling off in places, was evident after 100 hours.

Post-test metallography was inconclusive. Some areas showed negligible microstructural degradation while others were corroded and/or damaged by heavy grinding in metallographic preparation.

Performance of PWA 68 + Pt + PWA 273 was similar to that of aluminized PWA 68; i.e. the platinum overlayer had no apparent effect on the extent of visually discernable oxidation or microstructural degradation.

d) Diffusion Aluminide Coatings

No significant difference in performance of four specimens of diffusion aluminide coatings (PWA 273, PWA 70 + PWA 273, PWA 73, and Ti + PWA 273) on IN738 was discernable, except possibly for a thicker oxide and greater scale spallation on the Ti-modified coating. Post-test metallography showed a similar nature and extent of attack on all of the samples (Figure 70).

Somewhat surprisingly in view of the ineffectiveness of the Pt overlayer on CoCrAlY, the Pt-modified PWA 273 appeared distinctly better than the other aluminides. The initial visual inspection at 20 hours suggested relatively little degradation, although there was some evidence of selective attack after 100 hours. Metallographic examination showed a Pt-rich surface layer generally unaffected except for a thin scale (Figure 71).

d. $SO_3$ Effects at Higher Temperatures

Specimens of PWA 68 coated IN738 and bulk Co-25Cr-6Al were exposed for 100 hours (5 cycles with fresh $Na_2SO_4$ salt applied every 20 hours) at 899°C in a furnace atmosphere produced by equilibrating the input $SO_2$:$O_2$ mixture used in the previous experiments at the higher test temperature; calculated gas pressures under these conditions are $p_{SO_3} \approx 0.01$, $p_{SO_2} \approx 0.04$, $p_{O_2} \approx 0.95$ atm. In spite of the higher temperature, both alloys are known to be resistant to sulfate-induced hot corrosion and would be expected to suffer minimal degradation on heating in sulfur-free air for 100 hours.

Post-test metallography of the PWA 68 coating showed corrosive attack of the depth and morphological form illustrated in Figure 72a. Although the extent of corrosion is substantial, the shape of the nodules and extensive β-depleted zone do not resemble the features observed in the service hardware examined for this program.

The Co-25Cr-6Al showed several areas of very deep, localized attack as in Figure 72b. Again there was a substantial β-depleted zone with precipitates of Cr-rich sulfides (black arrows); a layer of corrosion product immediately adjacent to the scale/metal interface was highly enriched in aluminum and sulfur (area scans not presented).

Lastly, two specimens of PWA 68-coated IN738, one with a platinum underlayer, were tested at 760°C (1400°F); the equilibrated $SO_3$ pressure at this temperature is about 0.02 atm. Visual observations indicated the attack was more severe than at 649 or 899°C, and the test was terminated after 40 hours. Metallographic examination confirmed the extensive hot corrosion of both specimens. The PWA 68 coating was penetrated in numerous areas of highly localized attack, and the coating on one edge of the specimen was completely consumed (Figure 73). General surface degradation and material consumption was even more extensive on the specimen with the platinum underlayer, and two sites of penetration into the substrate were observed on the plane of polish being examined. However, there was a striking tendency for the attack front to stop at the platinum-containing diffusion zone, even on the curved edge which is almost always the initial site of localized coating failure (Figure 74).

e. Summary and Discussion of Results of $Na_2SO_4$ - $SO_3$ Experiments

These experiments have shown that the presence of $Na_2SO_4$ deposits plus $SO_3$ in the gaseous environment can result in substantial degradation of coatings which are highly resistant to $Na_2SO_4$ deposits heated in air. Also apparent is the ability to reproduce the microstructural features and element distribution of service degradation in short-time laboratory furnace experiments involving only thin $Na_2SO_4$ deposits and $SO_3$ in the furnace gas.

A series of low temperature (649°C) tests with 0.04 atm $SO_3$ pressure did not differentiate between the performance of state-of-the-art and modified coatings known to exhibit significant differences in resistance to sulfate-chloride attack and $Na_2SO_4$ deposits heated in sulfur-free air. In addition, the CoCrAlY-type alloys experienced general and highly uniform surface degradation rather than the localized nodular attack characteristic of service hardware. It is suspected that the $SO_3$ pressure is so high that effects which may become important at lower pressures are being masked. The potential for such a problem is always present when a laboratory test is made severe to shorten testing time.

In spite of these drawbacks, the incidence of substantial hot corrosion without a zone of internal attack in advance of the scale/metal interface and the observation of pink, Co-containing sulfate crystals on test specimens and service hardware are strong indications that the $SO_3$ effects observed in the controlled atmosphere tube furnace experiments are indeed a factor in degradation of shipboard engines.

Pronounced nodular attack of CoCrAlY was observed in testing with $Na_2SO_4$-$SO_3$ at 760°C (1400°F). As frequently encountered in service hardware, small but well developed nodules, some of them penetrating into the substrate, were observed in areas of otherwise negligible coating degradation.

At a temperature of 899°C (1650°F), general surface degradation was again observed, and there was a thick β-depleted zone ahead of the scale/metal interface. Nodular attack was superimposed on the general surface con-

sumption, but the morphology of the nodules and the extent of the β-depletion were markedly dissimilar to degradation microstructures developed in any of the turbine hardware from the Asiafreighter engine.

Testing at several temperatures (i.e. 649, 760, and 899°C) showed that $SO_3$ in the gas phase can result in substantially increased degradation over the entire temperature range of sulfate-induced hot corrosion. However, the features observed in a shipboard engine operated at low shaft horsepower were more closely reproduced at low (649 - 760°C) rather than high (899°C) temperatures. While not offering conclusive proof, such observations support the hypothesis that the service engine experienced degradation via a low temperature process involving the presence of condensed deposits of $Na_2SO_4$ and $SO_3$ in the combustion gases.

## SECTION III

## SUMMARY AND CONCLUDING REMARKS

The approach to this program involved work in the following areas: 1) examination of service hardware, 2) hot corrosion testing with sulfate-chloride salt deposits, and 3) hot corrosion testing with $SO_3$ gas in the furnace atmosphere. Conclusions drawn from each phase of the investigation and the correlation of service experience with results of the various types of laboratory tests were as follows:

1) Service-Induced Degradation in the Marine Environment

A significant extent of hot corrosion attack was observed in a marine gas turbine operating at low shaft horsepower. The microstructural features of the coating and substrate, both in heavily corroded and in virtually unaffected areas, were consistent with the relatively low metal temperatures expected from the operating history of the engine, suggesting that most of the observed degradation had indeed occurred at temperatures of less than 800°C. This inference was strongly supported by subsequent experimentation in which the microstructure and element distribution of the attack front were reproduced in laboratory furnace tests in the temperature range of 649-760°C.

2) Effect of NaCl on $Na_2SO_4$ - Induced Hot Corrosion

It was shown that CoCrAlY-type alloys are highly susceptible to degradation by chloride-containing deposits; the mechanism of attack involves dealloying of aluminum by the sulfate-chloride melt. Platinum overlayers on CoCrAlY significantly extend the coating lifetime against this type of attack, especially at low temperatures where dissolution of the single phase platinum aluminide overlayer is slow. Alloying of CoCrAlY with titanium also improves resistance to chlorides, although the effect is not as dramatic as that of the platinum overlayer.

Ni-base diffusion aluminide coatings are more resistant than CoCrAlY to chloride-containing salt deposits, although degradation again occurs by a type of dealloying mechanism and coating lifetime is less than expected in equivalent testing with deposits of 100% $Na_2SO_4$.

In spite of the potency of chlorides in degrading CoCrAlY, comparison of microstructures from sulfate-chloride hot corrosion tests with those of service degradation indicate that chloride-induced dealloying is not a significant mechanism involved in hot corrosion of shipboard engines. The microstructure and element distribution of the attack front developed in the sulfate-chloride hot corrosion tests was fundamentally different from that observed in engine hardware. In addition, service experience being accumulated during the course of this work was showing that platinum overlayers on CoCrAlY were ineffective, in spite of their demonstrated resistance to chloride-induced attack.

3) Hot Corrosion Induced by $Na_2SO_4$ Deposits and $SO_3$ Gas

As shown earlier by Navy work, microstructural features essentially the same as those of service degradation were produced in a 760°C test with a thick deposit of mixed sulfate salts (in which the $CoSO_4$ component served to lower the melting point and supply $SO_3$ via its decomposition). The microstructure and element distribution of the attack front in service hardware were also reproduced in a 649°C tube furnace test with $Na_2SO_4$ deposits and 0.04 atm $SO_3$ in the furnace atmosphere. Also in the $SO_3$ tube furnace experiments, pink crystals of $Na_2Co(SO_4)_2$, equivalent to those observed on Asiafreighter vanes, were developed on CoCrAlY specimens.

The similarity of degradation microstructures and the formation of Co-containing sulfates are strong evidence that marine hot corrosion is related to the presence of sulfate deposits on the turbine hardware and $SO_3$ in the combustion gas.

Several CoCrAlY and aluminide coatings were evaluated in a low temperature (649°C) test with 1 mg/cm$^2$ of $Na_2SO_4$ and 0.04 atm $SO_3$ pressure; all showed significant attack (but not coating penetration) in 100 hour exposure times. The degradation mechanism is believed to involve acid fluxing of alumina scales. Other factors which must be invoked to fully explain the microstructure developed in the propagation stage of hot corrosion attack are not well understood.

Although extreme caution must be used in drawing conclusions from a test in which the $SO_3$ pressure is much higher than that expected in the engine, the similar performance of coatings which exhibited strikingly different behavior in the sulfate-chloride tests strongly implies that chloride-resistant coatings will not necessarily be resistant to $SO_3$ effects. An understanding of chloride-induced hot corrosion is still essential to protect against the possibility of this type of attack, but a different approach to development of $SO_3$ resistant coatings will apparently be required.

The correlation of microstructures observed in degraded coatings from service and from laboratory simulation tests is not straightforward, and knowledgeable investigators may be capable of supporting different interpretations of the same or very similar observations. However, it is maintained that two very important points have been established beyond reasonable doubt by the work of this program and the referenced studies at other laboratories:

- The presence of NaCl in condensed deposits of $Na_2SO_4$ salt will cause more severe hot corrosion than the sulfate-induced attack which would occur in the absence of the chloride.

- Chloride effects, either alone or in combination with $Na_2SO_4$, are not the only cause of the more severe hot corrosion of turbine materials which is usually encountered in marine service.

While a synergistic effect of condensed or vaporous chloride phases cannot yet be ruled out, it appears well demonstrated that hot corrosion mechanisms related to the presence of $SO_3$ in combustion gases play a far more significant role than chlorides in the hot corrosion of shipboard engines.

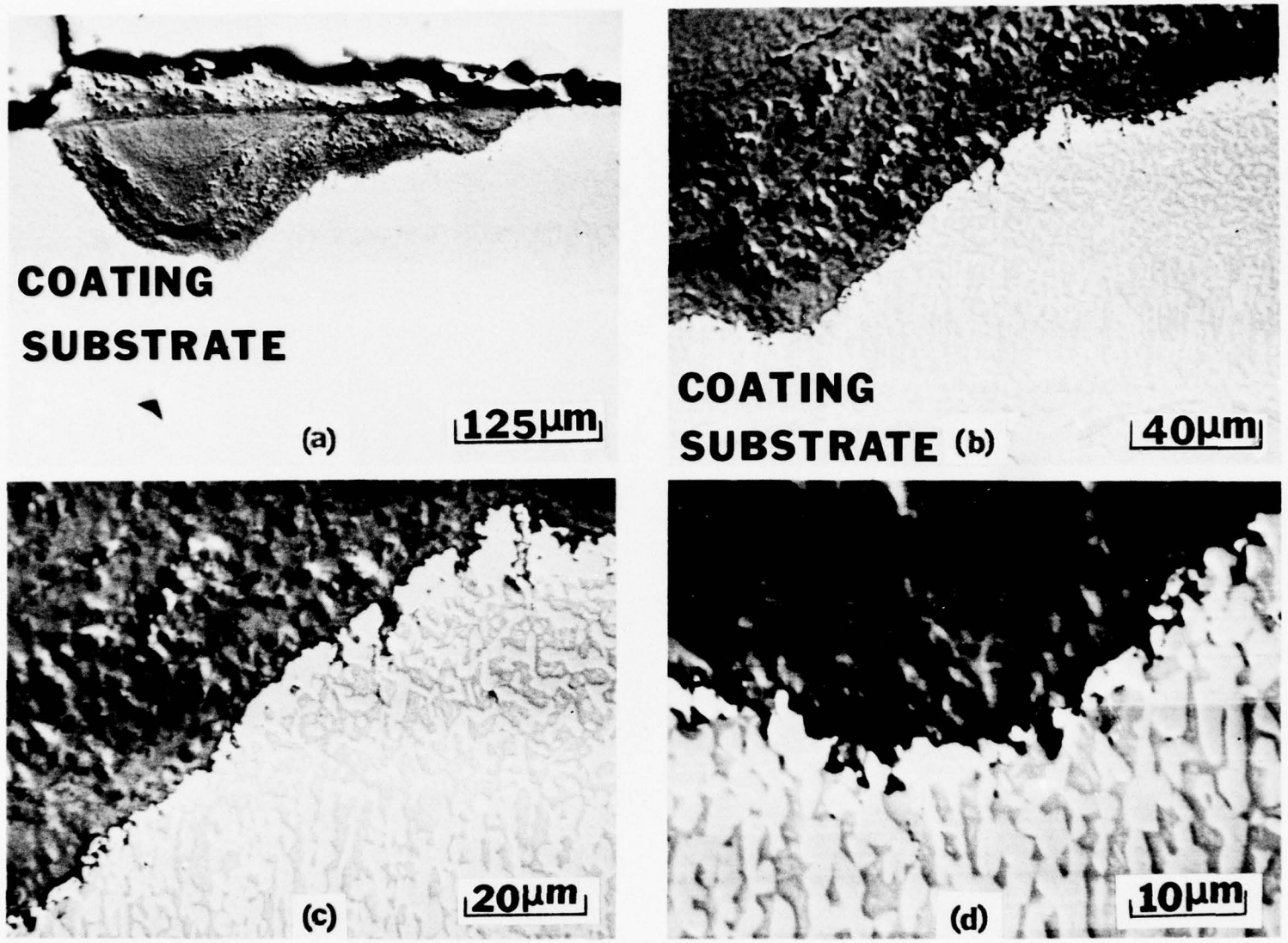


Figure 1. Typical coating protrusion in CoCrAlY-coated (IM 6250; 18-24%Cr, 11-13%Al, 0.1-0.5%Y) IN 792 first stage turbine blade operated 4801 hours in Asiafreighter engine.

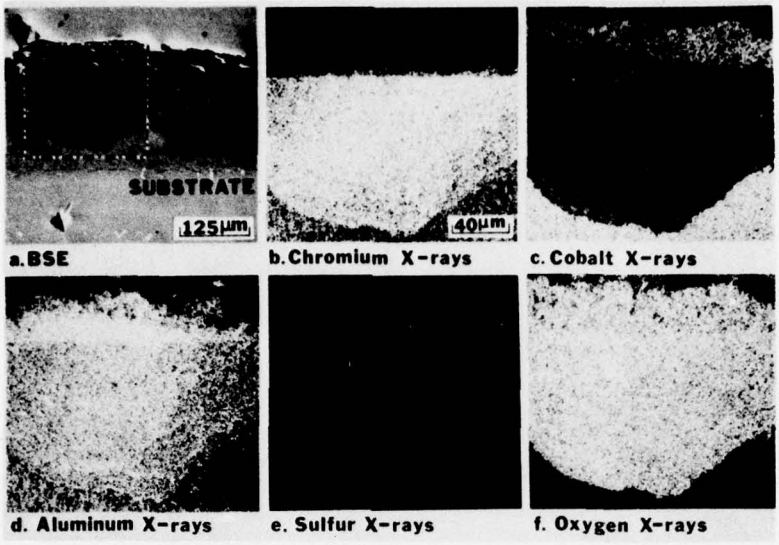


Figure 2. Low magnification X-ray images showing composition of oxides in coating protrusion and overlying mound. Box in (a) is area of X-ray scans.

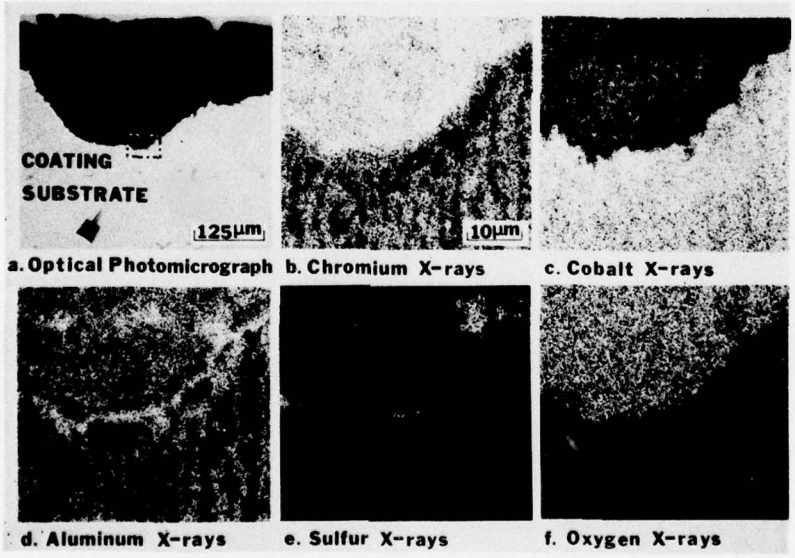


Figure 3. High magnification X-ray images showing element distribution in attack front at bottom of coating protrusion. Area of X-ray scans (box in 3a) is approximately that of Fig. 1d.

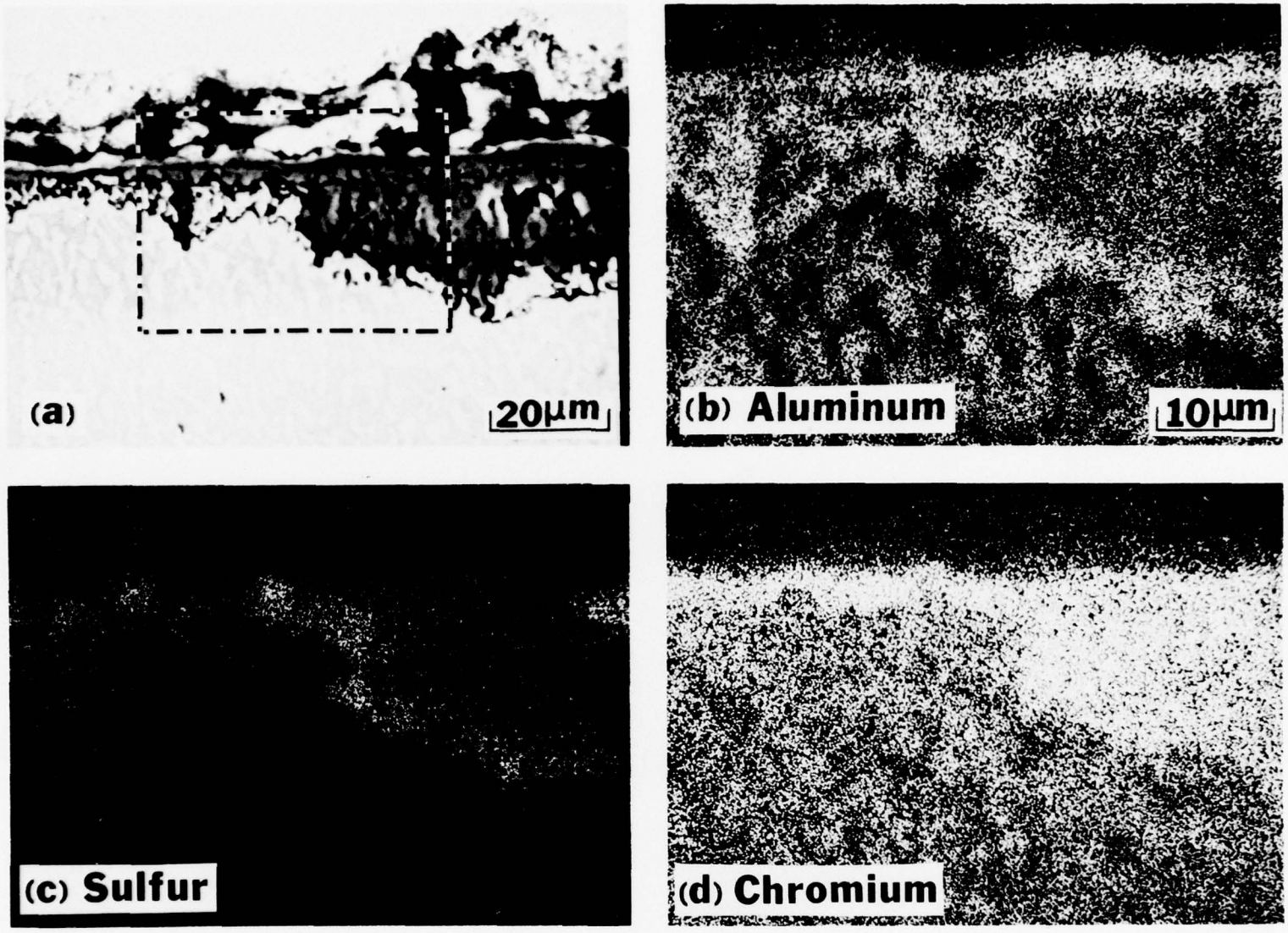


Figure 4. Surface degradation and shallow pitting characteristic of some areas of Asiafreighter blades.


(a)

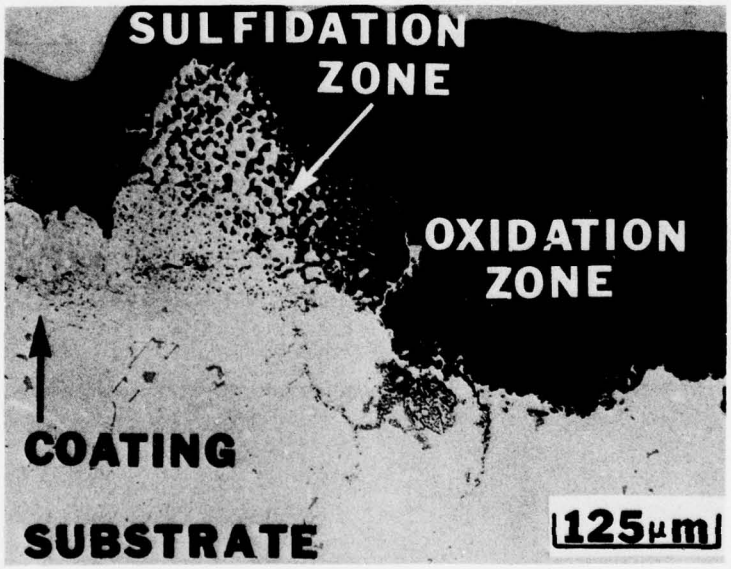


(b)

Figure 5. Additional photomicrographs showing typical microstructural features developed in engine operation of CoCrAlY-coated turbine blades: (a) oxidized leaders are sometimes associated with nodular attack, (b) cut-edge degradation may be observed at sites of coating penetration.

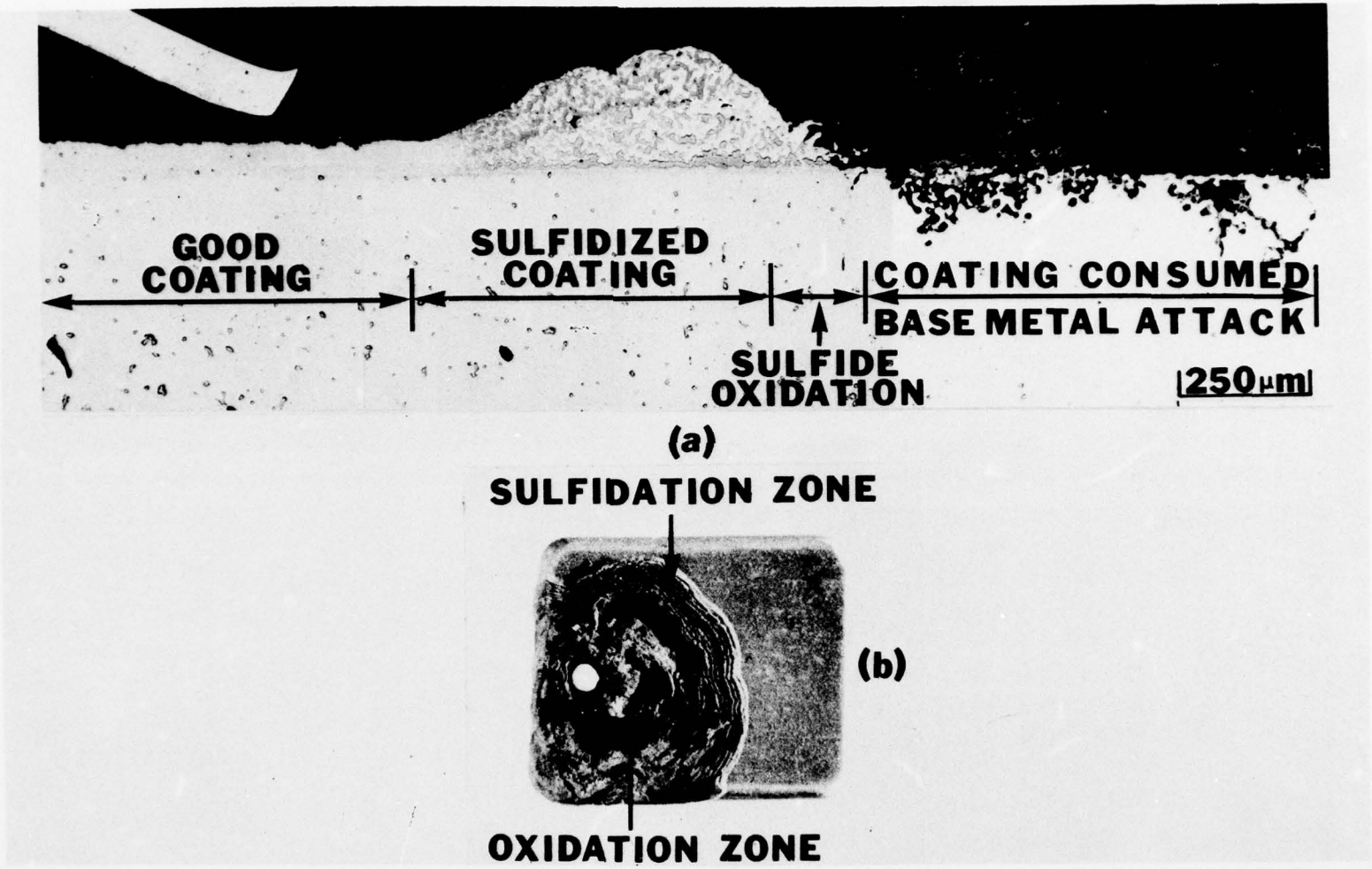


Figure 6. Cut-edge attack produced in furnace cyclic hot corrosion testing of diffusion aluminide coatings at 899°C: (a) microstructure of aluminized (PWA 73) IN 738 exposed 780 hours with $Na_2SO_4$, (b) macrograph of coupon of aluminized (LDC-2) MarM-200 exposed 380 hours with $Na_2SO_4$ + 2.5% $V_2O_5$.

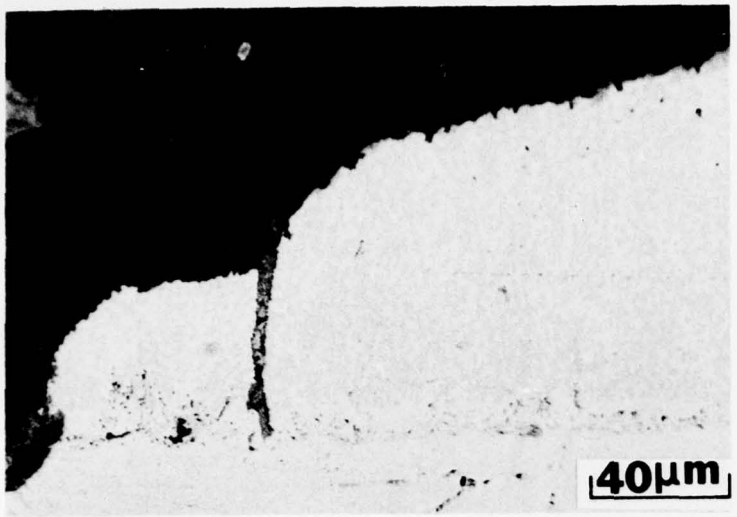


7a. Penetrated coating at leading edge


7b. Typical nodular attack and surface corrosion products near leading edge

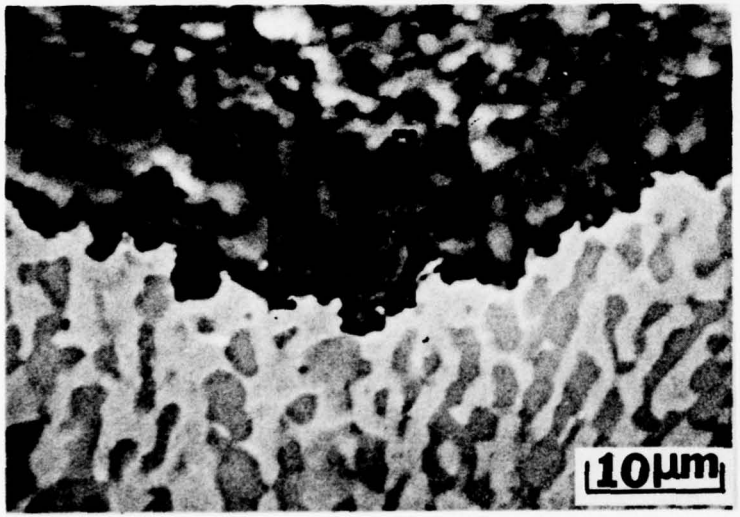


7c. Scale/metal interface; boxed area in 7b

Figure 7. Microstructure near failed leading edge of PWA 68-coated Mar-M509 first stage vane operated 2770 hours in Asiafreighter engine. Area of 7c is shown in X-ray images of Figure 8.

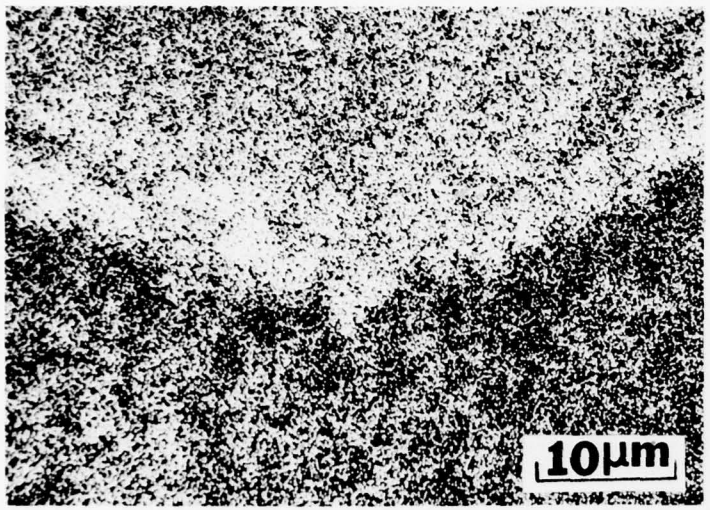


8a. Chromium

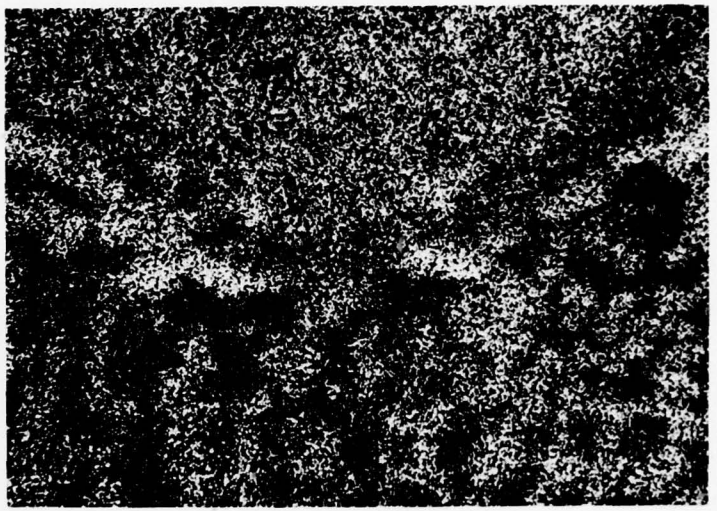

8b. Aluminum

8c. Sulfur

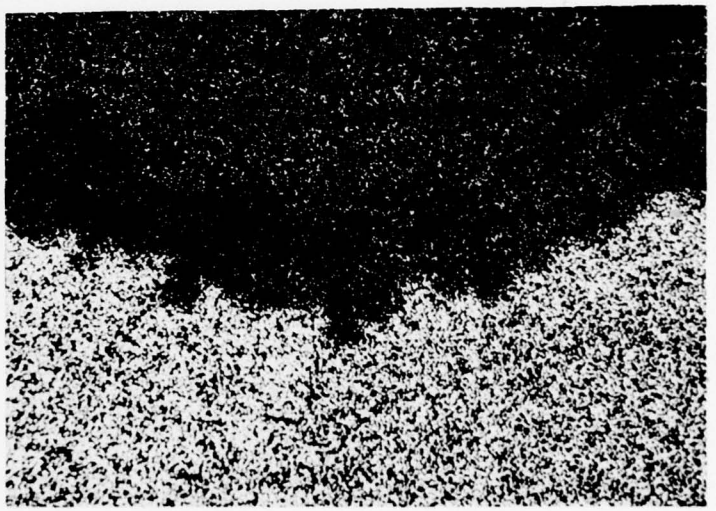

8d. Cobalt

Figure 8. Distribution of metallic elements and sulfur at bottom of coating protrusion in Asiafreighter vane. Sample was prepared by dry cutting and polishing with kerosene lubricant.

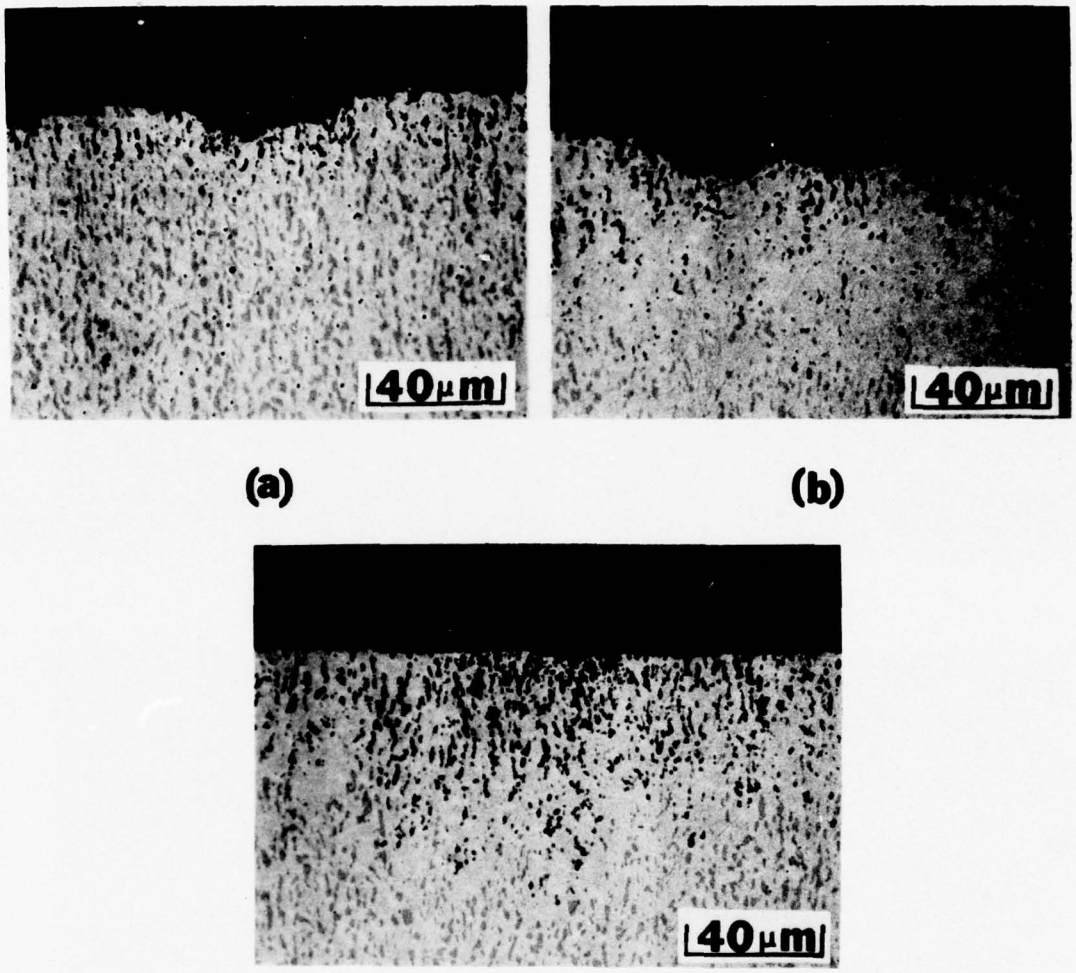


Figure 9. Surface microstructure of Co-25Cr-6Al-0.5Y after cyclic hot corrosion testing for 500 hours at 649°C (1200°F). Salt deposits were (a) 100% $Na_2SO_4$, (b) $Na_2SO_4$ - 1% NaCl, and (c) $Na_2SO_4$ - 10% NaCl.

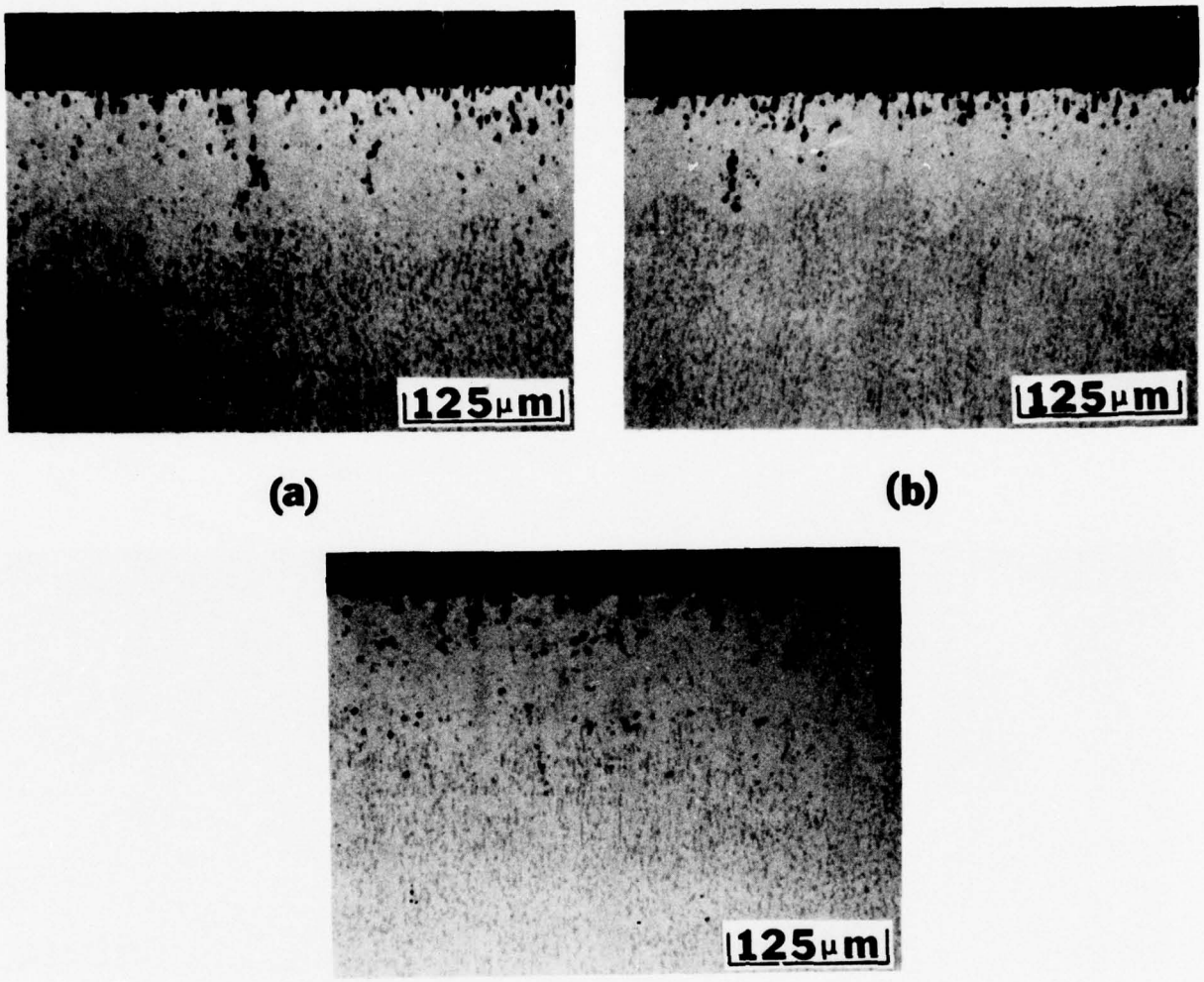


Figure 10. Surface microstructure of Co-25Cr-6Al-0.5Y after cyclic hot corrosion testing for 500 hours at 899°C (1650°F). Material, test conditions, and salt deposits are the same as those of Fig. 9 except for the higher temperature.

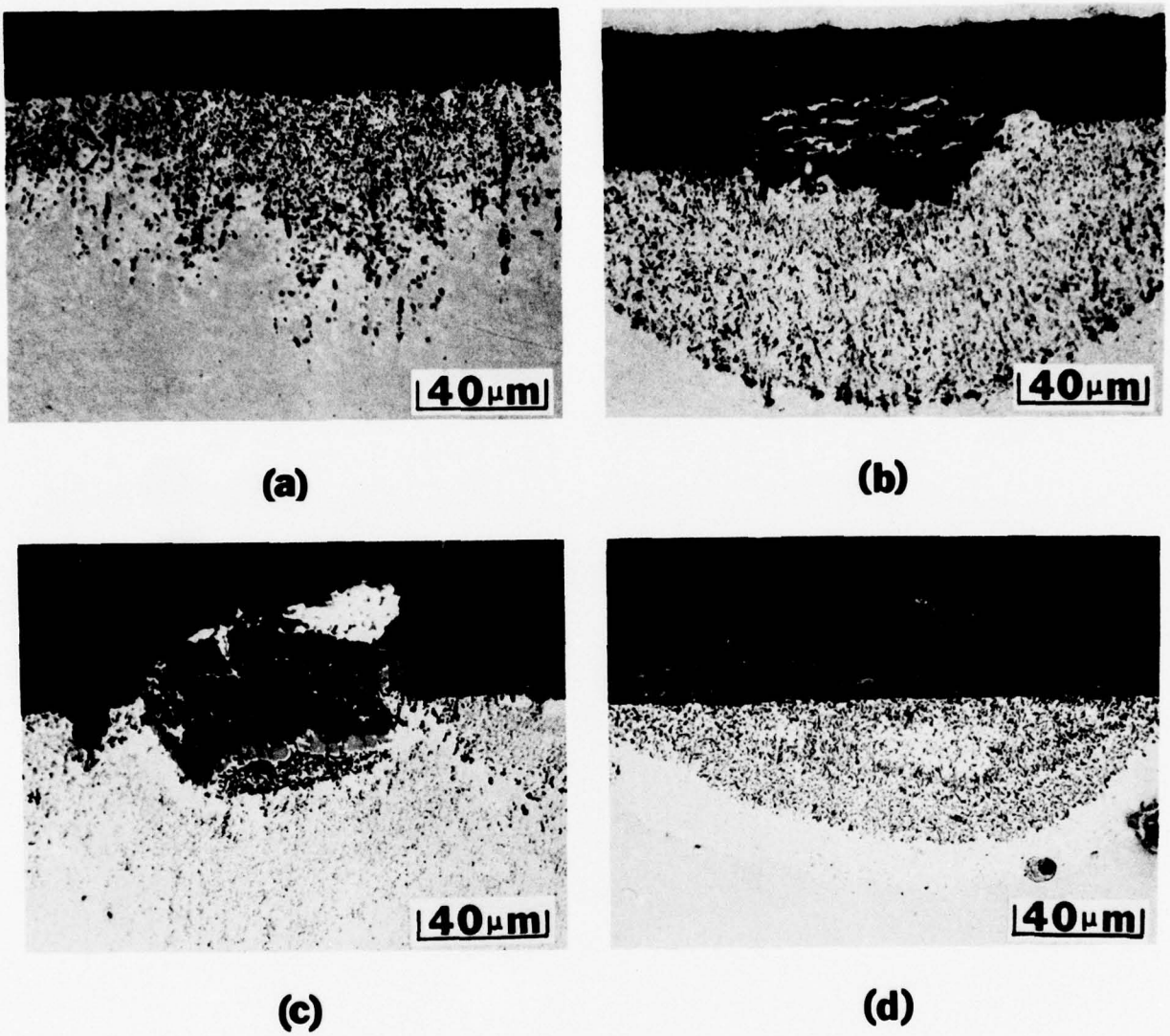


Figure 11. Degradation of state-of-the-art CoCrAlY (PWA 68), NiCrAlY (PWA 267), and NiCoCrAlY (PWA 270) coatings (a, b, and c respectively) and an experimental high-chromium CoCrAlY alloy after cyclic hot corrosion testing for 500 hours at 649°C (1200°F) with $Na_2SO_4$ - 10% NaCl.

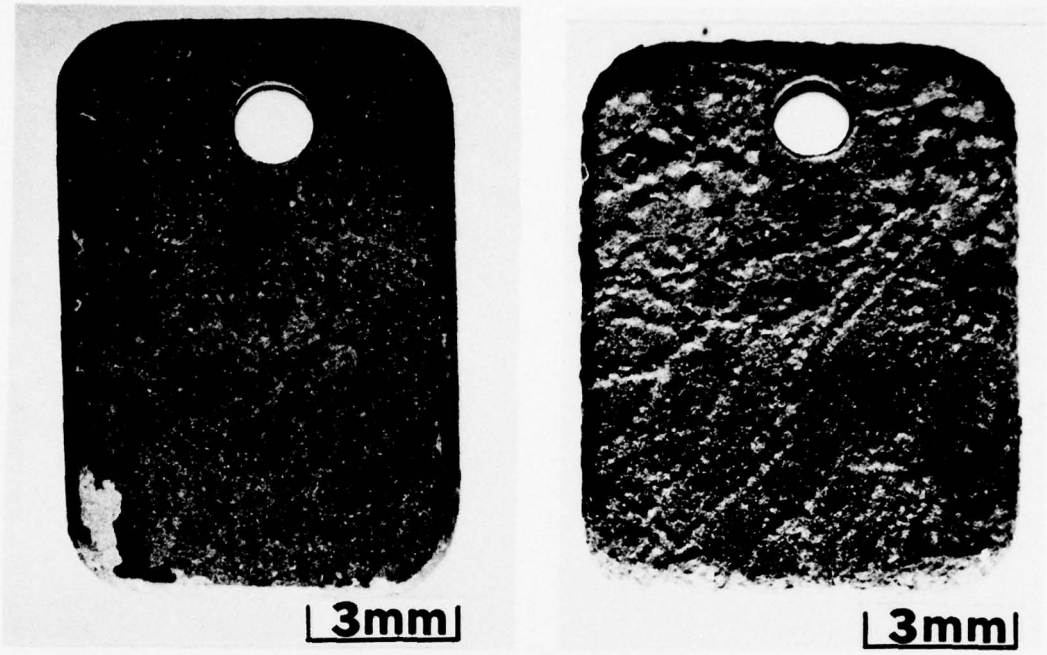


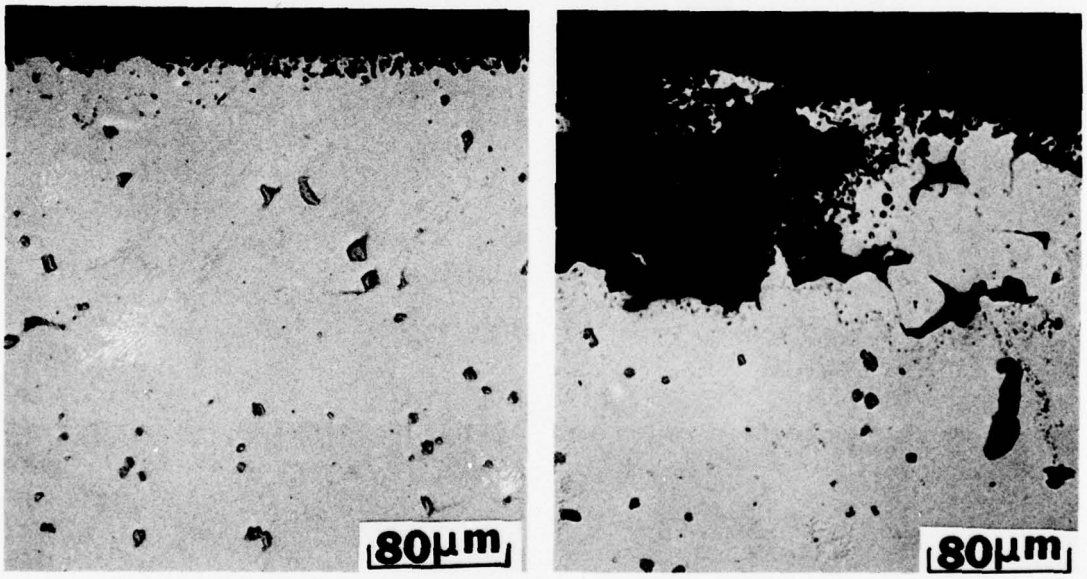


with NaCl vapor

without NaCl

Figure 12. Surface condition and corresponding microstructures of uncoated IN 738 (Ni-16Cr-8.5Co-3.4Ti-3.4Al-1.75Mo-2.6W-1.75Ta-0.12Zr-0.85Nb-0.012B after 300 hour hot corrosion test at 899°C (1650°F). Specimens were washed and recoated with 1 mg/cm$^2$ of $Na_2SO_4$ every 20 hours. The specimen heated in air containing about 300 ppm NaCl vapor was less attacked than that exposed in chloride-free air.

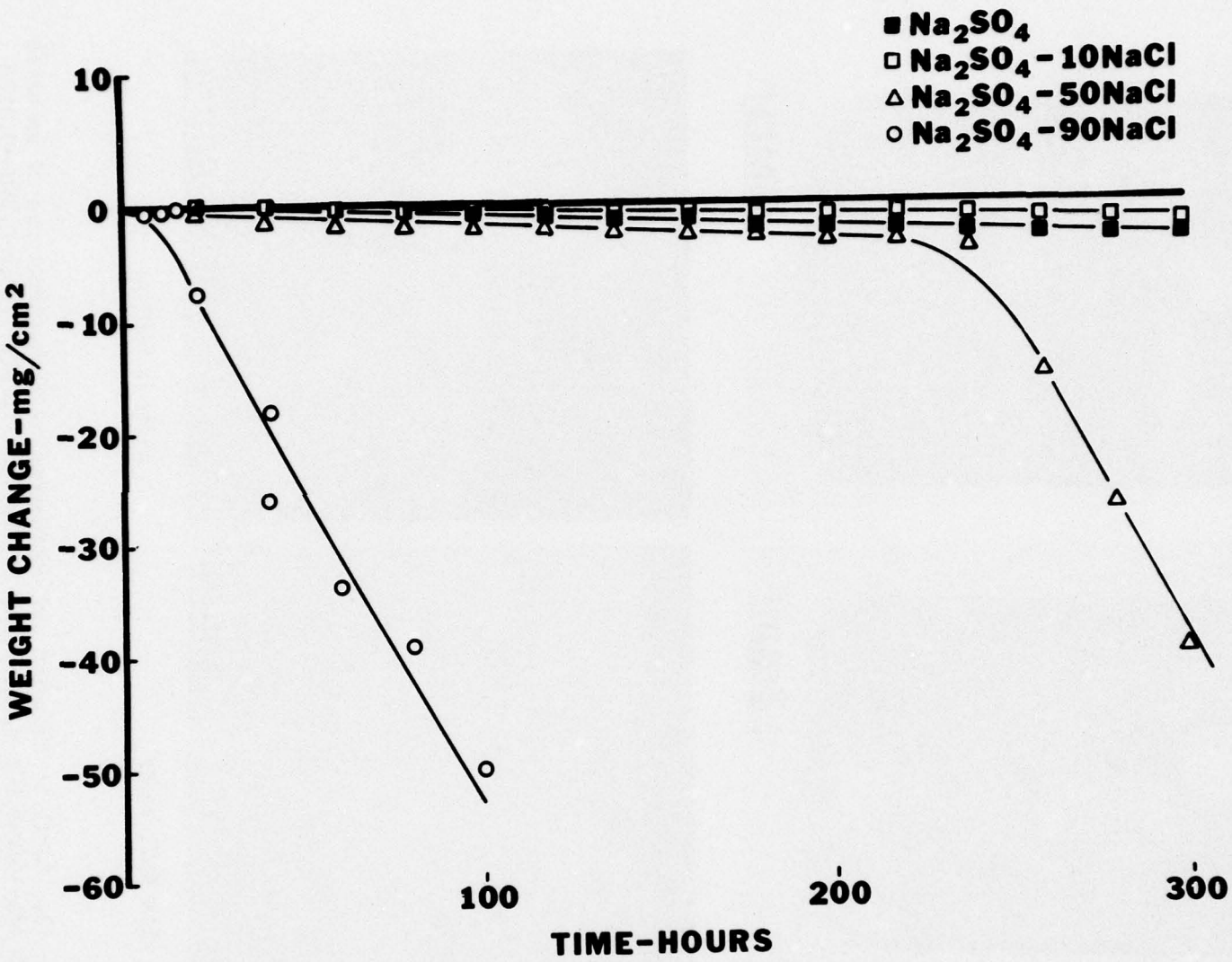


Figure 13. Weight change vs. time data for 899°C (1650°F) cyclic hot corrosion of Co-25Cr-6Al-0.5Y with deposits of sulfate and sulfate-chloride salts. Data show increasing severity of attack (as indicated by decreasing time to start of large weight losses) with increasing chloride content of the deposit.

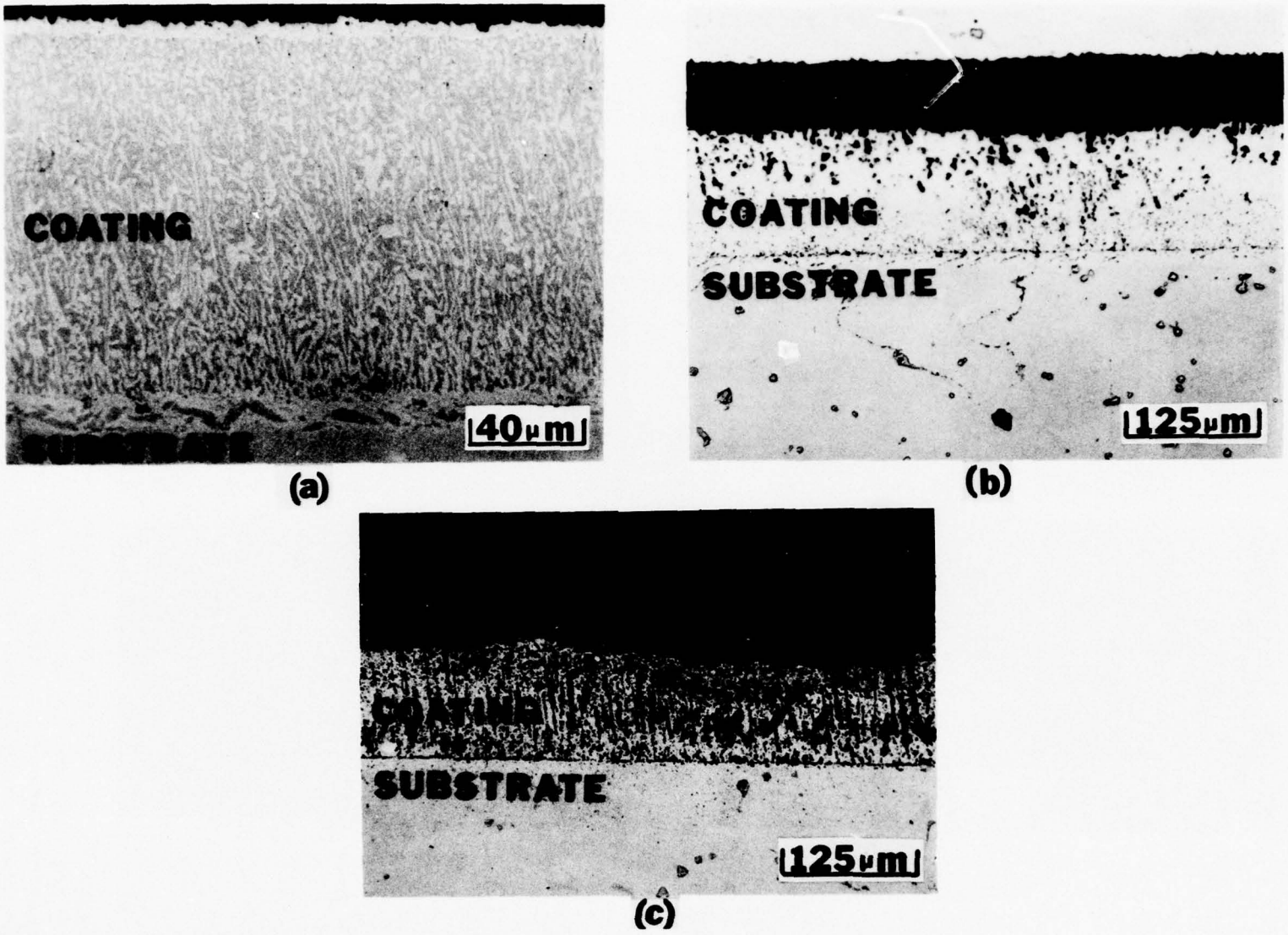


Figure 14. Effect of chloride-containing deposits on degradation of CoCrAlY-coated IN 738 in 899°C cyclic hot corrosion test: (a) 500 hours with $Na_2SO_4$, (b) 500 hours with $Na_2SO_4$ - 5%NaCl, (c) 40 hours with $Na_2SO_4$ - 90% NaCl.

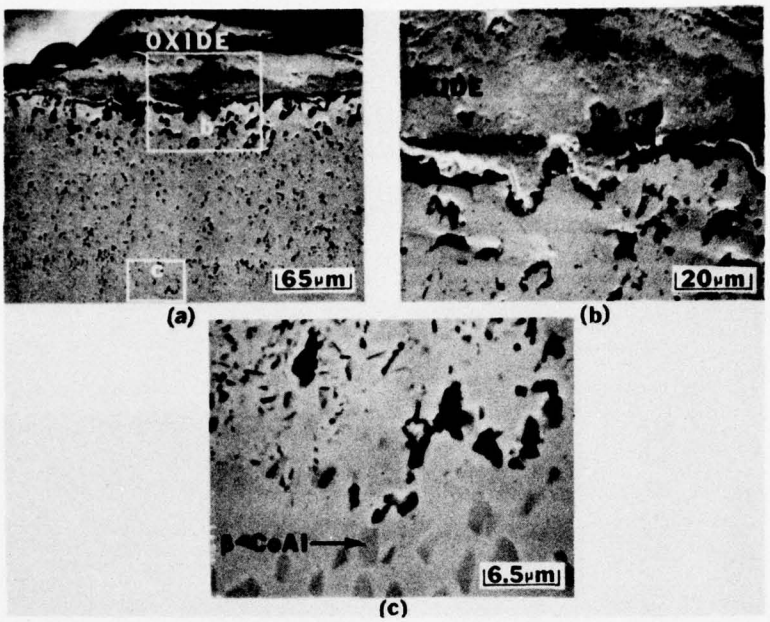


Figure 15. Cross sections through Co-25Cr-6Al-0.5Y after 100 hours in 899°C cyclic hot corrosion test with $Na_2SO_4$ - 90% NaCl. Boxes in (a) are areas of X-ray images in Figure 16.

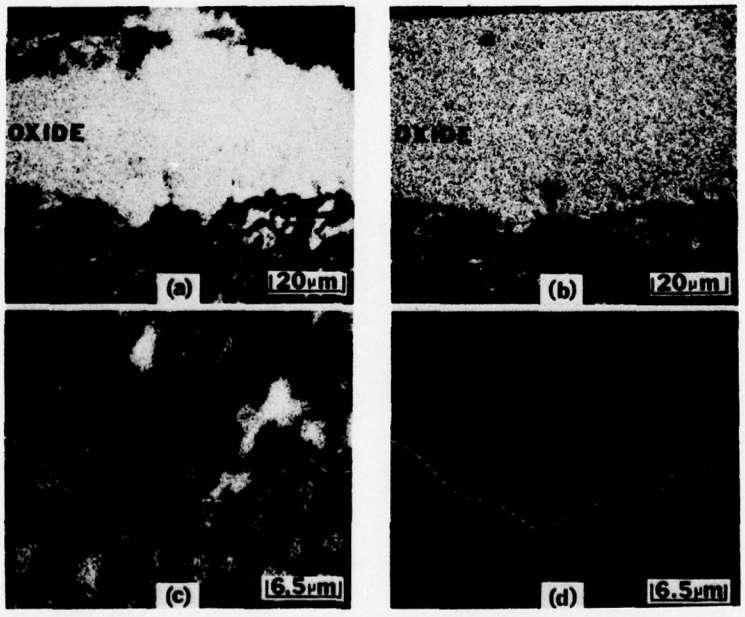


Figure 16. X-ray images of the specimen illustrated in Fig. 15; (a) and (c) are aluminum, (b) and (d) are oxygen. Dashed line in (c) and (d) is interface between innermost zone of internal attack and unaffected alloy. Al-rich areas in top half of (c) are believed to be Cl-containing pores.

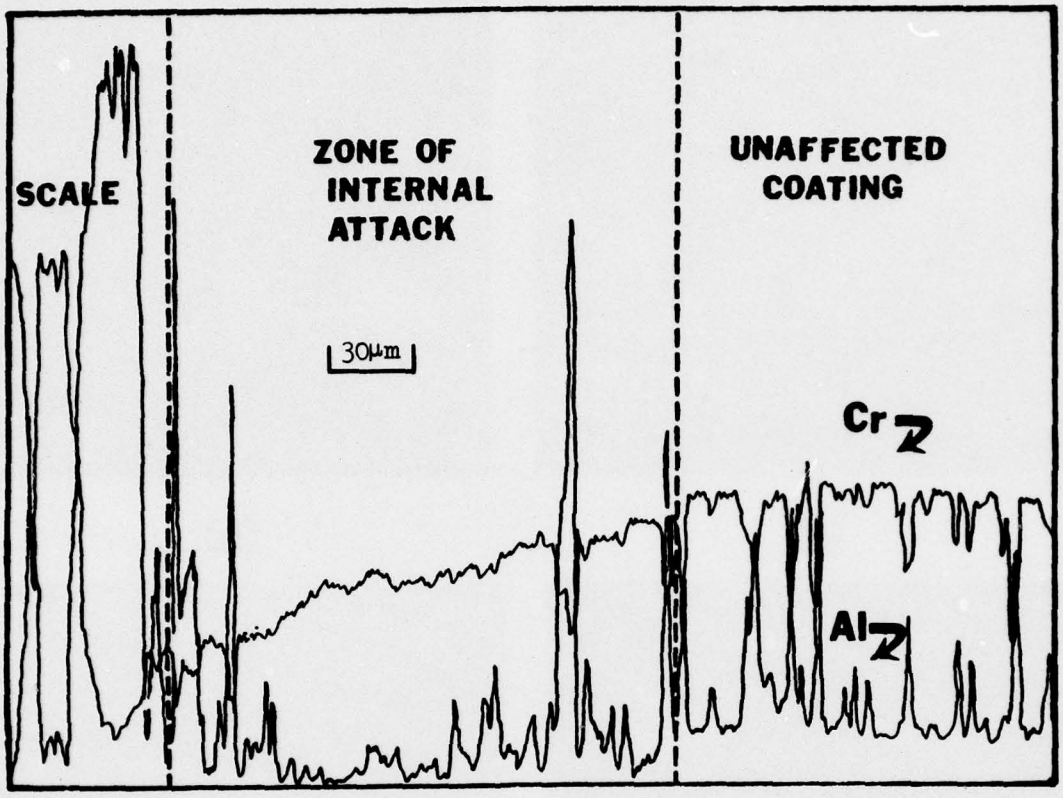


Figure 17. Semiquantitative line scans for Cr and Al in the specimen of Figs. 15 and 16. Peaks and valleys in unaffected material reflect different Cr and Al content of the $\alpha$-Co and $\beta$-CoAl phases but a uniform average composition. Zone of internal attack includes Al-rich phases, but Cr content decreases smoothly across the zone.

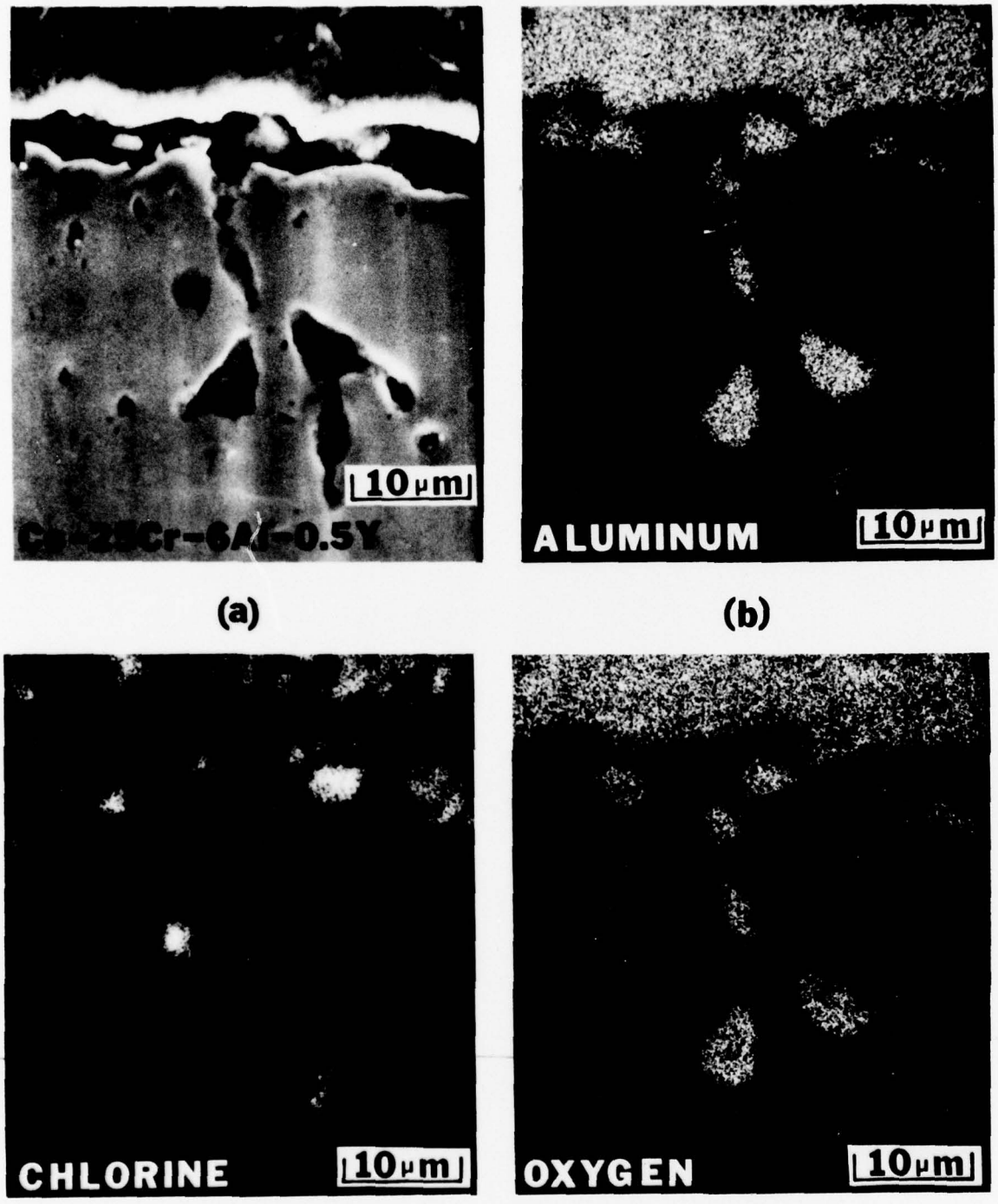


Figure 18. Back scattered electron (a) and X-ray images of CoCrAlY specimen exposed 20 hours at 899°C in crucible hot corrosion test with $Na_2SO_4$ - 90% NaCl salt. Note cavities filled with nonmetallic reaction product containing Al, Cl, and O.

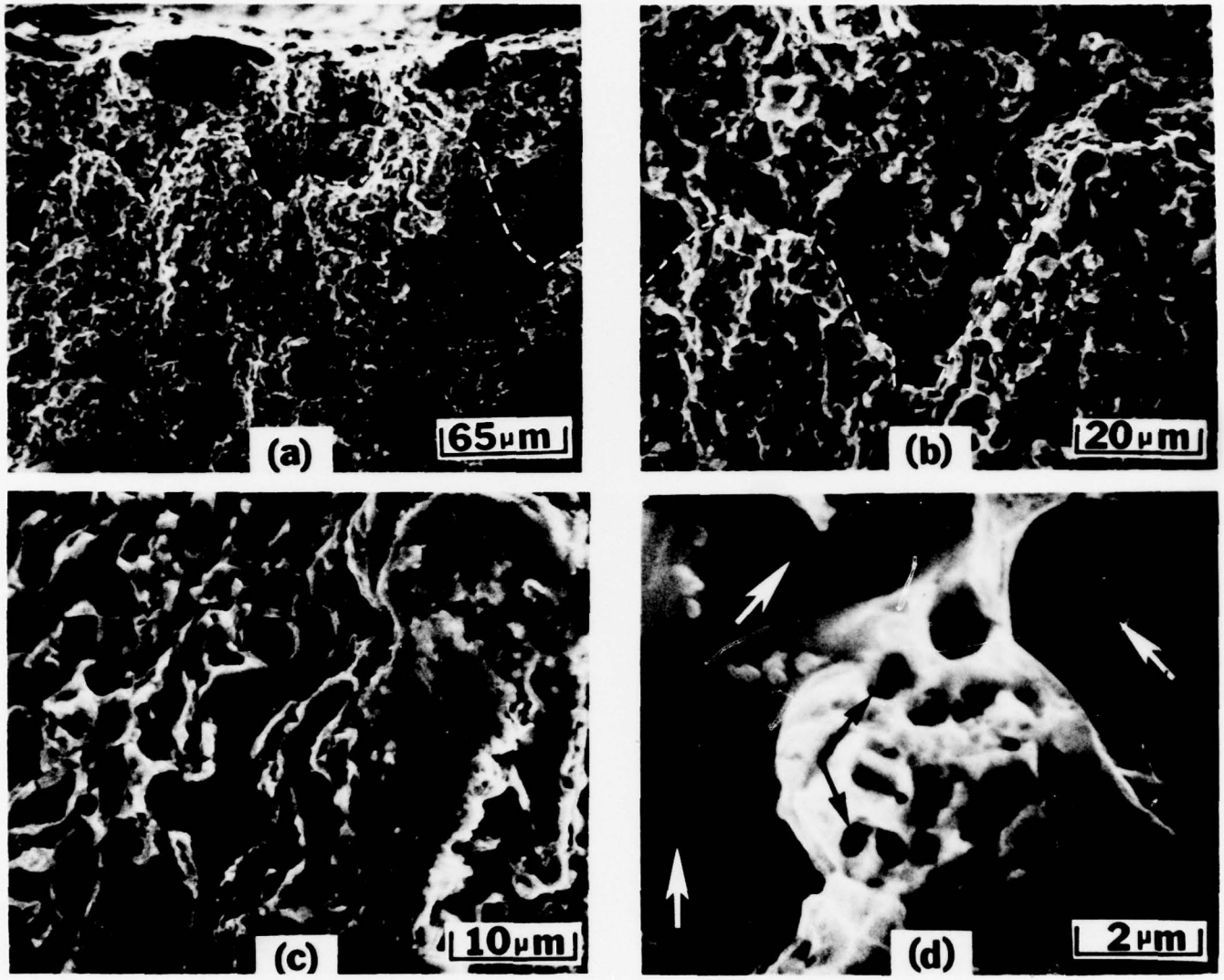


Figure 19. Scanning micrographs of fractured Co-25Cr-6Al-0.5Y specimen exposed 20 hours to cyclic hot corrosion at 899°C. Dashed lines in (a) and (b) mark extent of porous zone of internal attack. The pores appear to form a continuous network (c) which includes both large and very small pores (arrows in d).

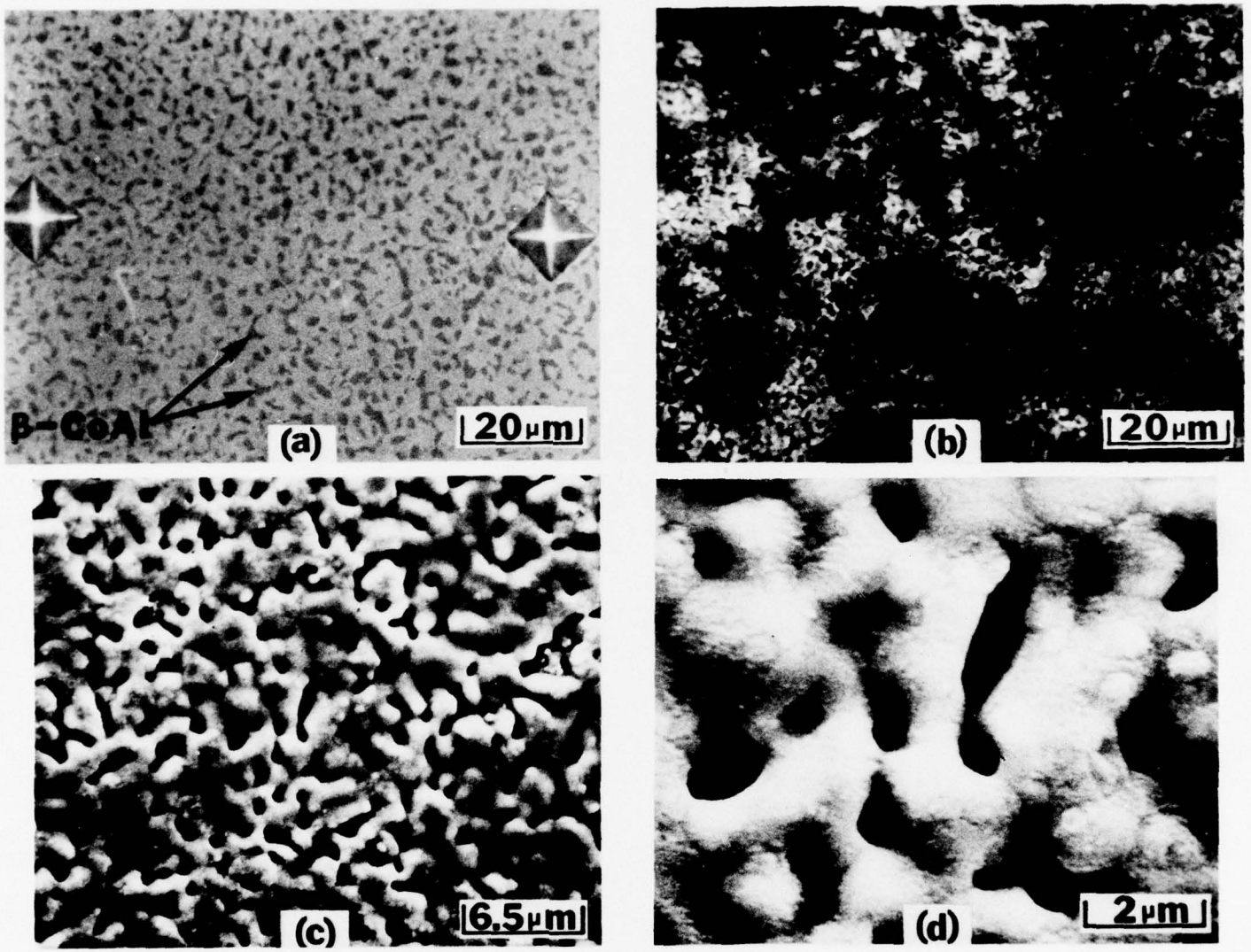


Figure 20. Pre-test polished surface and features developed in 10 minute exposure to $Na_2SO_4$ - 90%NaCl at 899°C. Numerous pores are evident, the size and distribution of which are similar but not identical to the distribution of the β-CoAl phase in the pre-test microstructure.

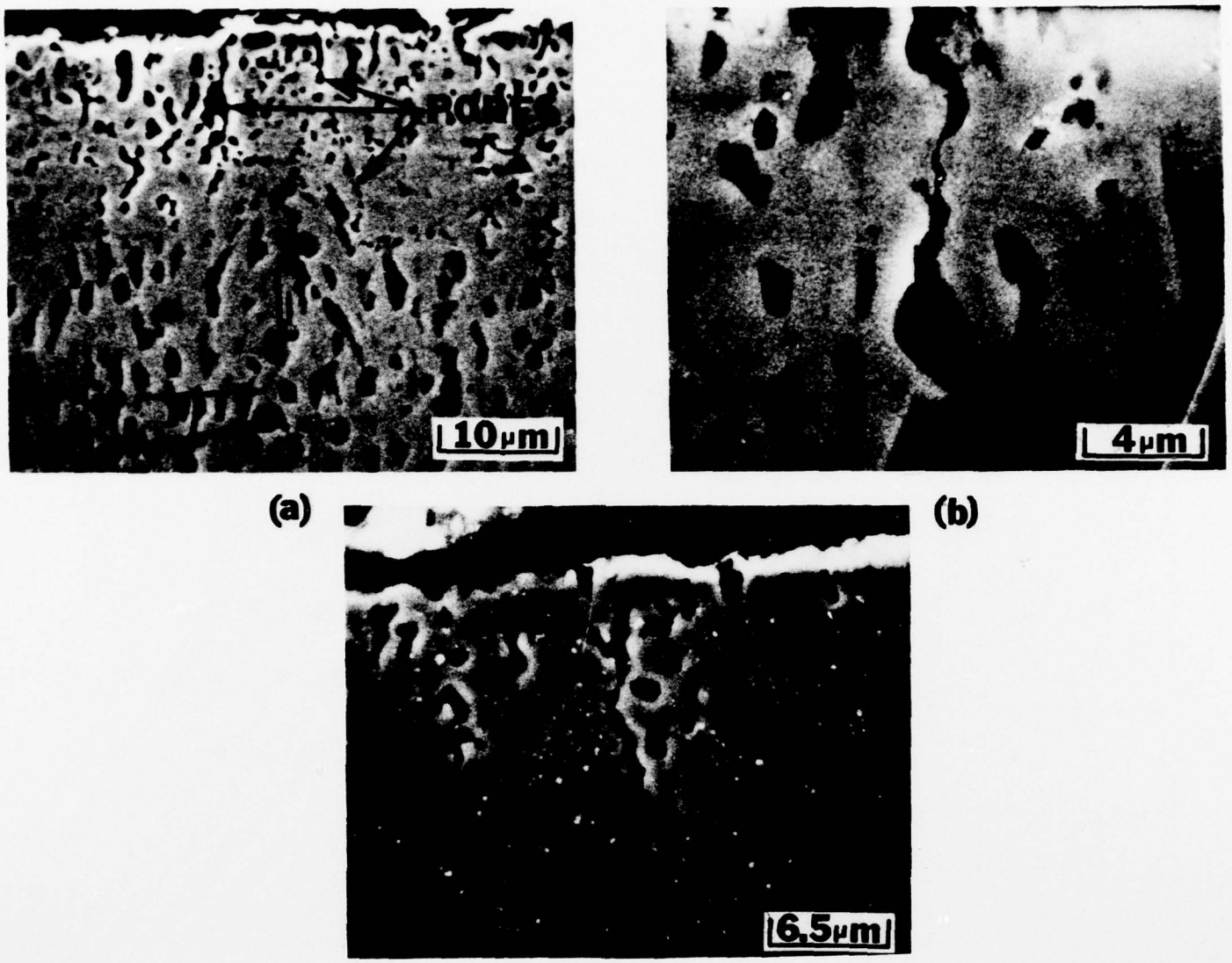


Figure 21. Scanning electron micrographs of polished section through specimen of Fig. 20. Note that large pores are similar but not identical in shape and distribution to those of the β-CoAl phase in the unaffected microstructure.

(a) $(Na_2SO_4, NaCl)_{liq} + (Al,Cr)_{alloy} \rightarrow Al_2O_3 + Cr_2O_3 + (Na_2SO_4, \textcircled{Na_2S}\ \textcircled{NaCl})_{liq}$

(b) $(Na_2SO_4, Na_2S, NaCl)_{liq} + (Cr)_{alloy} \rightarrow CrS - (Na_2SO_4, Na_2S, \textcircled{NaCl})_{liq}$

(c) $(2\,NaCl)_{liq} + Al_2O_3 + \frac{1}{2}\,O_2 \rightarrow 2NaAlO_2 + (Cl_2)_{gas}$

(d) $\frac{1}{2}Cl_2 + (Al)_{alloy} \rightarrow (AlCl)_{gas}$

(e) $2\,AlCl + \frac{3}{2}O_2 \rightarrow Al_2O_3 + Cl_2$

Figure 22. Sequence of reactions possibly involved in attack of CoCrAlY coatings by sulfate-chloride salts. Circles designate components of the liquid deposit which become capable of subsequent reaction as the melt becomes depleted in oxygen and sulfur by formation of $Al_2O_3$, $Cr_2O_3$, and CrS. The process is partially self-sustaining due to recycling of $Cl_2$ in reaction (e) but eventually stops because some of the $Cl_2$ is lost to the environment in each cycle.

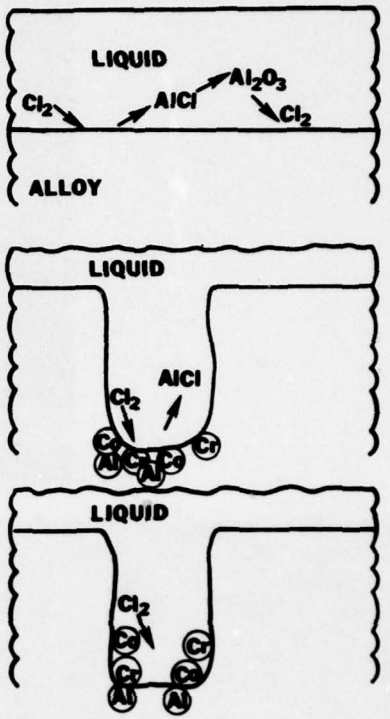


Figure 23. Schematic diagrams showing development of a pore in a CoCrAl alloy due to formation of aluminum chloride and surface diffusion of cobalt and chromium.

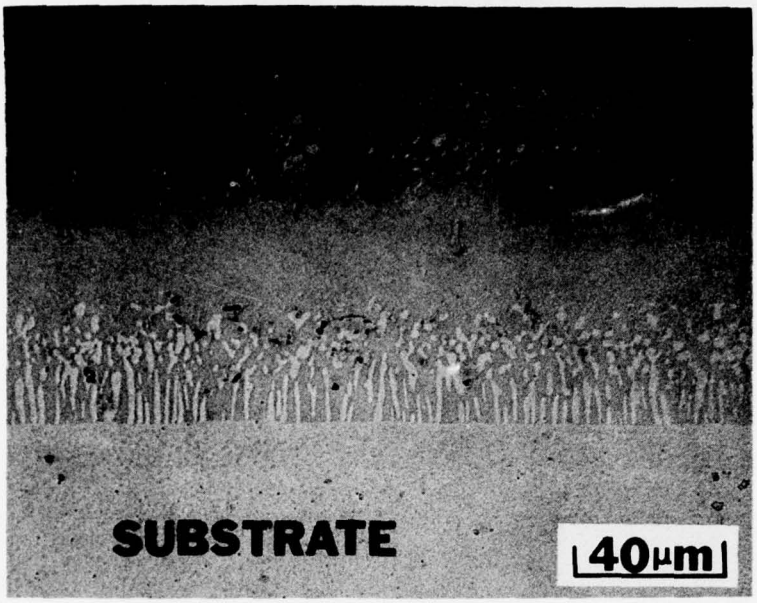


Figure 24. Pre-test microstructure of PWA 273 diffusion aluminide coating on IN 738 substrate.

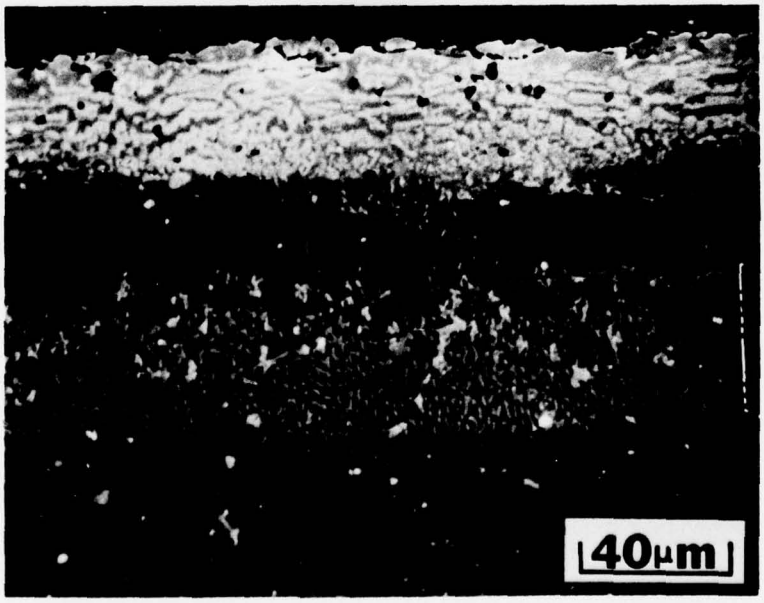


Figure 25. Scanning electron micrograph (secondary electrons) of LDC-2A coating. Note layered structure similar to PWA 273 but with Pt-rich phases in the outer layer.

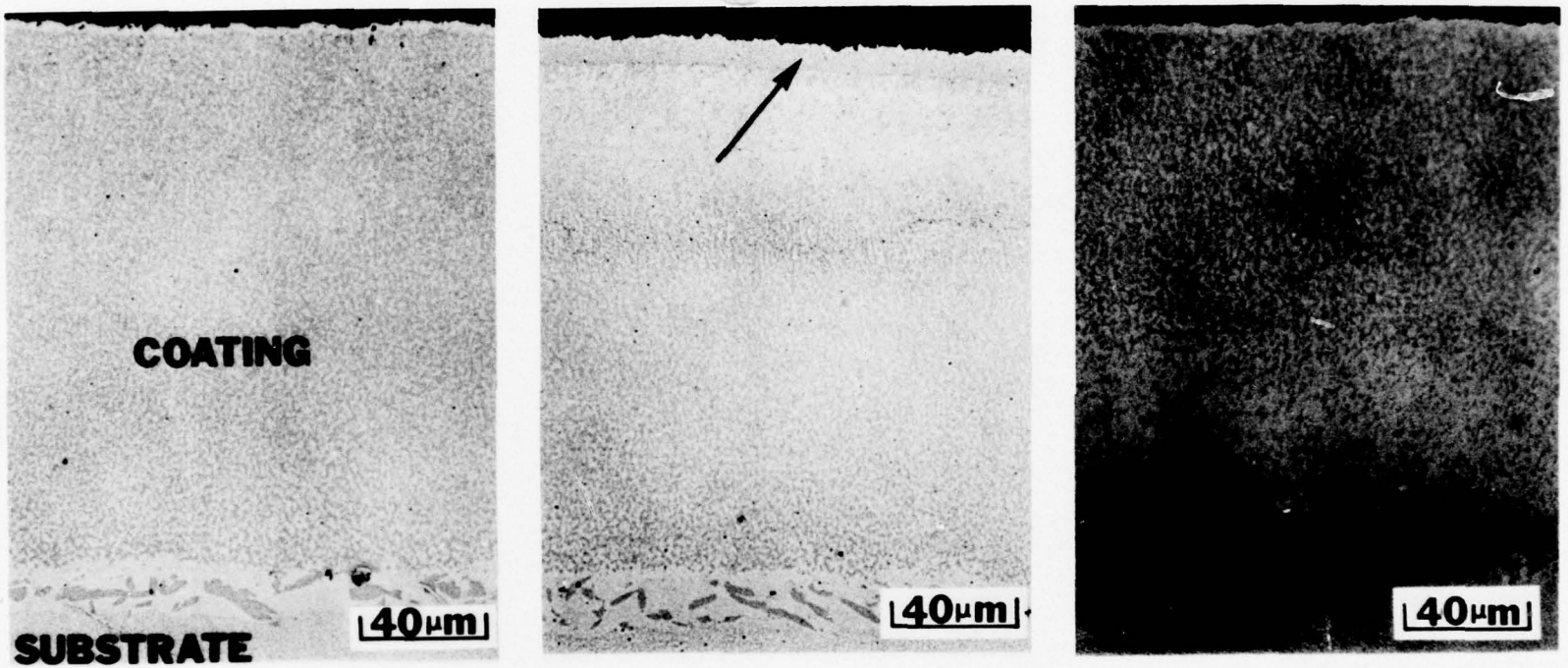


26a. PWA 68 CoCrAlY

26b. PWA 68 + Pt overlayer

26c. Pt underlayer + PWA 68

Figure 26. Pre-test microstructure of PWA 68 and platinum-modified CoCrAlY coatings. Arrows in b and c mark platinum aluminide overlayer and underlayer respectively.

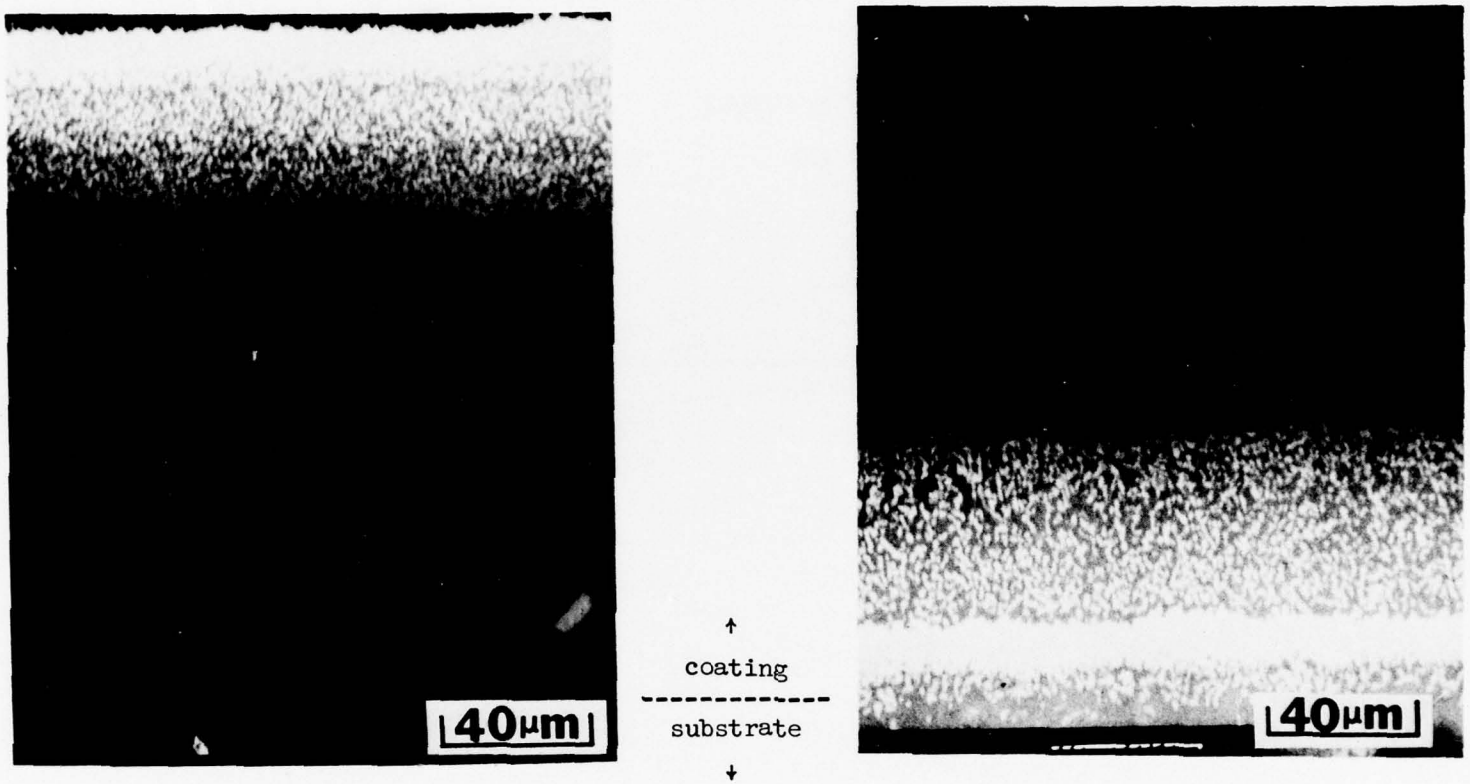


Figure 27. Back scattered electron images of platinum-modified CoCrAlY coatings shown in Figs. 26b and 26c. Overlayer and underlayer and extent of platinum-containing diffusion zones are defined by atomic number contrast which renders Pt-rich phases very bright due to high back scattering power of heavy elements.

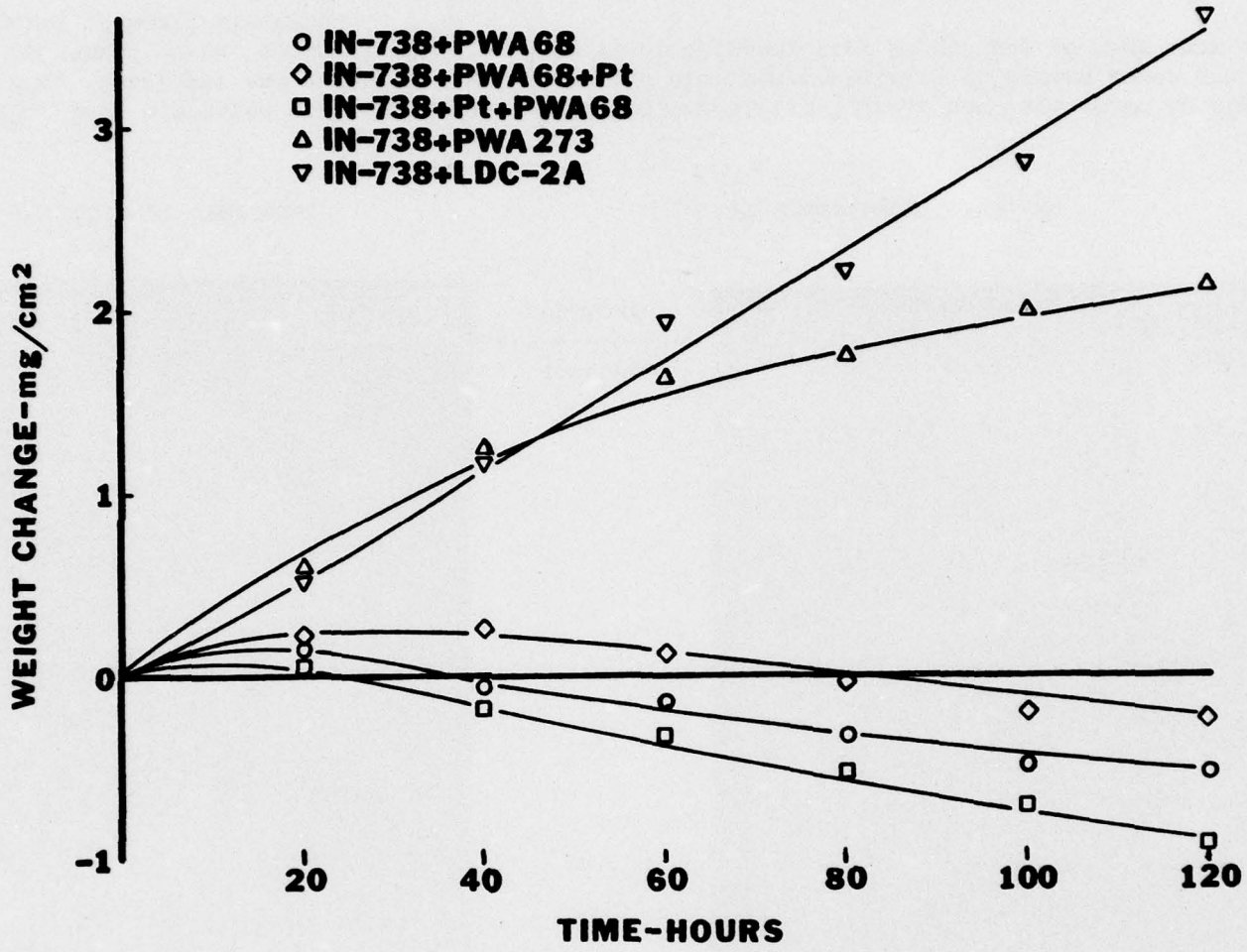


Figure 28. Weight change vs. time data for state-of-the-art coatings exposed in the cyclic hot corrosion test (1 hour cycles, washed and recoated with 1 mg/cm$^2$ of $Na_2SO_4$ - 50% NaCl every 20 hours) at 899°C (1650°F).

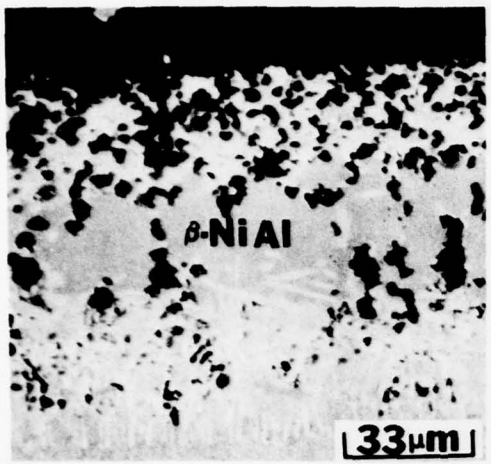


29a. Back scattered electrons

29b. Aluminum X-rays

29c. Chromium X-rays

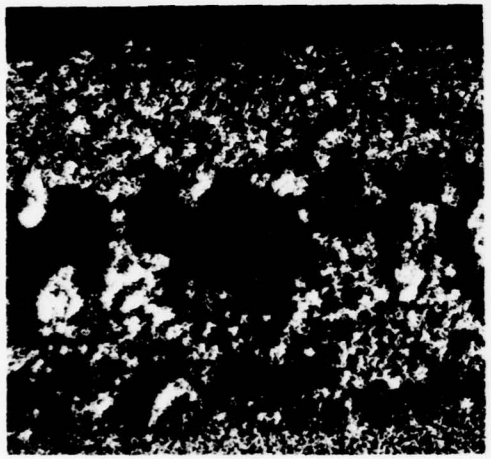

29d. Titanium X-rays

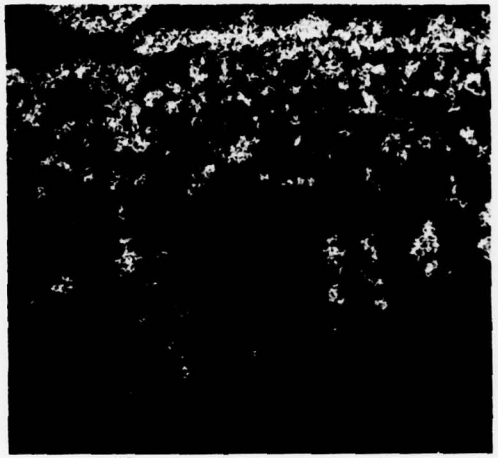

29e. ~~Chromium~~ Oxygen X-rays

29f. Sulfur X-rays

Figure 29. Typical microstructure of PWA 273 coating after 500 hours cyclic hot corrosion testing at 899°C. Note retention of substantial amounts of β-NiAl phase, as shown in BSE and Al X-ray images.

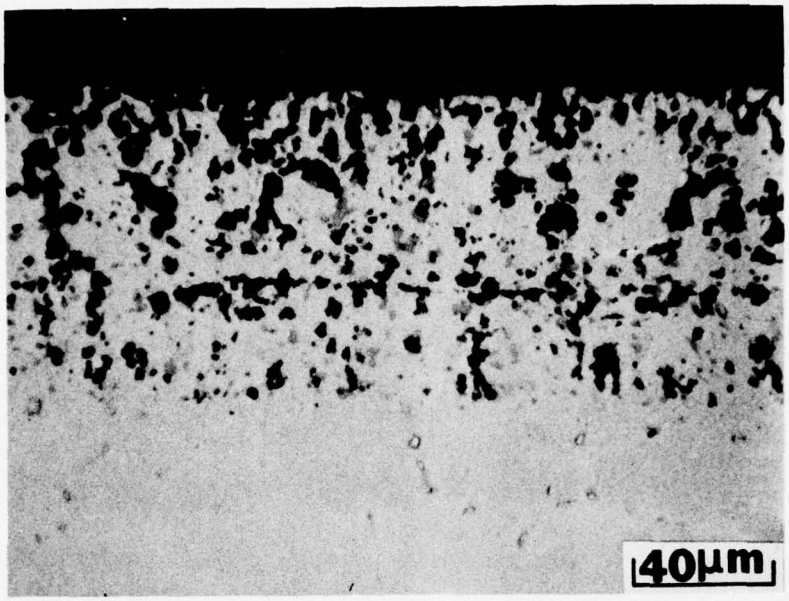


30a. Typical extent of dealloying and sulfide precipitation

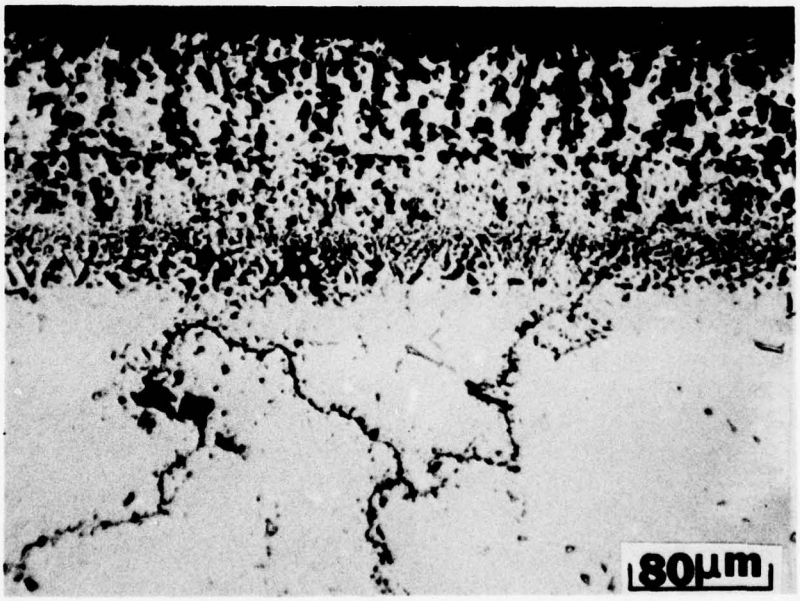


30b. Coating failure and substrate attack

Figure 30. Microstructure of LDC-2A platinum modified diffusion aluminide coating after 500 hours in the 899°C (1650°F) cyclic hot corrosion test with $Na_2SO_4$ - 50% NaCl. Note different magnification of 30a and 30b.

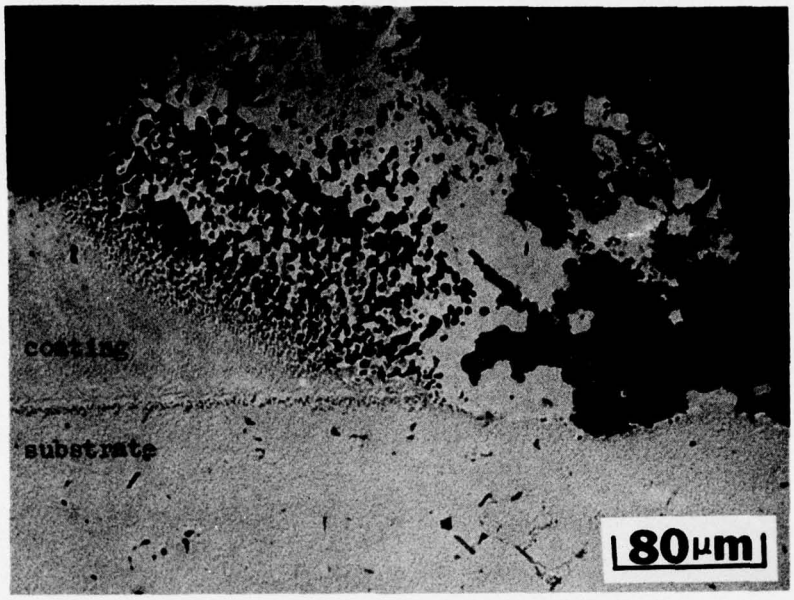


Figure 31a. Sidewise consumption of PWA 68 emanating from massive edge failure.

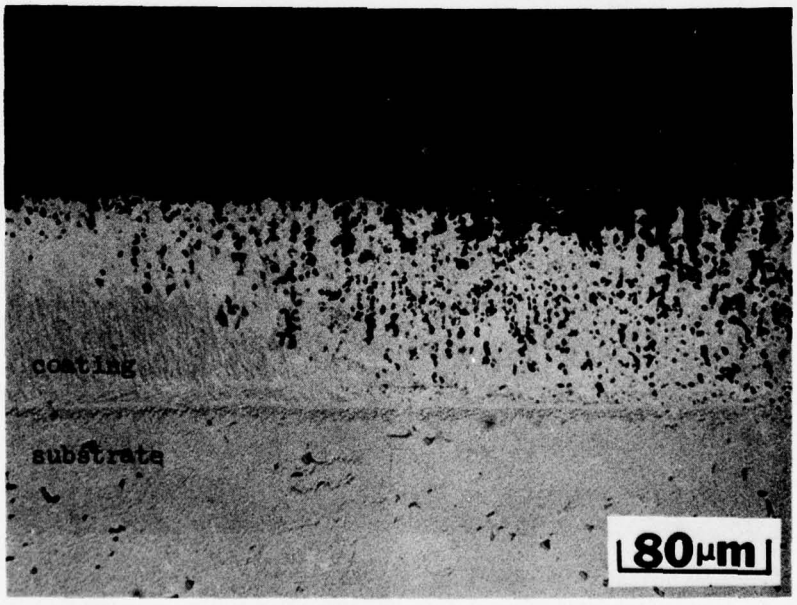


Figure 31b. Localized dealloying and internal oxidation of PWA 68, apparently the mechanism of coating penetration.

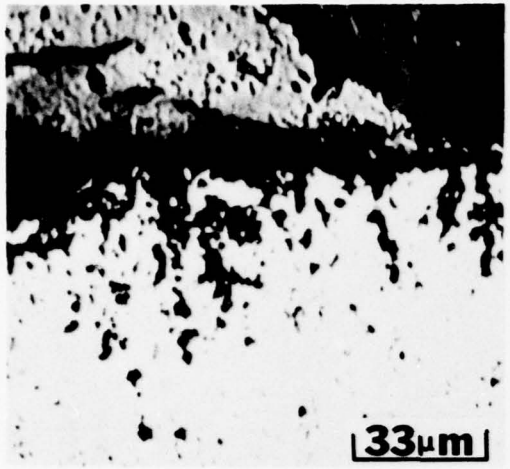


32a. Back scattered electrons

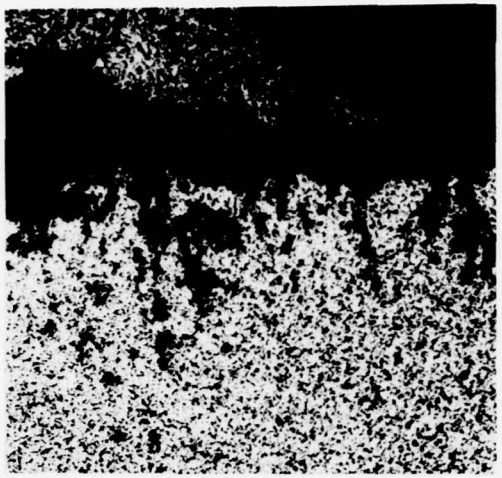

32b. Cobalt X-rays

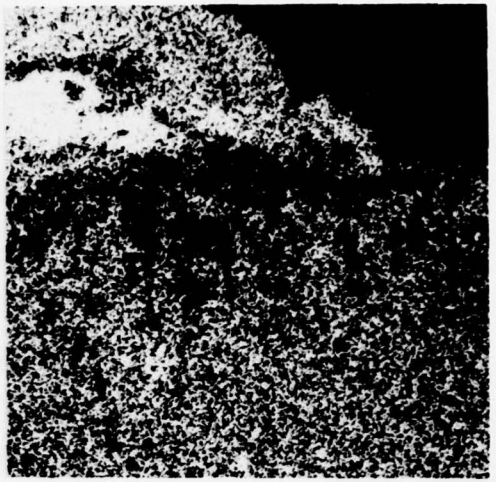

32c. Chromium X-rays

32d. Aluminum X-rays

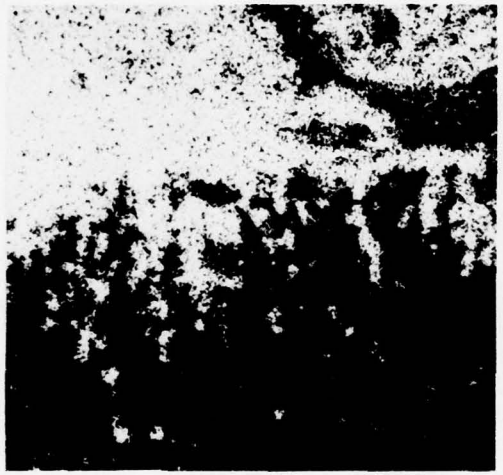

32e. Oxygen X-rays

32f. Sulfur X-rays

Figure 32. Scanning electron micrographs of coating protrusion in PWA 68, showing composition of oxide mound and penetration of oxygen and sulfur.


Figure 33. Penetration and cut-edge attack of Pt + PWA 68 coating. Features illustrated are typical of hot corrosion failure of CoCrAlY-type coatings, and Pt underlayer appears ineffective in modifying the mechanism or rate of sulfate-chloride degradation.

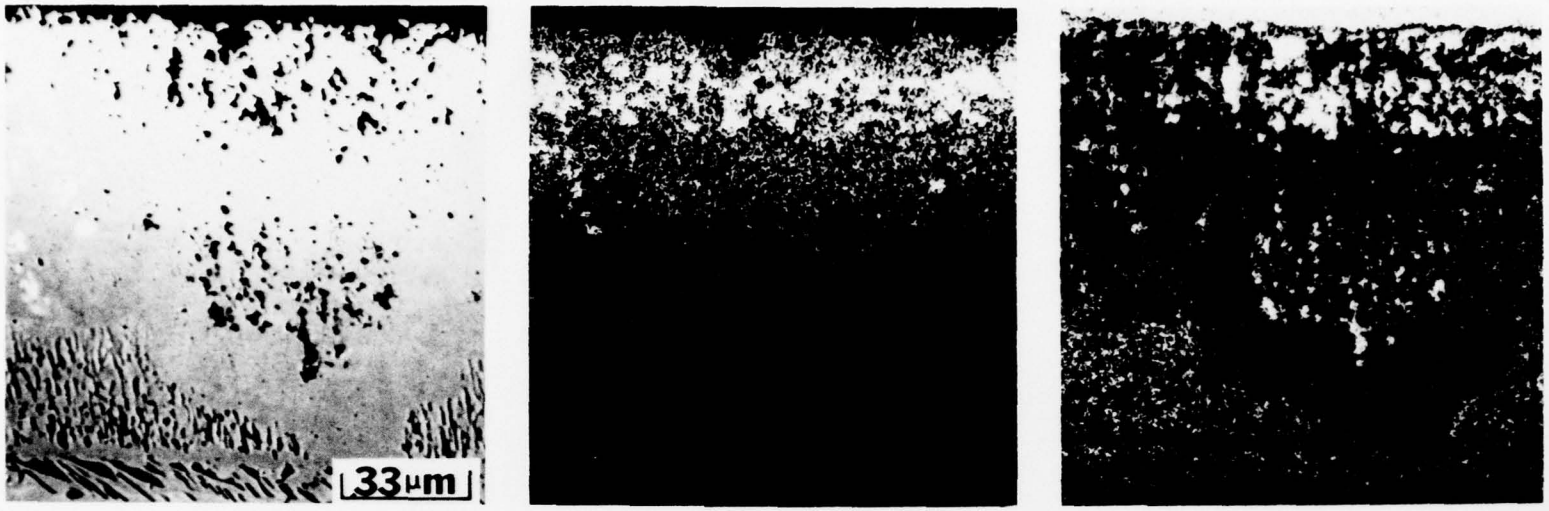


a. Back scattered electrons b. Platinum X-rays c. Aluminum X-rays

d. Titanium X-rays e. Oxygen X-rays e. Sulfur X-rays

Figure 34. Scanning electron micrographs of coating protrusion in PWA 68 + Pt overlayer coating. Structure and element distribution appear similar to those of PWA 68 (Fig. 32) except for the Pt-containing phases.

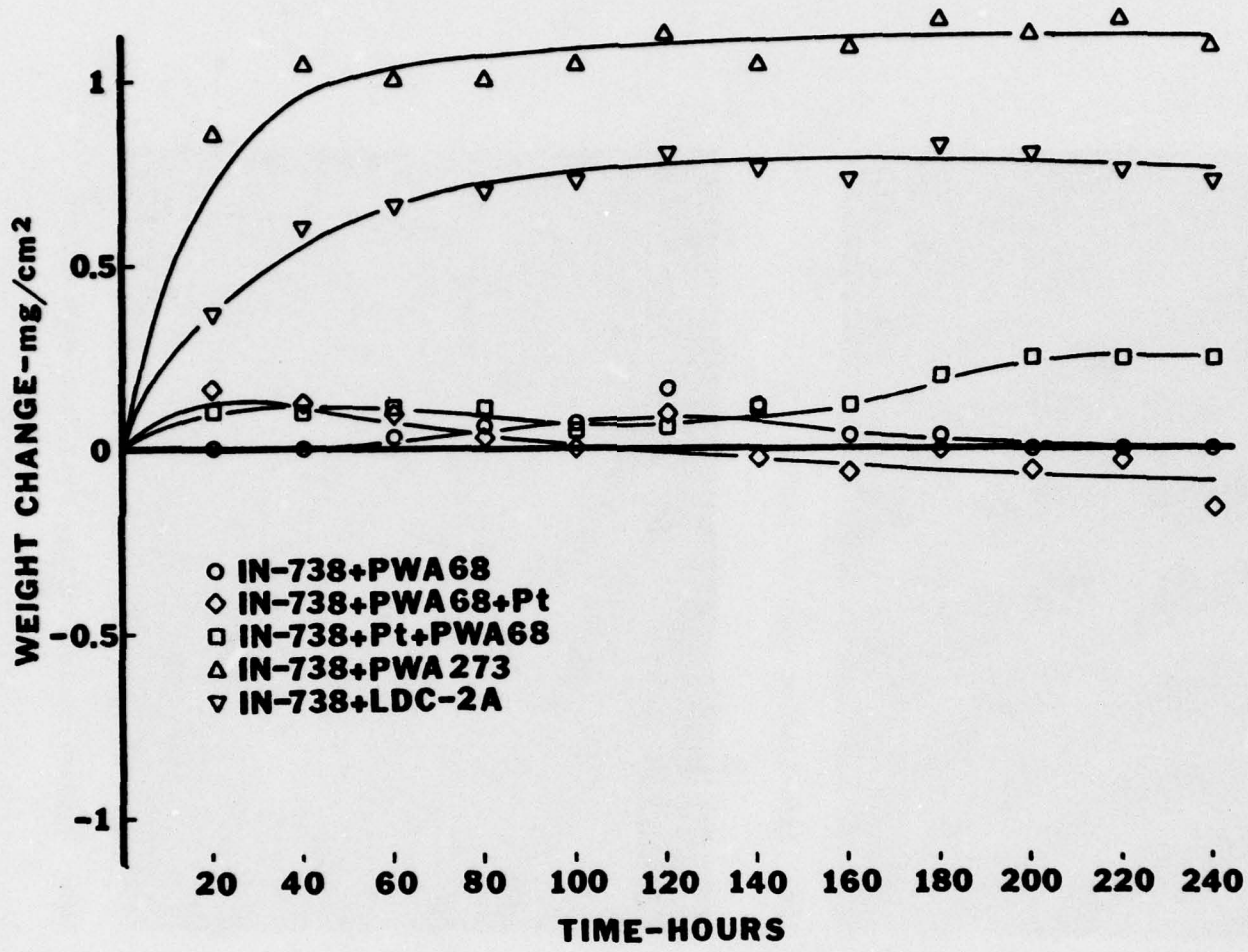


Figure 35. Weight change vs. time data for state-of-the-art coatings exposed in the cyclic hot corrosion test (1 hour cycles, washed and recoated with 1 mg/cm$^2$ of $Na_2SO_4$ - 50% NaCl every 20 hours) at 649°C (1200°F).

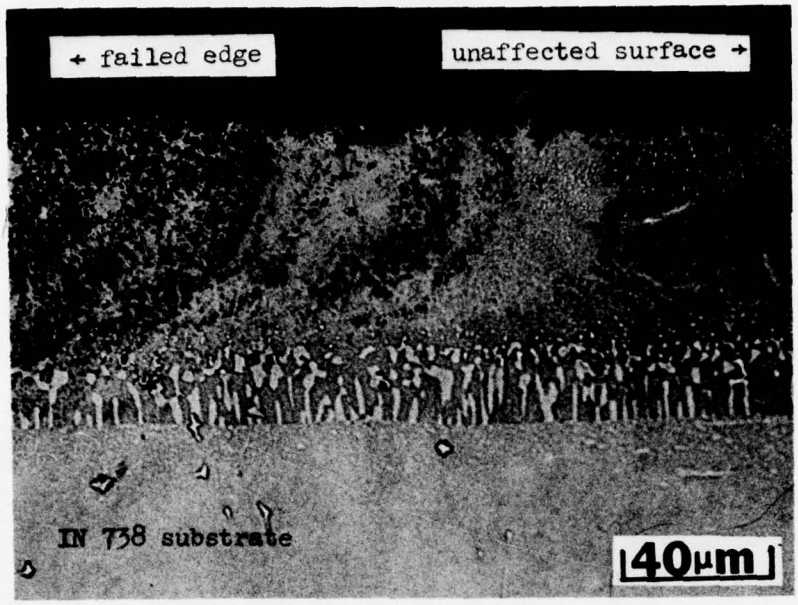


36a. Oxidation at edge of coupon

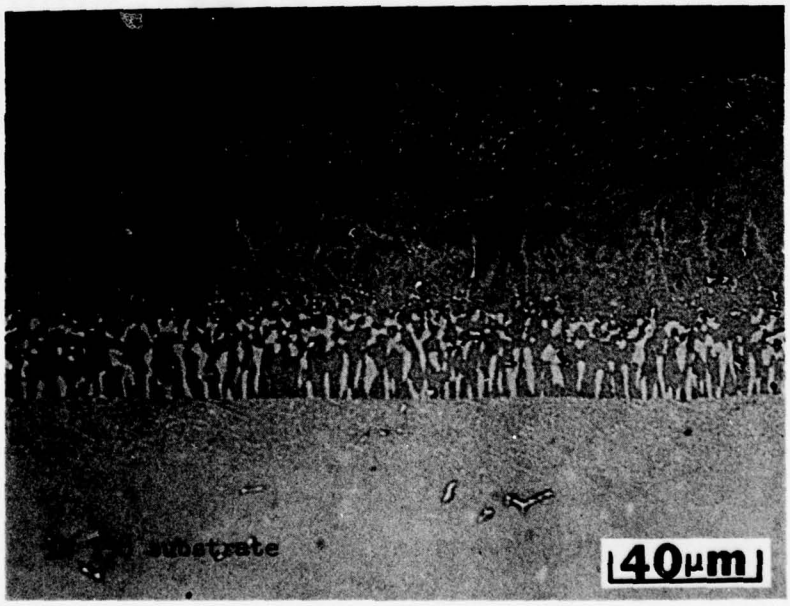


36b. Typical microstructure away from edge effect

Figure 36. PWA 273 diffusion aluminide coating after 1000 hours in 649°C cyclic hot corrosion test with $Na_2SO_4$ - 50% NaCl.

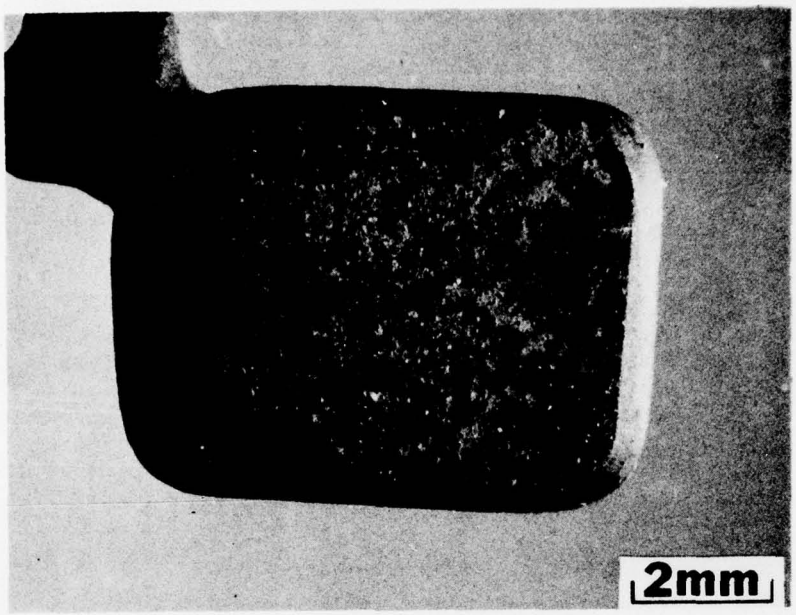


37a. Surface appearance

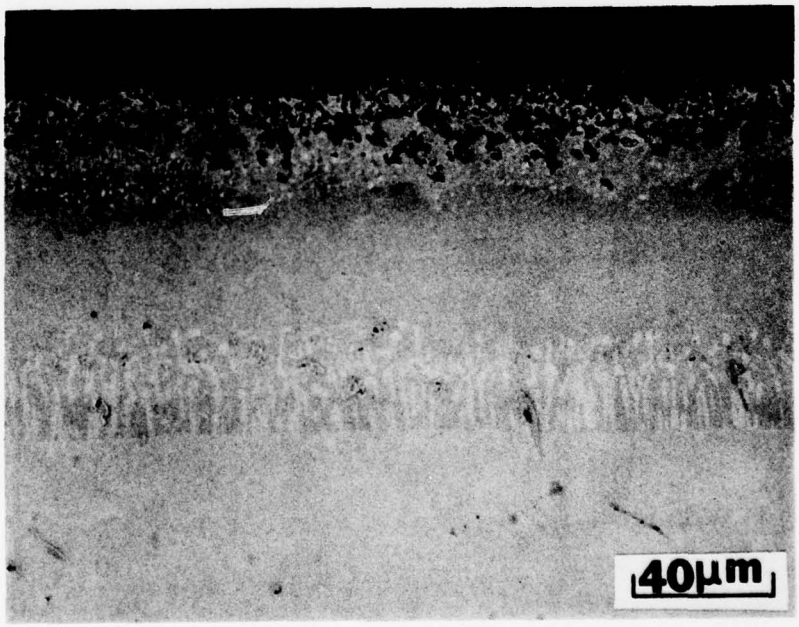


37b. Typical microstructure

Figure 37. Surface degradation of PWA 273 diffusion aluminide coating after 2000 hours of cyclic hot corrosion testing at 649°C with $Na_2SO_4$ - 50%NaCl salt.

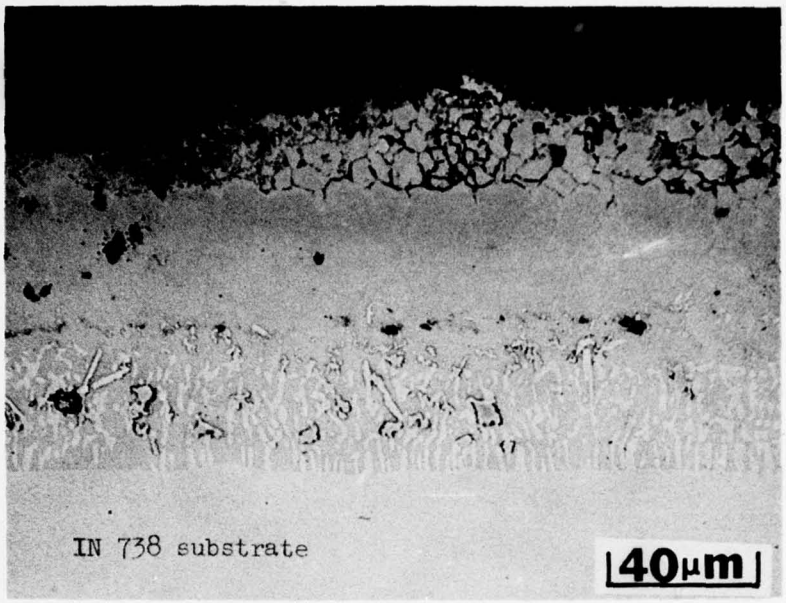


Figure 38. LDC-2A platinum modified diffusion aluminide. Surface microstructure was noticeably degraded in comparison with PWA 273, but there was no incidence of coating failure.

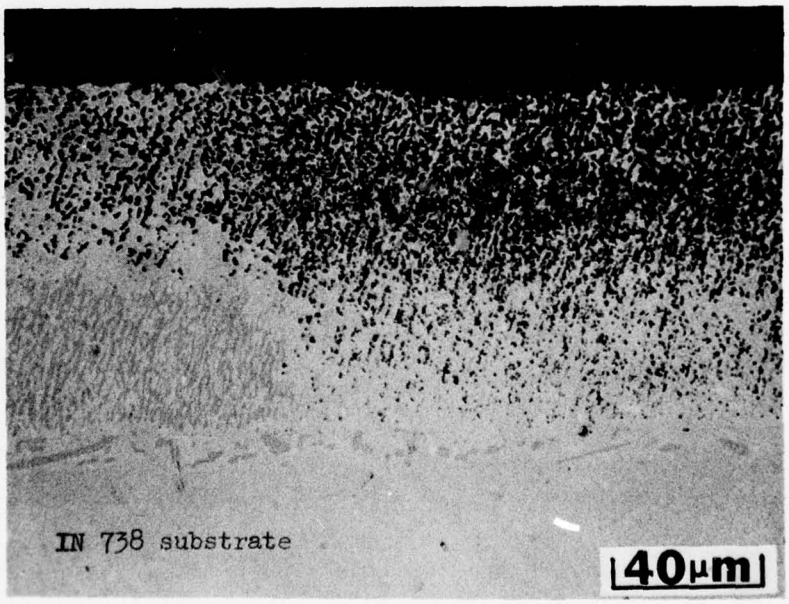


Figure 39. PWA 68 CoCrAlY after 1000 hours in 649°C cyclic hot corrosion showed general surface degradation and many areas of dealloying and precipitation of $Al_2O_3$ through entire coating thickness.

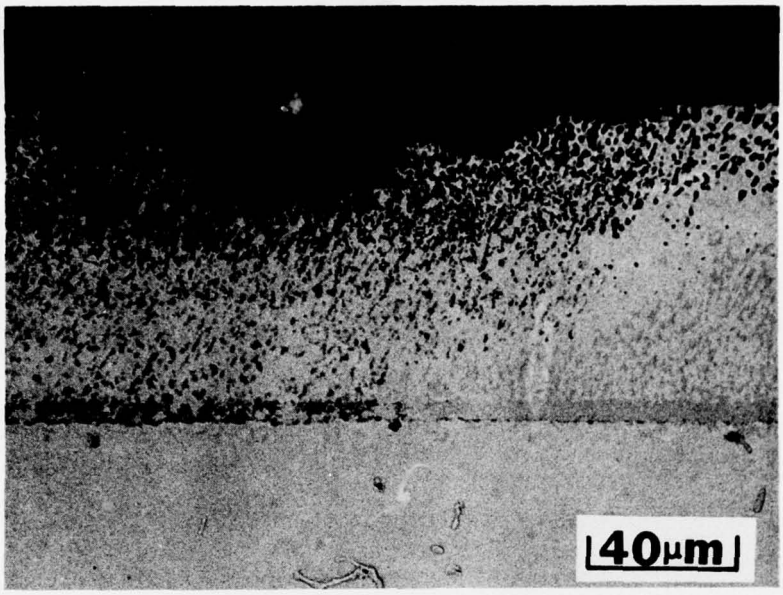


← Pt underlayer

40a. 1000 hour coupon

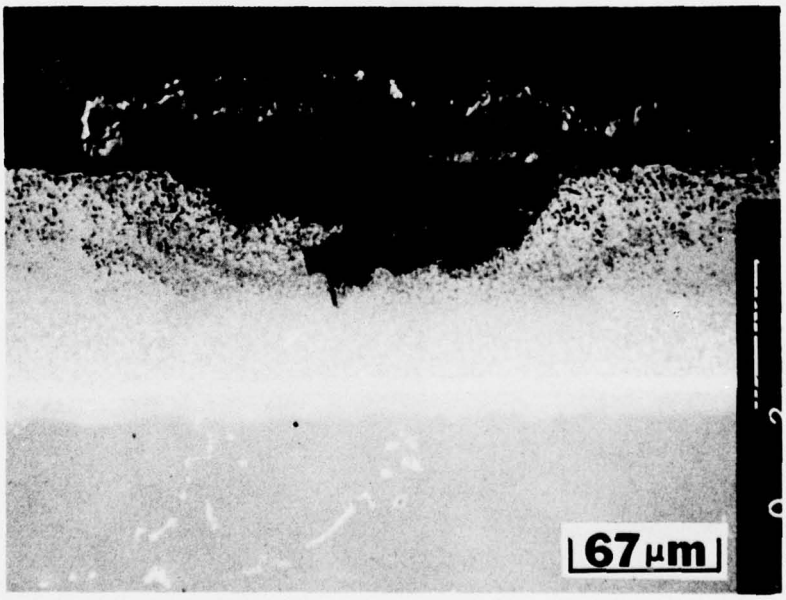


40b. Back scattered electron image of coating protrusion shown in Fig. 41. (Platinum underlayer and Pt-containing diffusion zone appear white due to high average atomic number).

Figure 40. Platinum underlayer between IN 738 substrate and PWA 68 CoCrAlY coating had no apparent effect on typical surface degradation or incidence of localized coating protrusions.

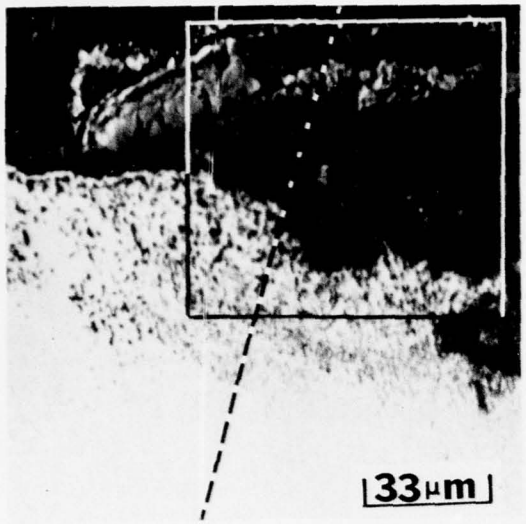


41a. Back scattered electrons

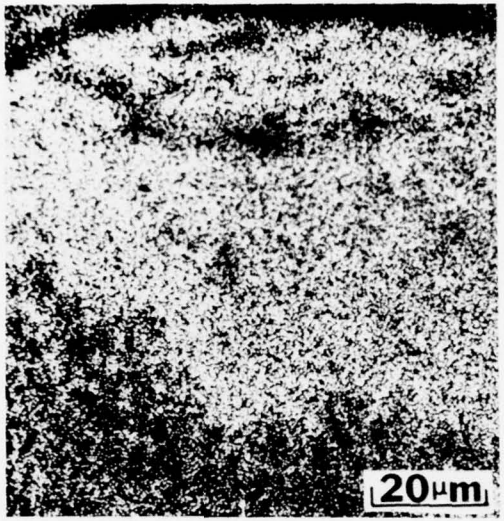


41b. Oxygen X-rays

41c. Sulfur X-rays

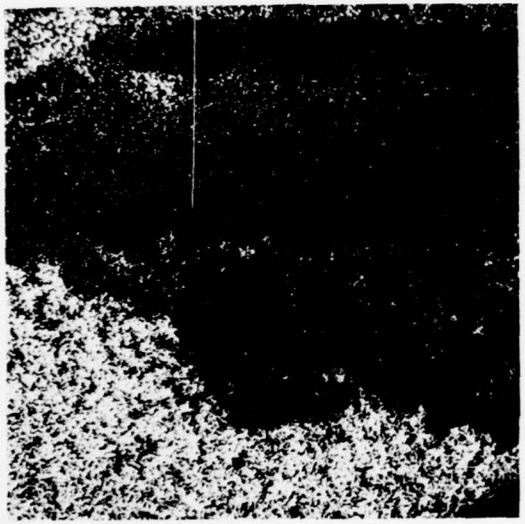

41d. Cobalt X-rays

41e. Chromium X-rays

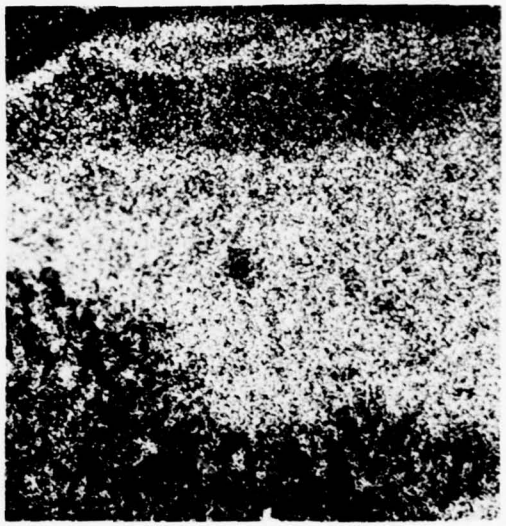

41f. Aluminum X-rays

Figure 41. Coating protrusion in PWA 68 after cyclic hot corrosion testing for 780 hours at 649°C with $Na_2SO_4$ - 50%NaCl. Box in 41a is area of X-ray images; dotted line is path of line scan discussed in text.

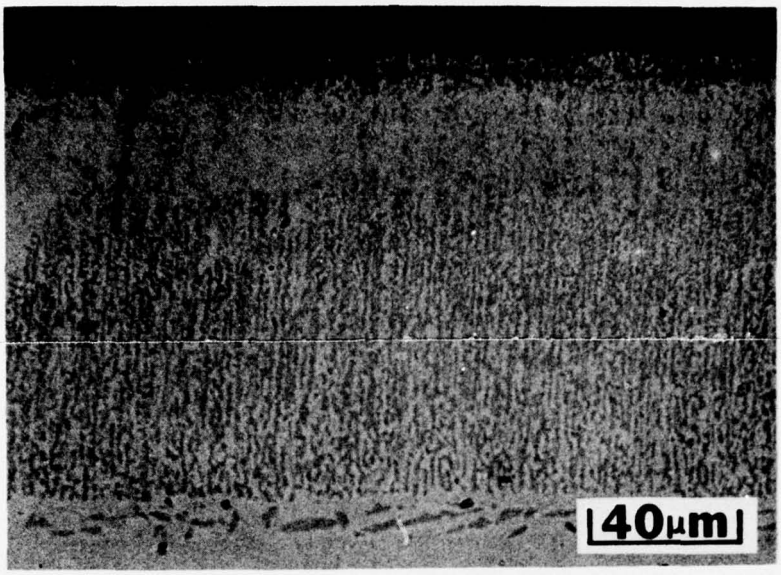


42a. PWA 68 coating with platinum overlayer suffered minimal degradation in 1000 hour cyclic hot corrosion test at 649°C. Microstructures shown in Figs. 39 and 40 were produced by the same exposure of PWA 68 without the platinum overlayer.

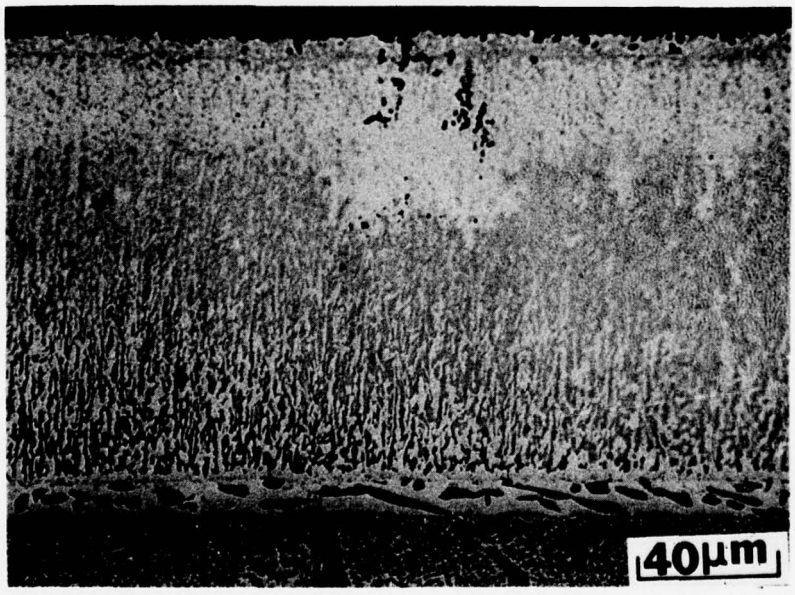


42b. Microstructure of PWA 68 + Pt after 2000 hours at 649°C

Figure 42. Minimal degradation of microstructure of PWA 68 + Pt coating was observed in the 649°C cyclic hot corrosion test with $Na_2SO_4$ - 50% NaCl.

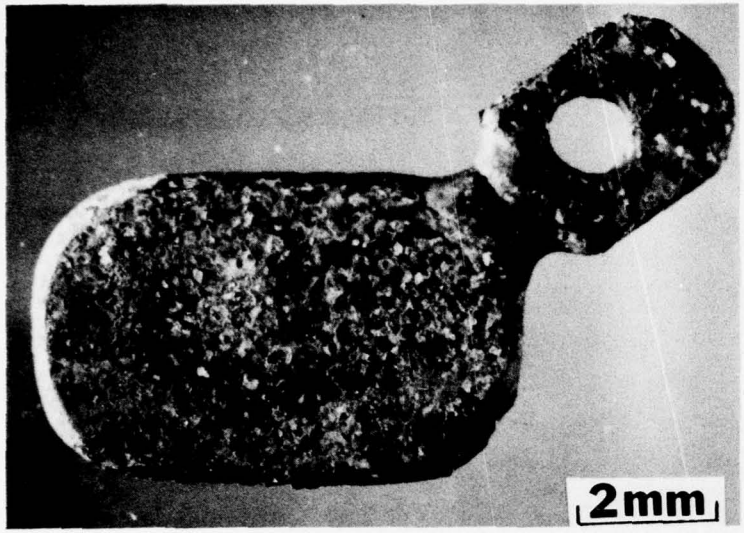


43a. Surface condition

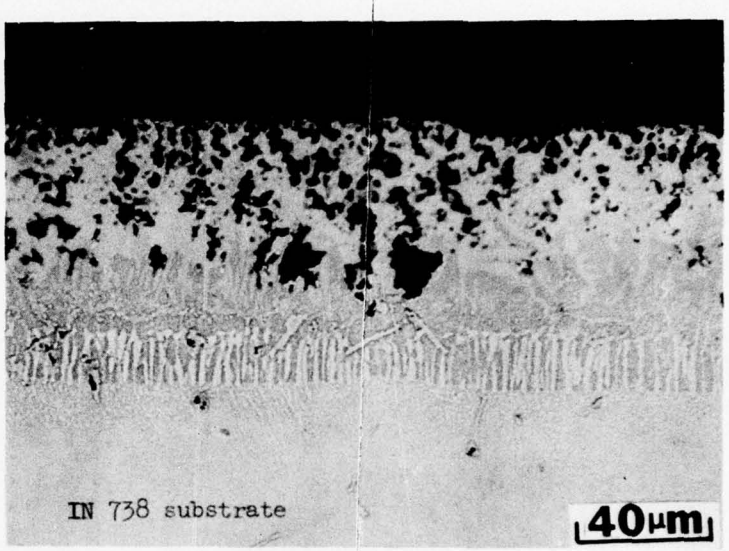


43b. Typical microstructure

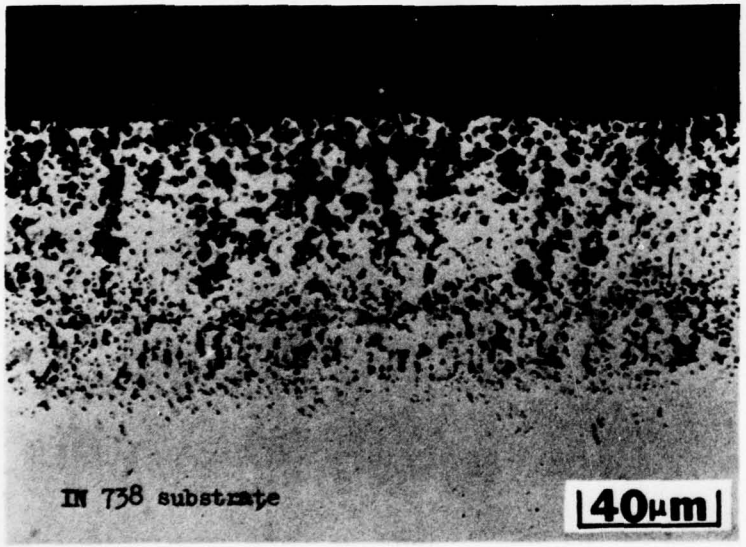


43c. Failed coating near edge

Figure 43. Surface condition and microstructure of PWA 73 diffusion aluminide coating after 120 hours in 899°C cyclic hot corrosion test with $Na_2SO_4$ - 50% NaCl. Test was terminated due to general surface degradation and corner failure.

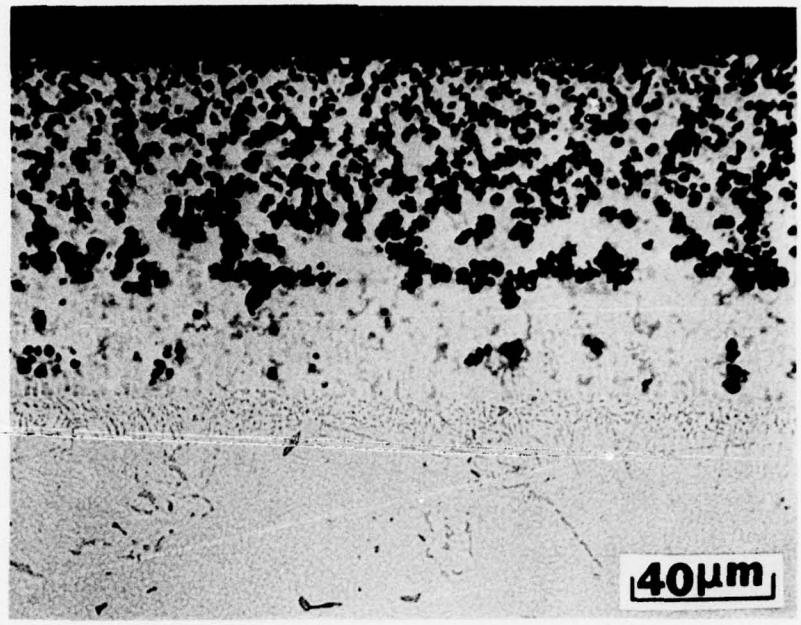


44a. 1000 hours

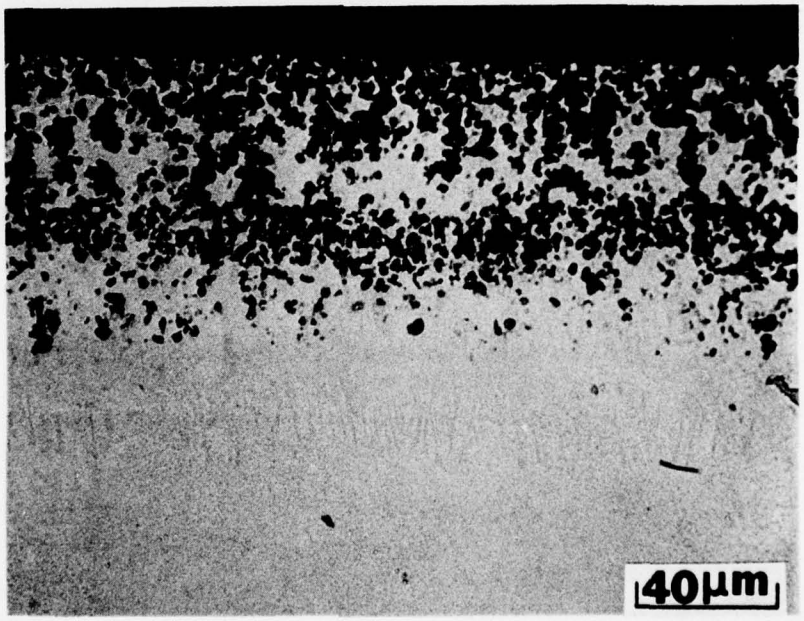


44b. 700 hours

Figure 44. Microstructural degradation of PWA 273 diffusion aluminide coating in 899°C (1650°F) cyclic hot corrosion test with $Na_2SO_4$ - 50% NaCl.

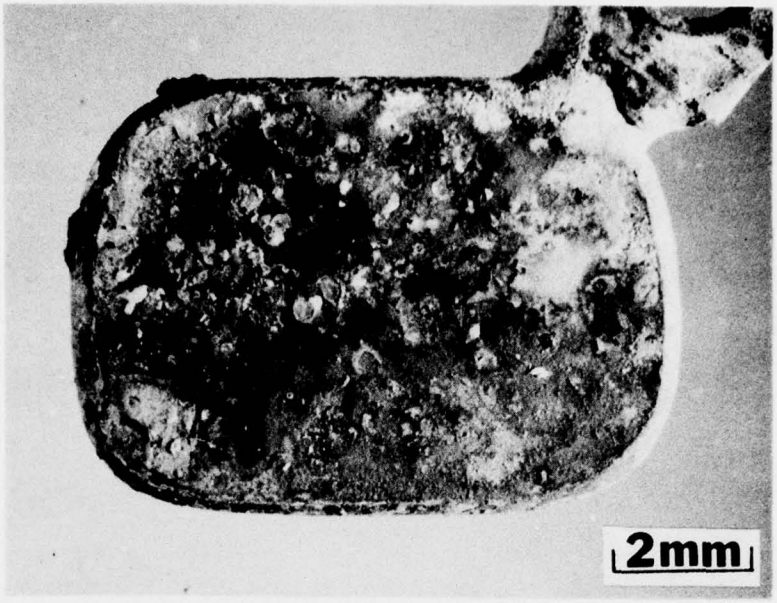


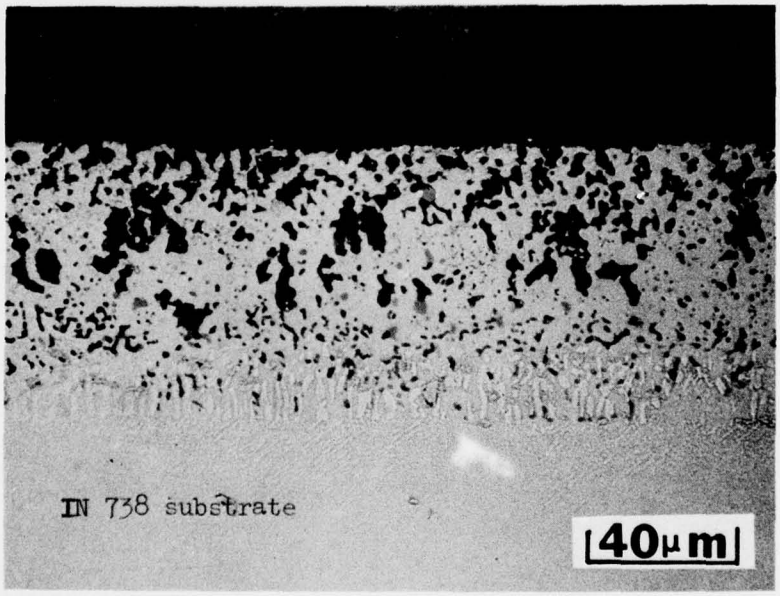


Figure 45. Surface condition and typical microstructure of chromized and aluminized (PWA 70 + PWA 73) IN 738 after 80 hours in 899°C cyclic hot corrosion test with $Na_2SO_4$ - 50% NaCl.

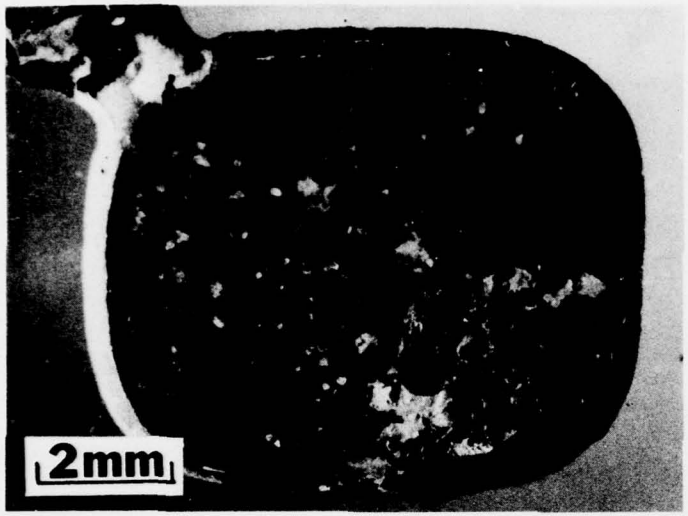


46a. Macrograph of test coupon

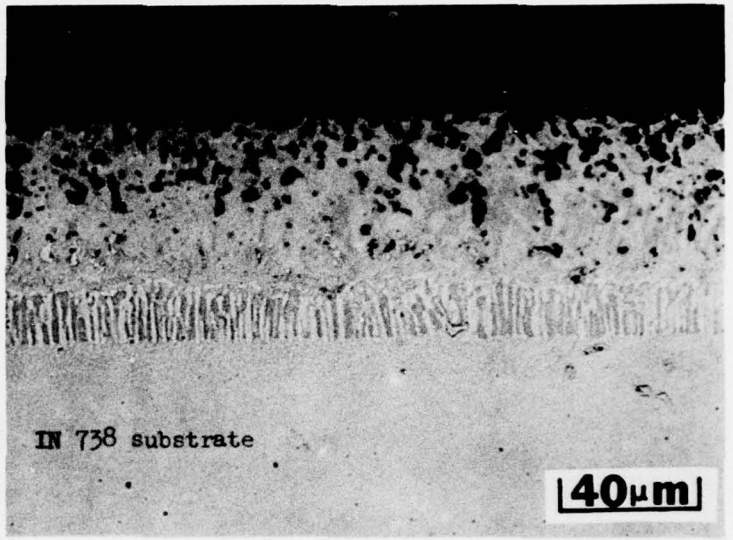


46b. Typical coating microstructure

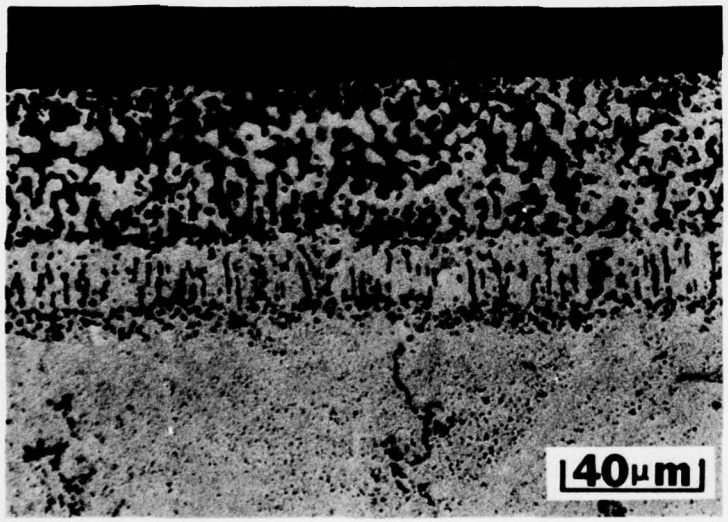


46c. Microstructure at failed corner

Figure 46. Surface condition and microstructure of chromized and aluminized (PWA 70 + PWA 273) IN 738 after 80 hours in 899°C cyclic hot corrosion test with $Na_2SO_4$ - 50% NaCl. Test was terminated due to corner failure.

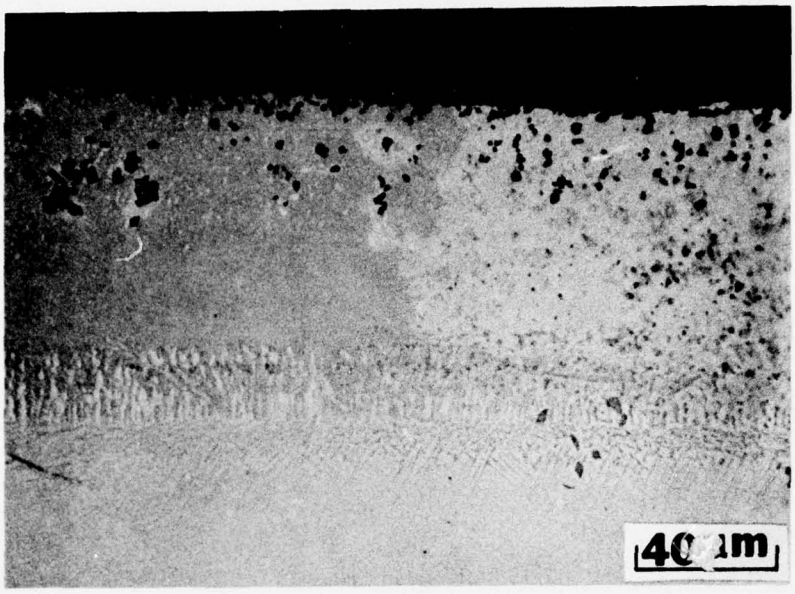


47a. Sharp transition in extent of dealloying

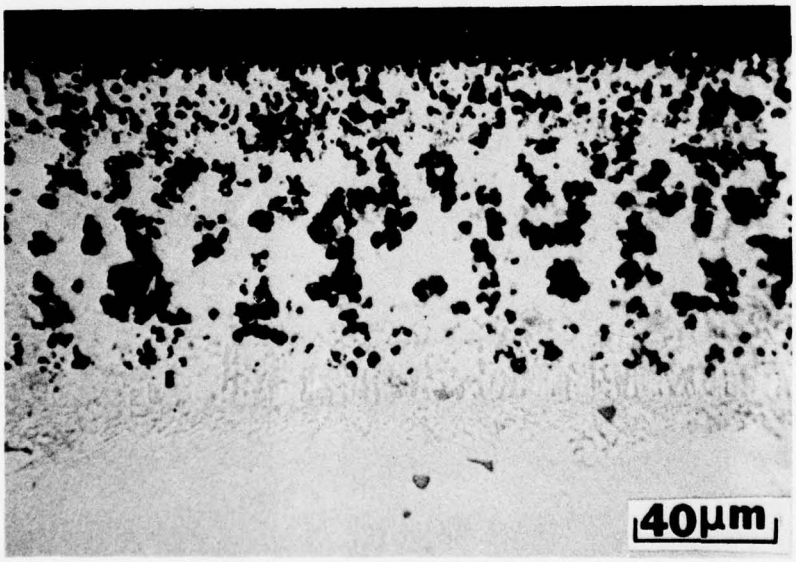


47b. Internal oxidation of entire coating thickness

**Figure 47.** Variable microstructural degradation of sputtered Pt + PWA 273 coating in 1000 hour 899°C cyclic hot corrosion test.

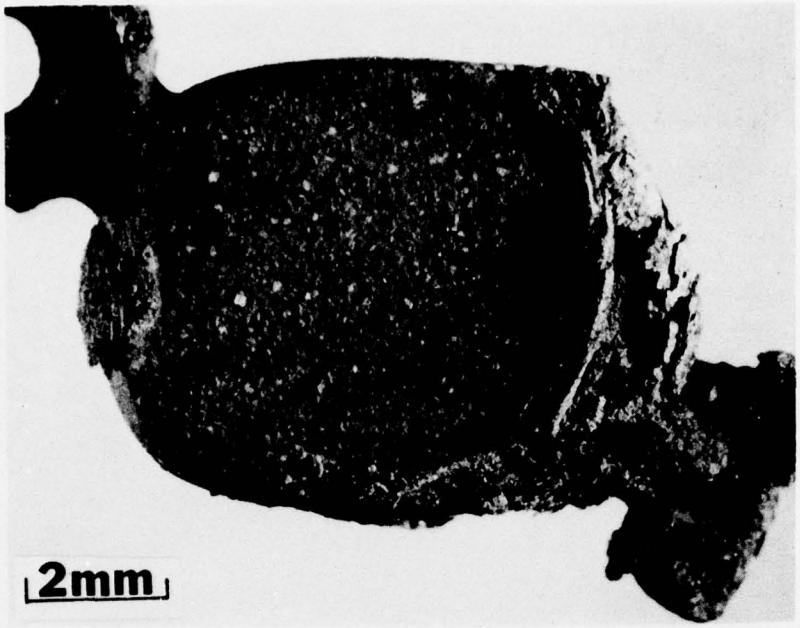


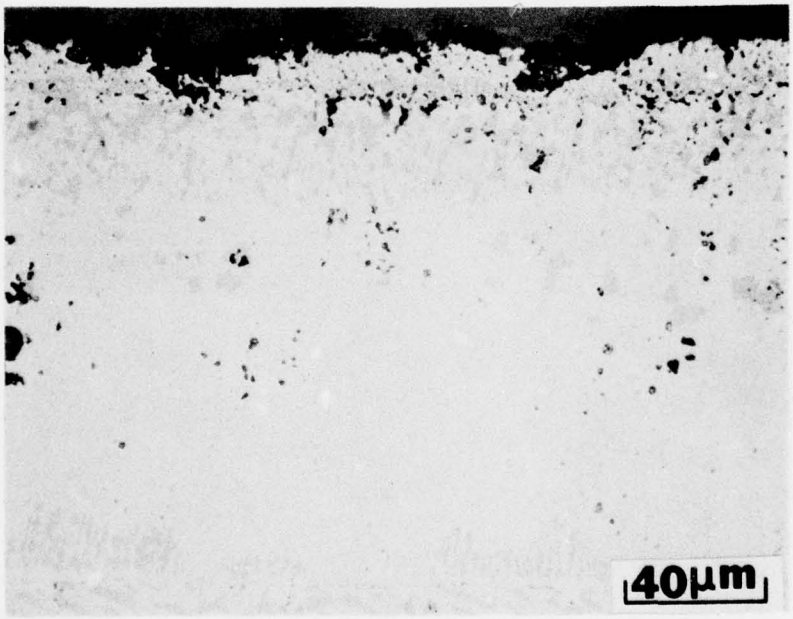


Figure 48. Surface condition and typical microstructure (away from cut edge attack) of PWA 68 coating with 6µm platinum overlayer; exposure time = 720 hours at 899°C.

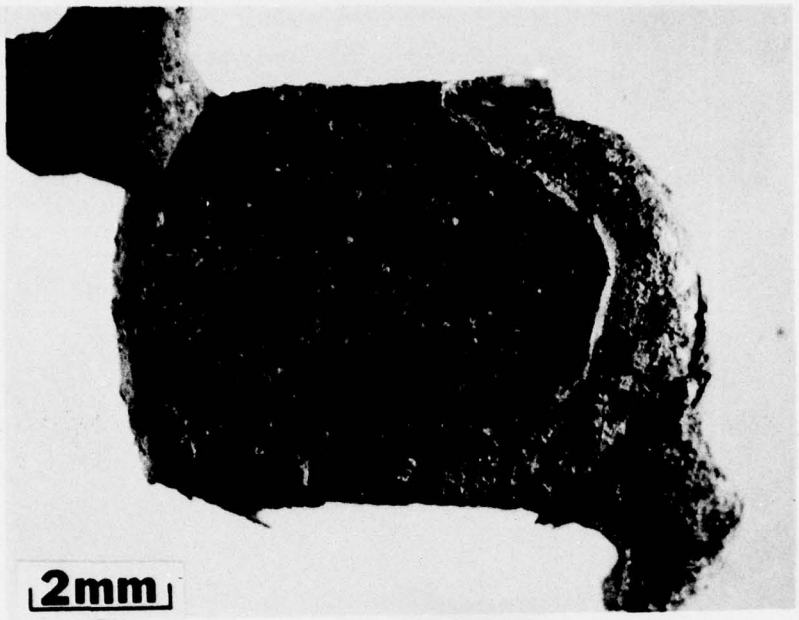


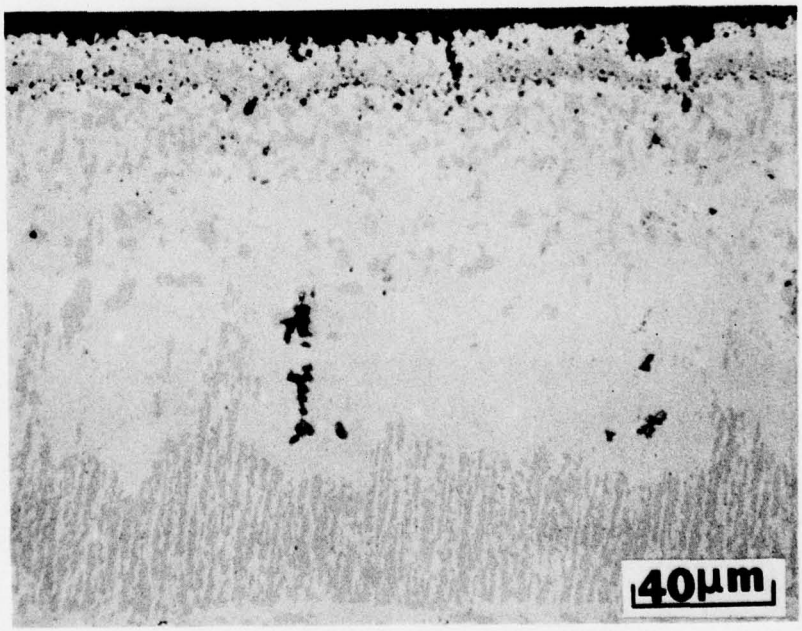


Figure 49. PWA 68 + ~12µm Pt overlayer; exposure time = 700 hours at 899°C. Thicker overlayer did not significantly improve performance (compare with Fig. 48).

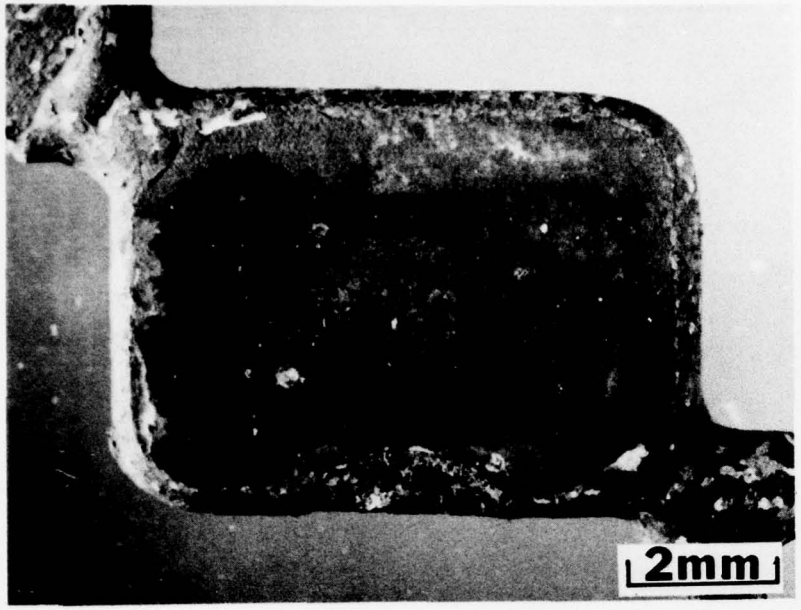


50a. Macrograph of test coupon

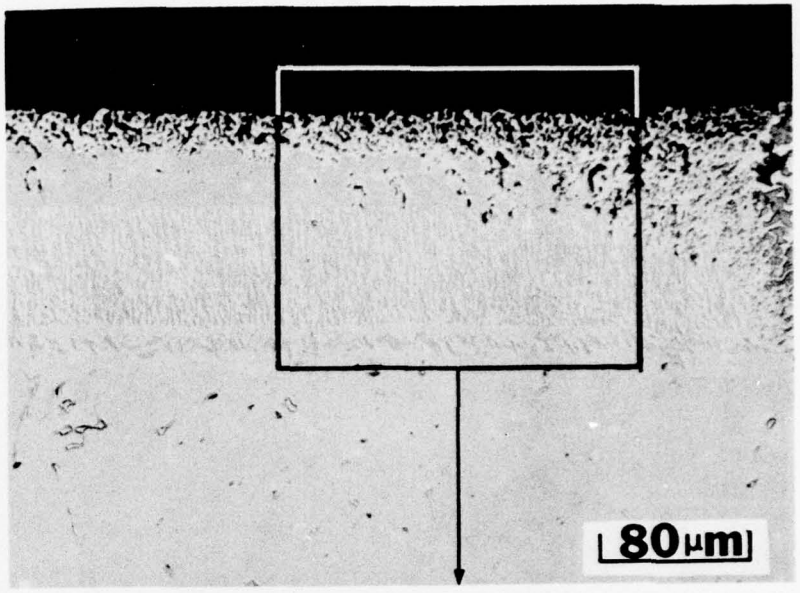


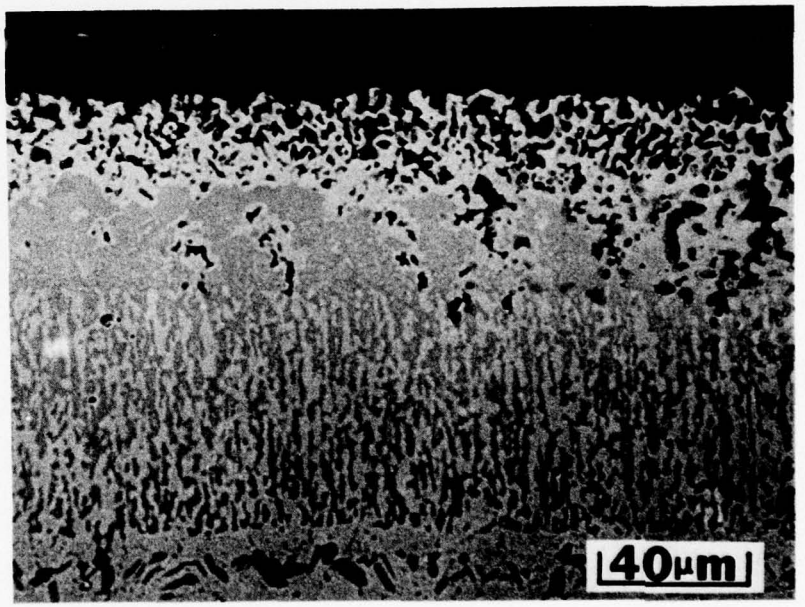


50b. Edge failure and uniform surface attack

Figure 50. Surface condition and microstructure of aluminized CoCrAlY (PWA 68 + PWA 273) after 80 hours in 899°C cyclic hot corrosion test with $Na_2SO_4$ - 50% NaCl. Test was terminated due to edge failure.

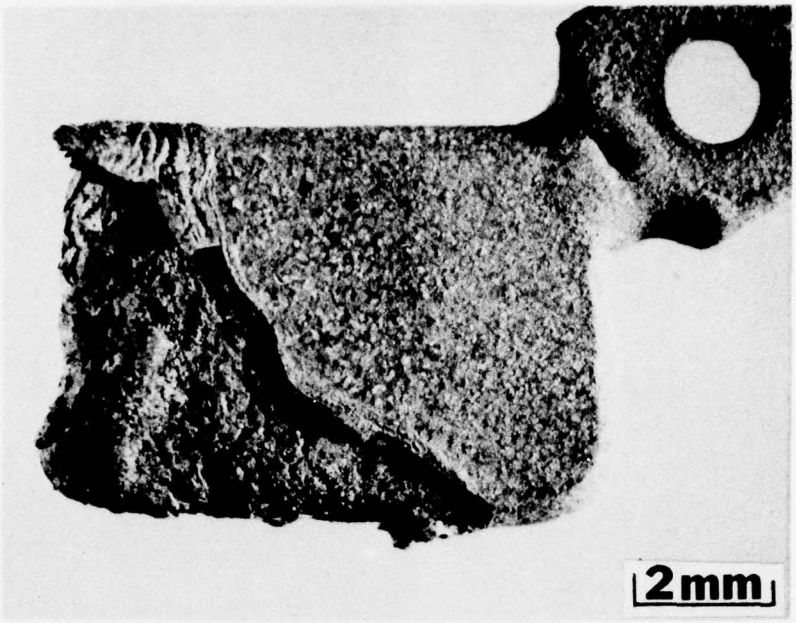


51a. Surface condition

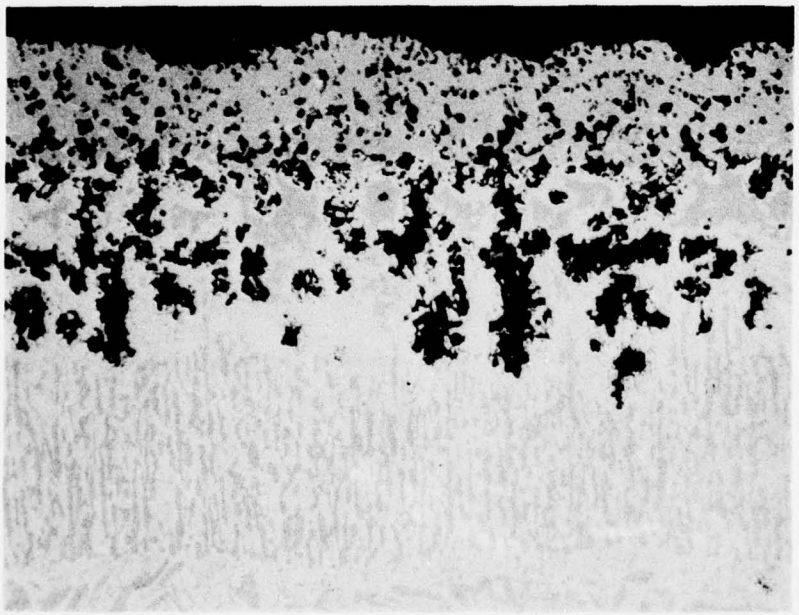

51b. Typical microstructure

Figure 51. Surface condition and microstructural degradation (away from cut-edge effect) of PWA 68 + Pt overlayer + PWA 273 coating; exposure time = 520 hours in 899°C cyclic hot corrosion. Uniform depth of attack on other face of coupon was about half that shown in 51b.

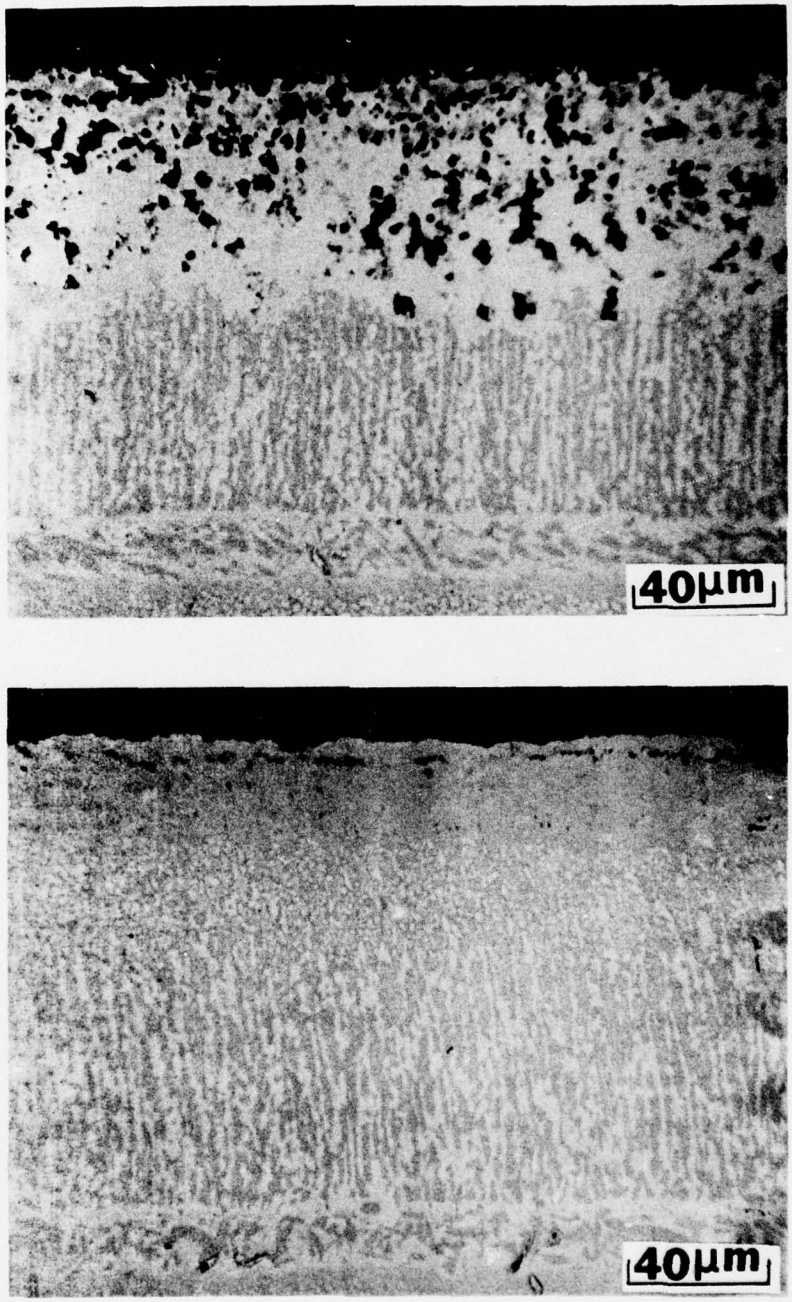


Figure 52. Variable extent of microstructural degradation after 940 hours exposure of PWA 68 + Pt + PWA 273 coating in 899°C cyclic hot corrosion.

AD-A056 574 PRATT AND WHITNEY AIRCRAFT GROUP EAST HARTFORD CT MAT--ETC F/G 11/6
DEGRADATION OF COATING ALLOYS IN SIMULATED MARINE ENVIRONMENTS.(U)
JUN 78 R H BARKALOW, F S PETTIT N00173-76-C-0146
UNCLASSIFIED PWA-FR-10225 NL

2 OF 2
AD
A056574

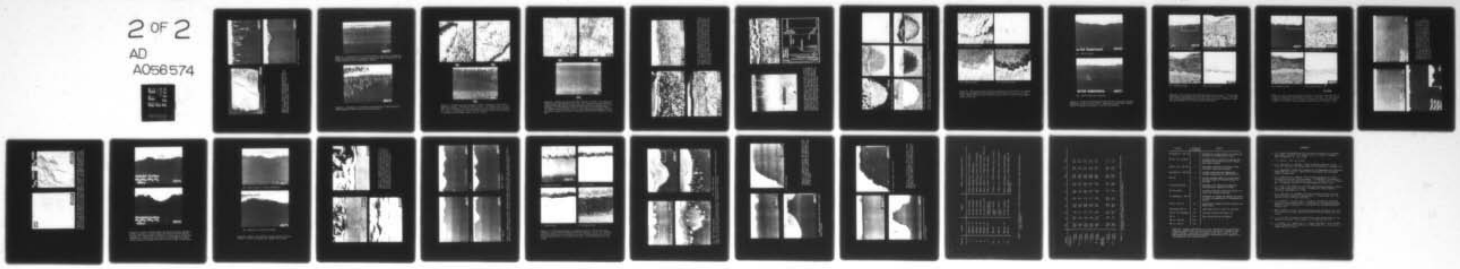

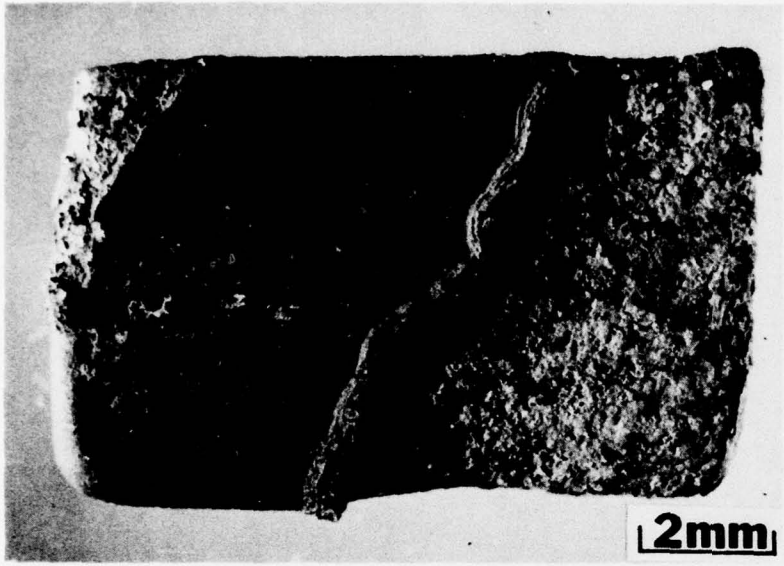


53a. Macrograph of test coupon

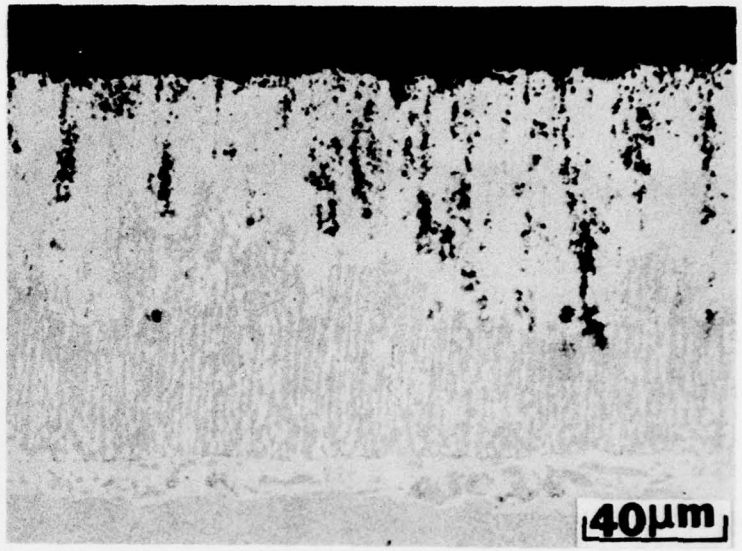


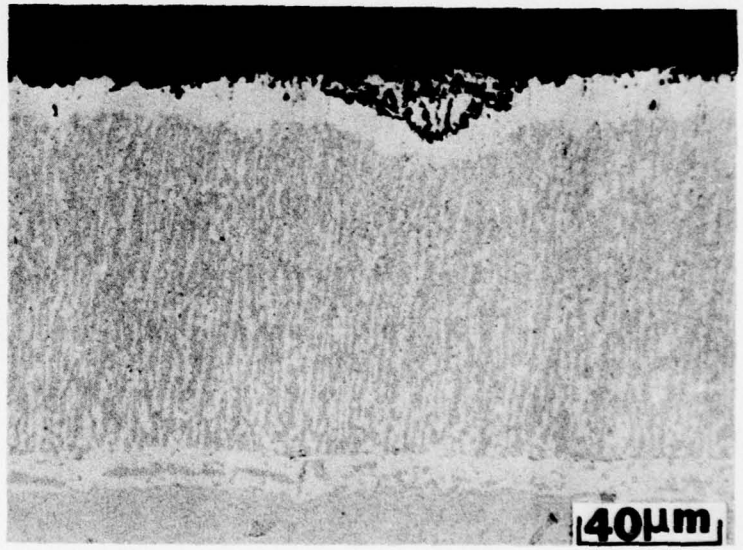


53b. Typical microstructures

Figure 53. Surface condition and microstructural degradation of Ti-modified PWA 68 coating; exposure time = 520 hours in 899°C cyclic hot corrosion with $Na_2SO_4$ - 50% NaCl.

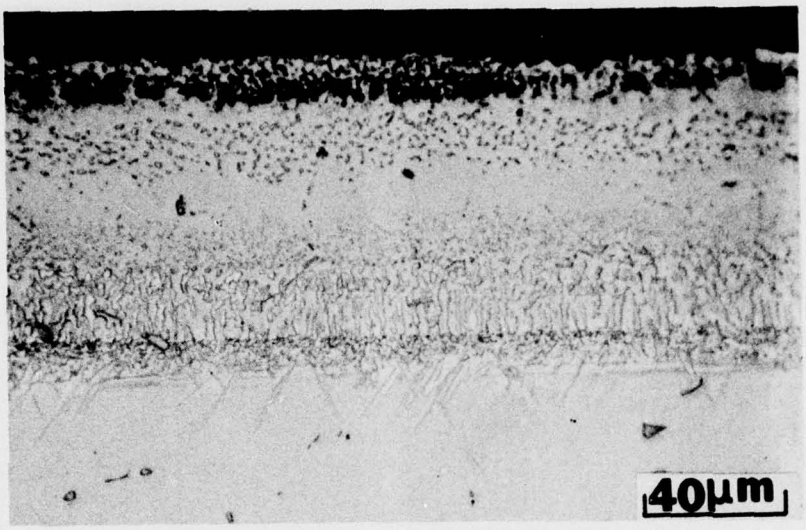


Figure 54. Microstructure of Ti-modified PWA 273 (6µm layer of sputtered titanium applied prior to aluminizing) after 1000 hours of cyclic hot corrosion testing at 899°C with $Na_2SO_4$ - 50% NaCl

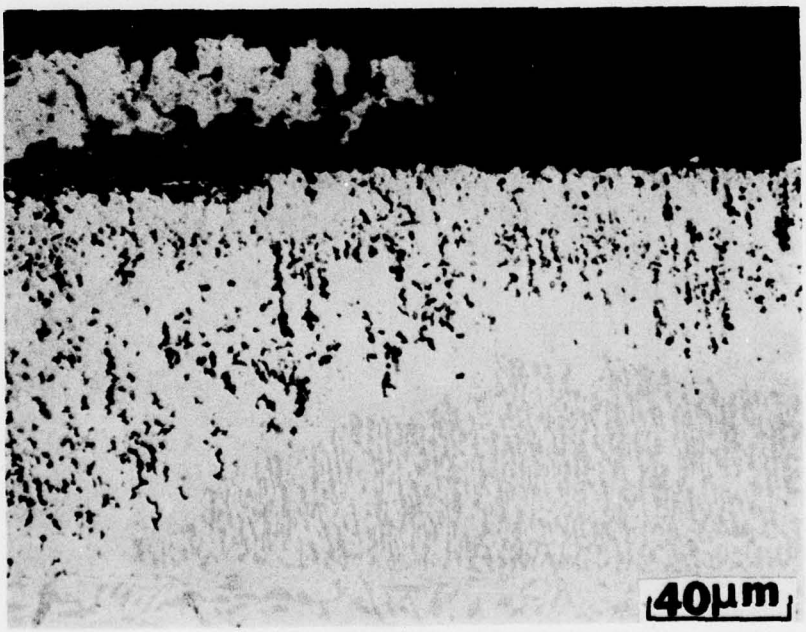


Figure 55. Oxidation of Ni overlayer and dealloying of PWA 68 after 80 hours exposure in 899°C cyclic hot corrosion test.

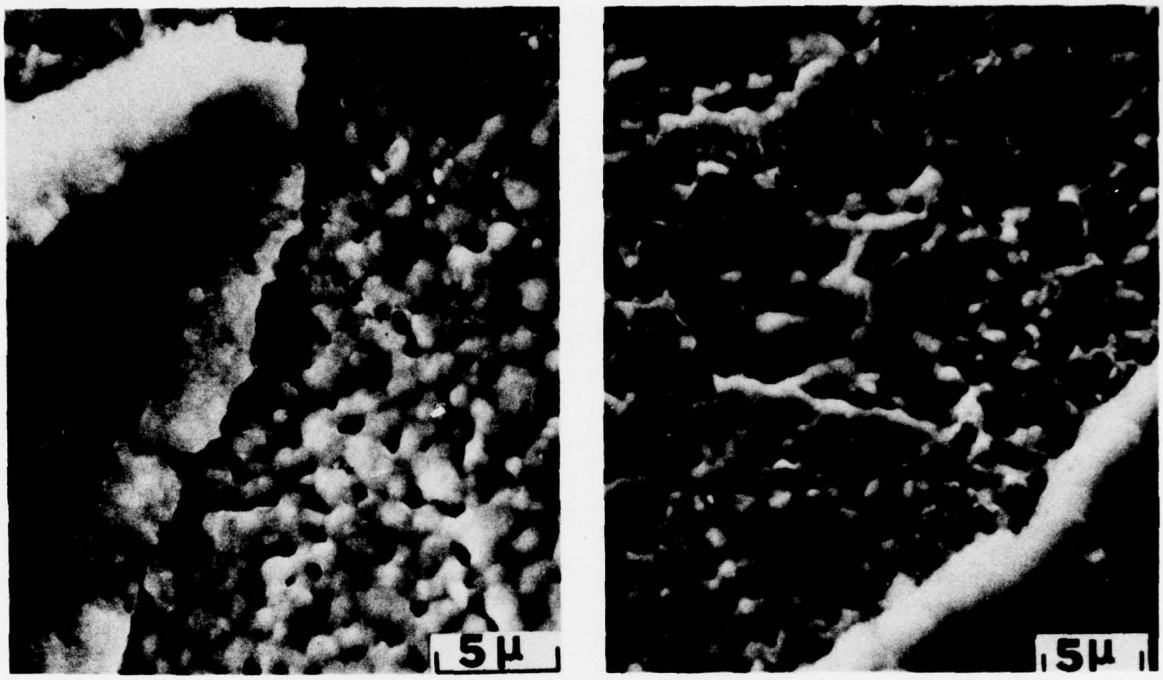


(a) (b)

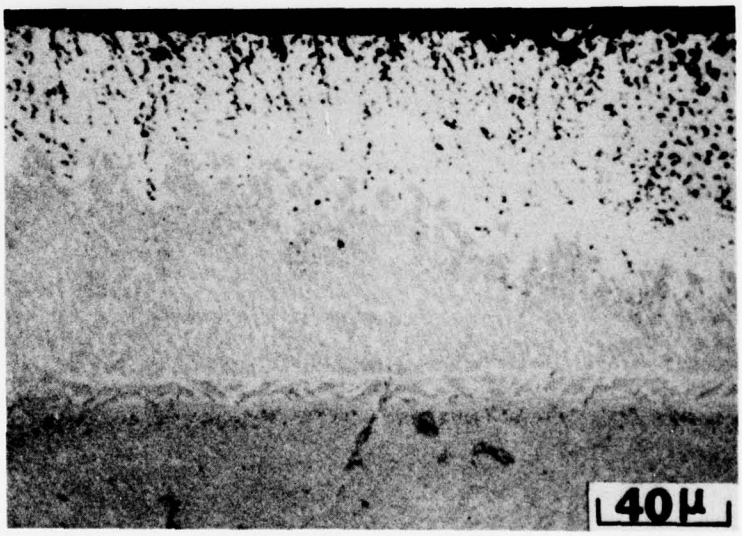


(c)

Figure 56. Surface and microstructural features developed on PWA 68 after exposure to $Na_2SO_4$ - 50% NaCl at 899°C (1650°F). (a) Surface pores are evident after 20 minutes. (b) Pores are larger and more numerous after exposure for 1 hour. (c) Transverse section after 22 hours shows that the porous zone of internal attack extends deeply into the coating.

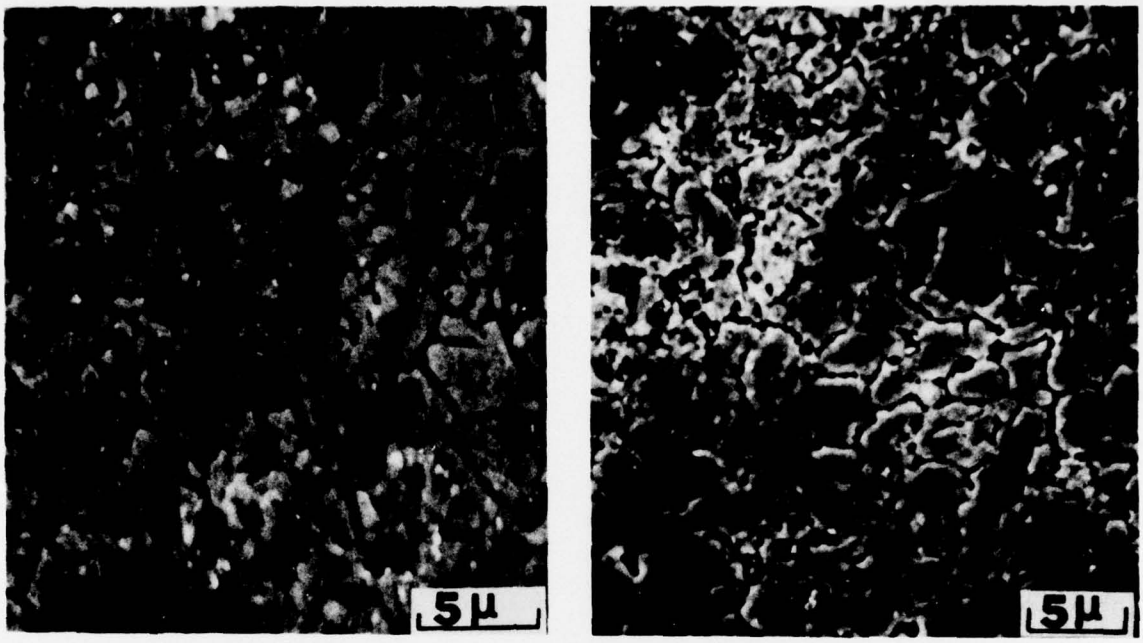


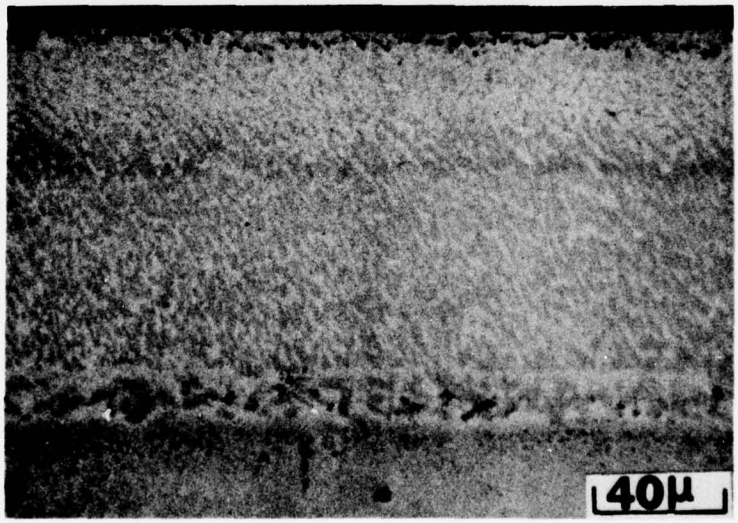


Figure 57. Surface and microstructural features on PWA 68 + Pt tested concurrently with the specimen of Fig. 56. (a) Scanning microscopy after 20 minutes shows preferential attack, apparently at grain boundaries of the Pt overlayer. (b) Re-examination after 1 hour shows no additional attack. (c) Transverse section after 22 hours shows negligible degradation of microstructure; compare with extensive dealloying and internal oxidation in Fig. 56c.

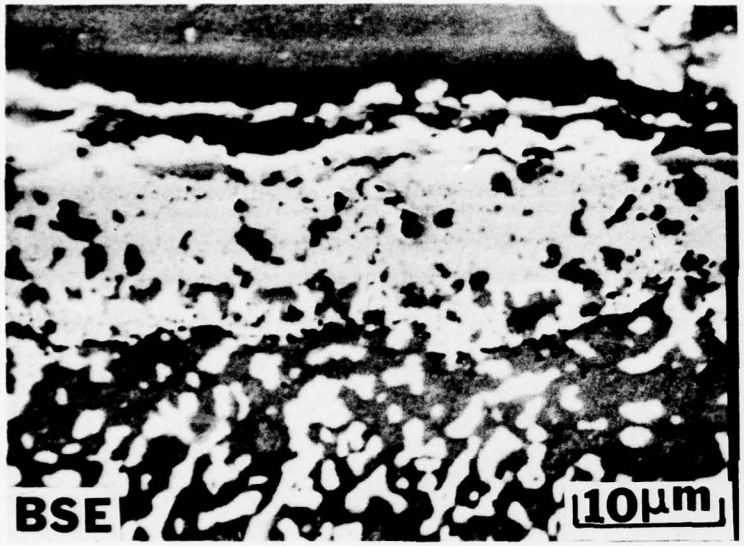


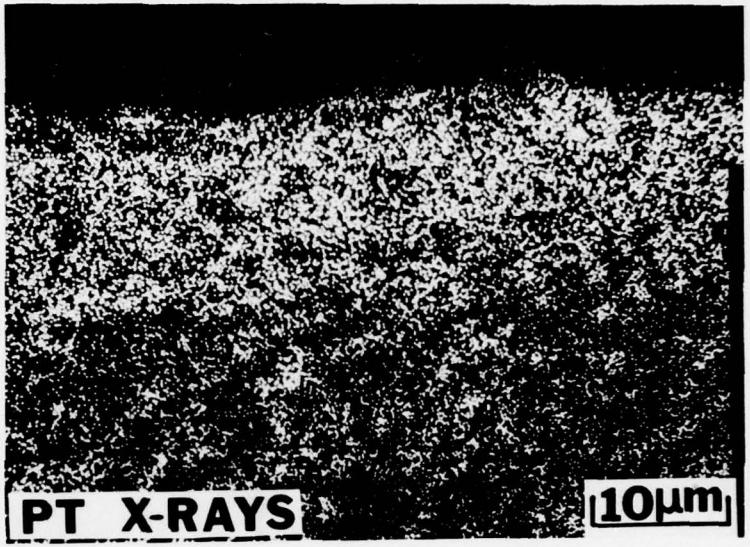


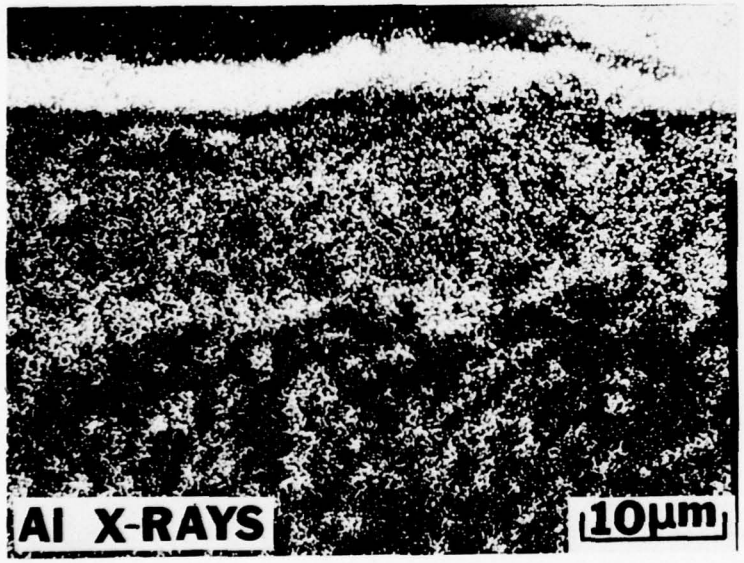


Figure 58. High magnification SEM photomicrographs of the platinum overlayer shown in Fig. 57c. Pt-rich phases appear bright in the back scattered electron image, which shows that the overlayer includes small islands of α-Co in a continuous matrix of the platinum aluminide phase. The Al X-ray image shows the alumina scale formed during the 22 hour hot corrosion test at 899°C.

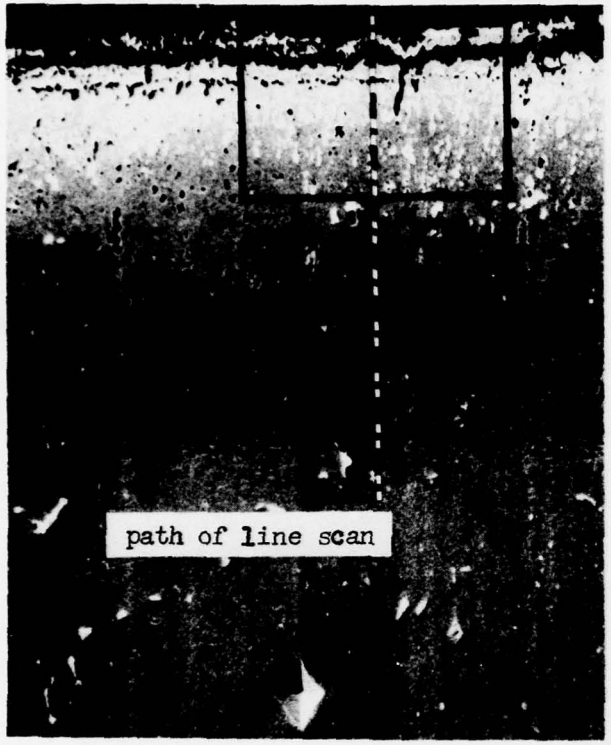



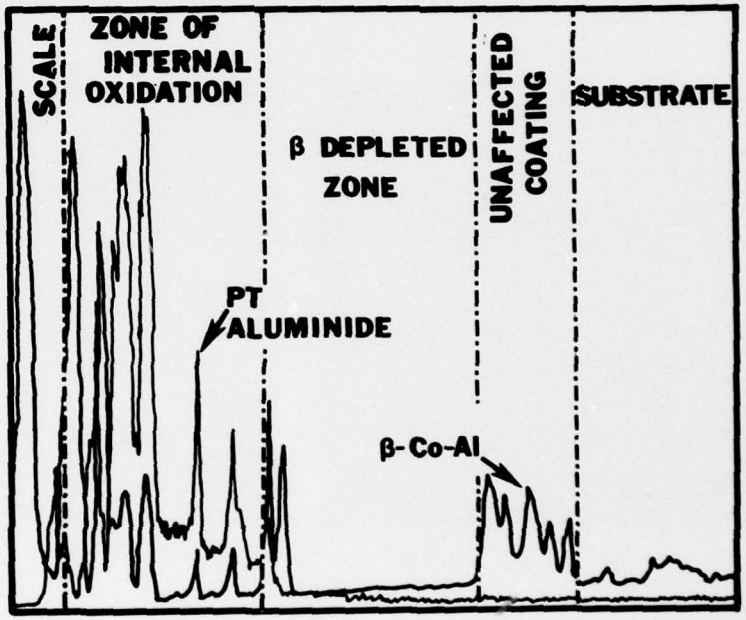


*Figure 59. Degradation of Pt overlayer + PWA 68 coating produced by 700 hours in the cyclic hot corrosion test at 899°C. Break-up of originally continuous platinum aluminide phase in the overlayer (see Figs. 57c, 58) apparently exposes the CoCrAlY to dealloying by the sulfate-chloride melt, as shown by β-dissolution, pore formation, and Al line scans through the coating.*

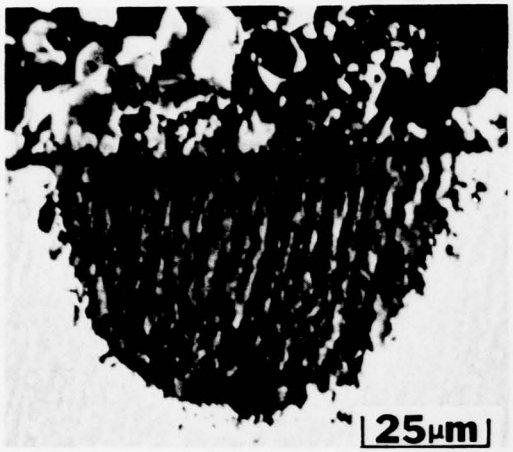


60a. Back scattered electrons

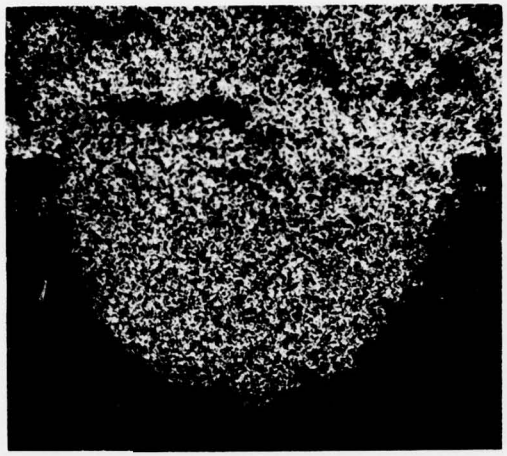

60b. Oxygen X-rays

60c. Sulfur X-rays

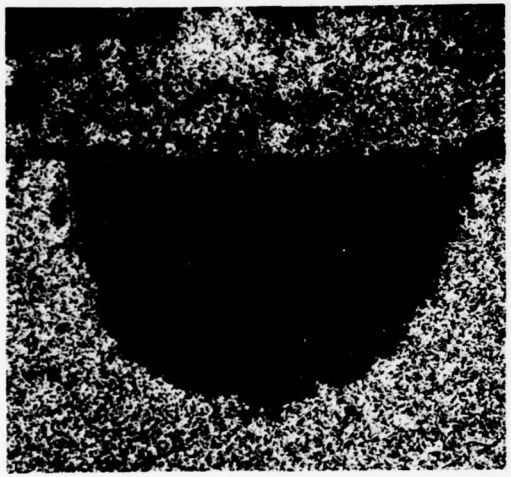

60d. Cobalt X-rays

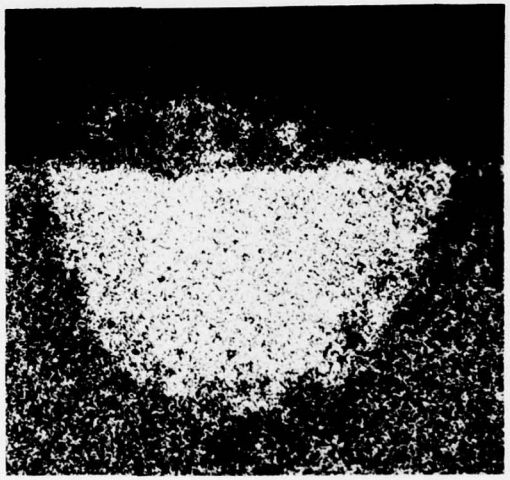

60e. Chromium X-rays

60f. Aluminum X-rays

Figure 60. Scanning electron micrographs of coating protrusion in PWA 68 CoCrAlY exposed 41 hours in static air at 760°C (1400°F) with thick deposit of $Na_2SO_4$ - 50mol% $CoSO_4$.

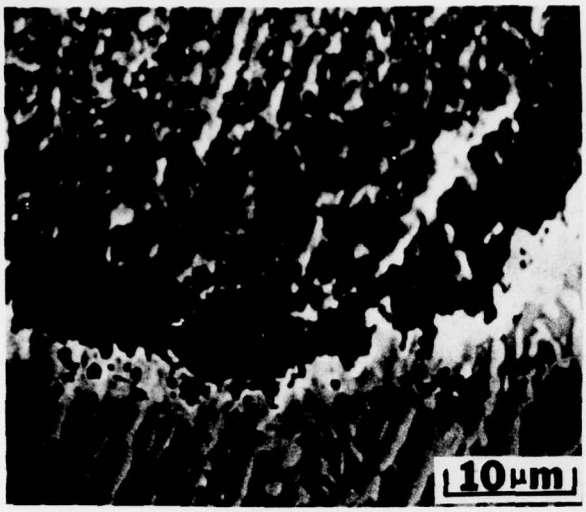


61a. Secondary electrons

61b. Sulfur X-rays

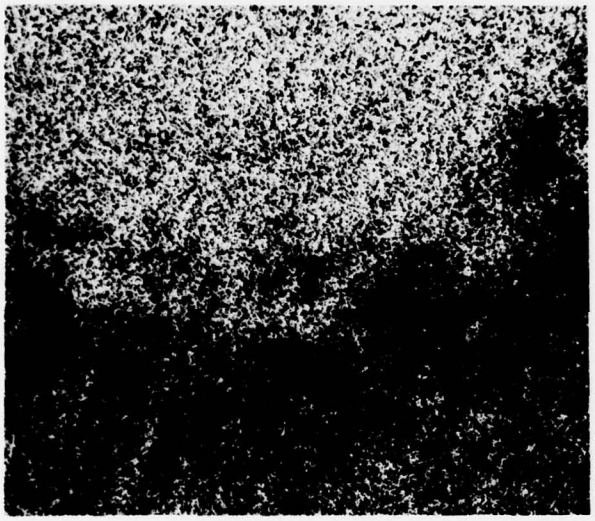

61c. Chromium X-rays

61d. Aluminum X-rays

Figure 61. Microstructure and element distribution of attack front in coating protrusion developed by 760°C exposure to thick deposit of $Na_2SO_4$ - 50 mol% $CoSO_4$. Entire protrusion and overlying oxide mound are shown at lower magnification in Fig. 60.

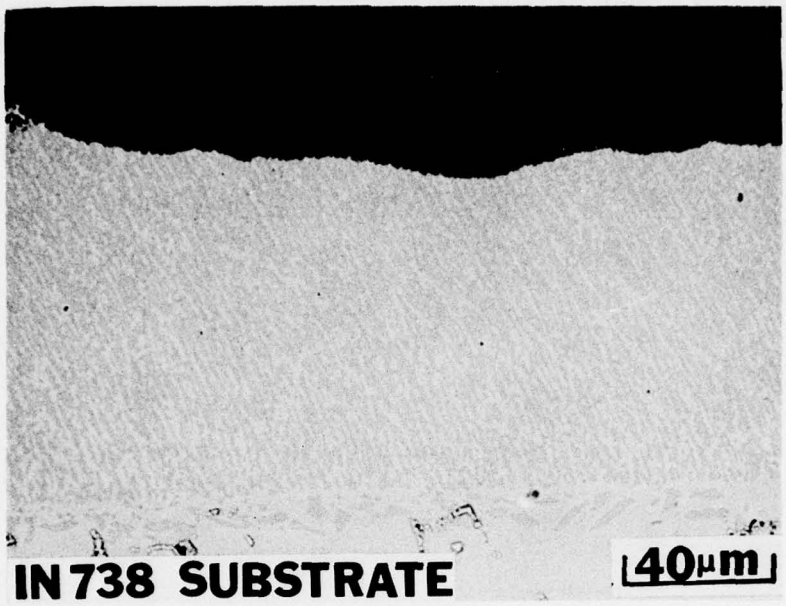


62a. PWA 68 CoCrAlY

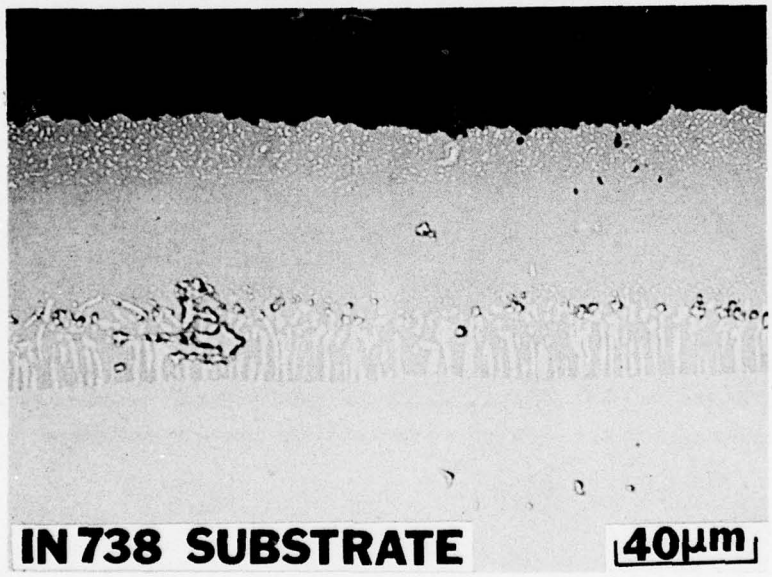


62b. PWA 273 diffusion aluminide

Figure 62. Attack of CoCrAlY and Ni-base diffusion aluminide coatings produced in 20 hour test at 649°C. Samples were coated with ~1mg/cm$^2$ deposit of $Na_2SO_4$ and exposed to ~0.2 atm $SO_3$ pressure.

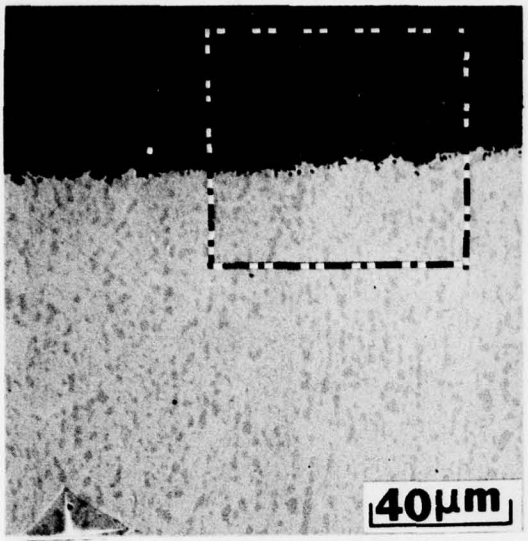


63a. Optical photomicrograph

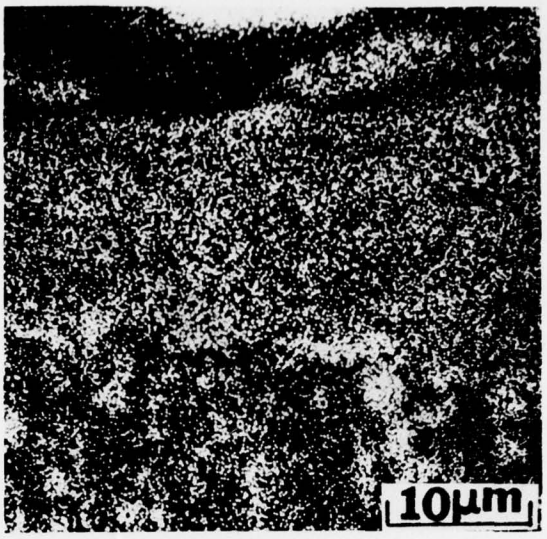


63b. Aluminum X-rays

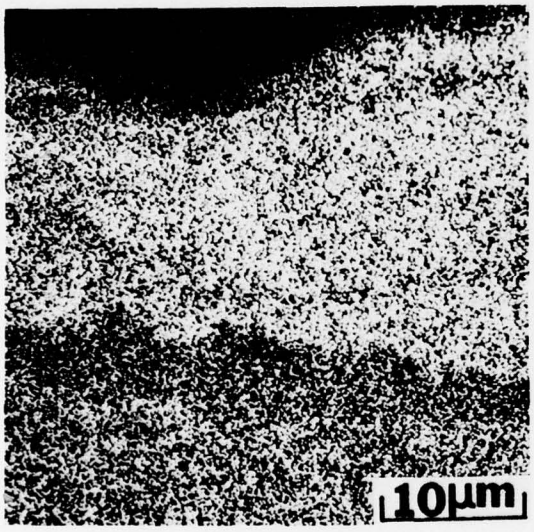


63c. Chromium X-rays

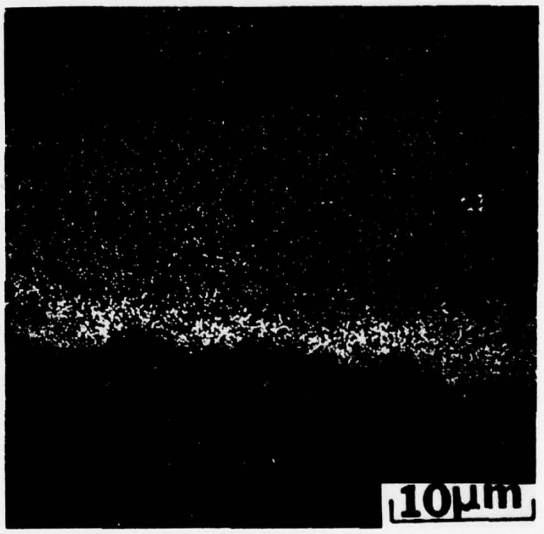


63d. Sulfur X-rays

Figure 63. Hot corrosion of Co-25Cr-6Al produced in 100 hour (5 cycles with fresh $Na_2SO_4$ salt applied every 20 hours) test at 649°C with $p_{SO_3}$ = 0.04 atm. Box in 63a is approximate area of X-ray images showing Al- and Cr-rich scale and concentration of S at the scale/metal interface.

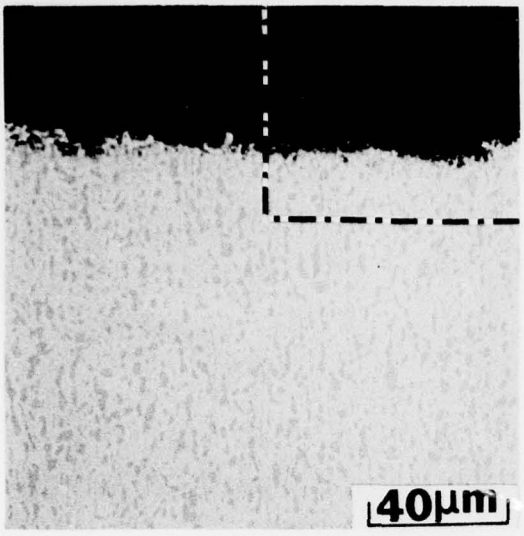


64a. Optical photomicrograph

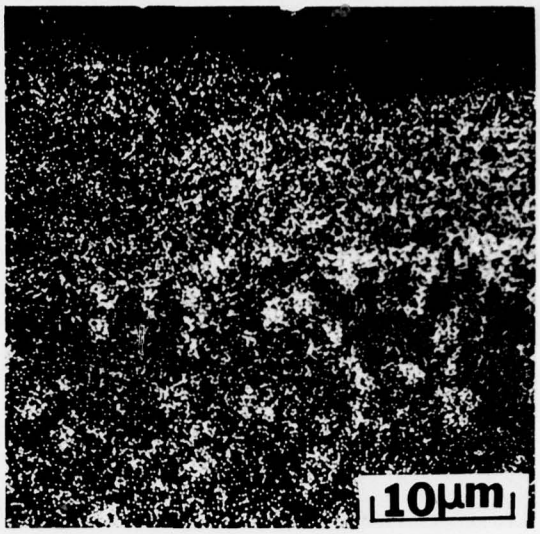


64b. Aluminum X-rays

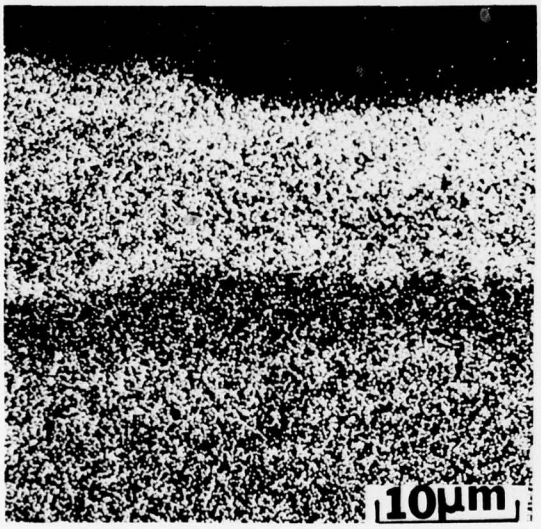


64c. Chromium X-rays

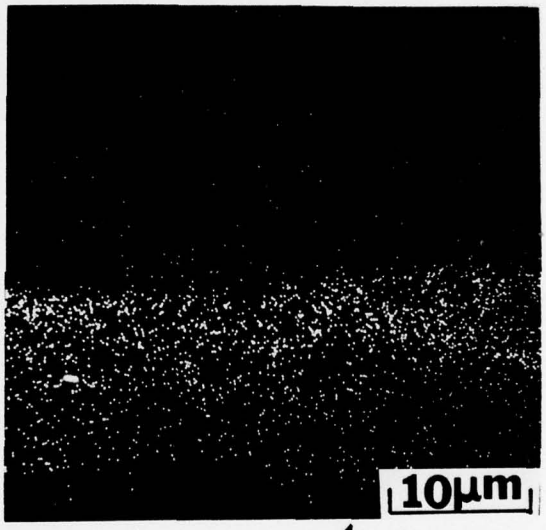


64d. Sulfur X-rays

inverted

Figure 64. Hot corrosion observed with same material and test conditions as in Fig. 63 except that salt deposit was $Na_2SO_4$ - 50% NaCl. The salt mixture instead of 100% $Na_2SO_4$ did not produce a discernable difference in severity of attack or microstructure and element distribution at the attack front.

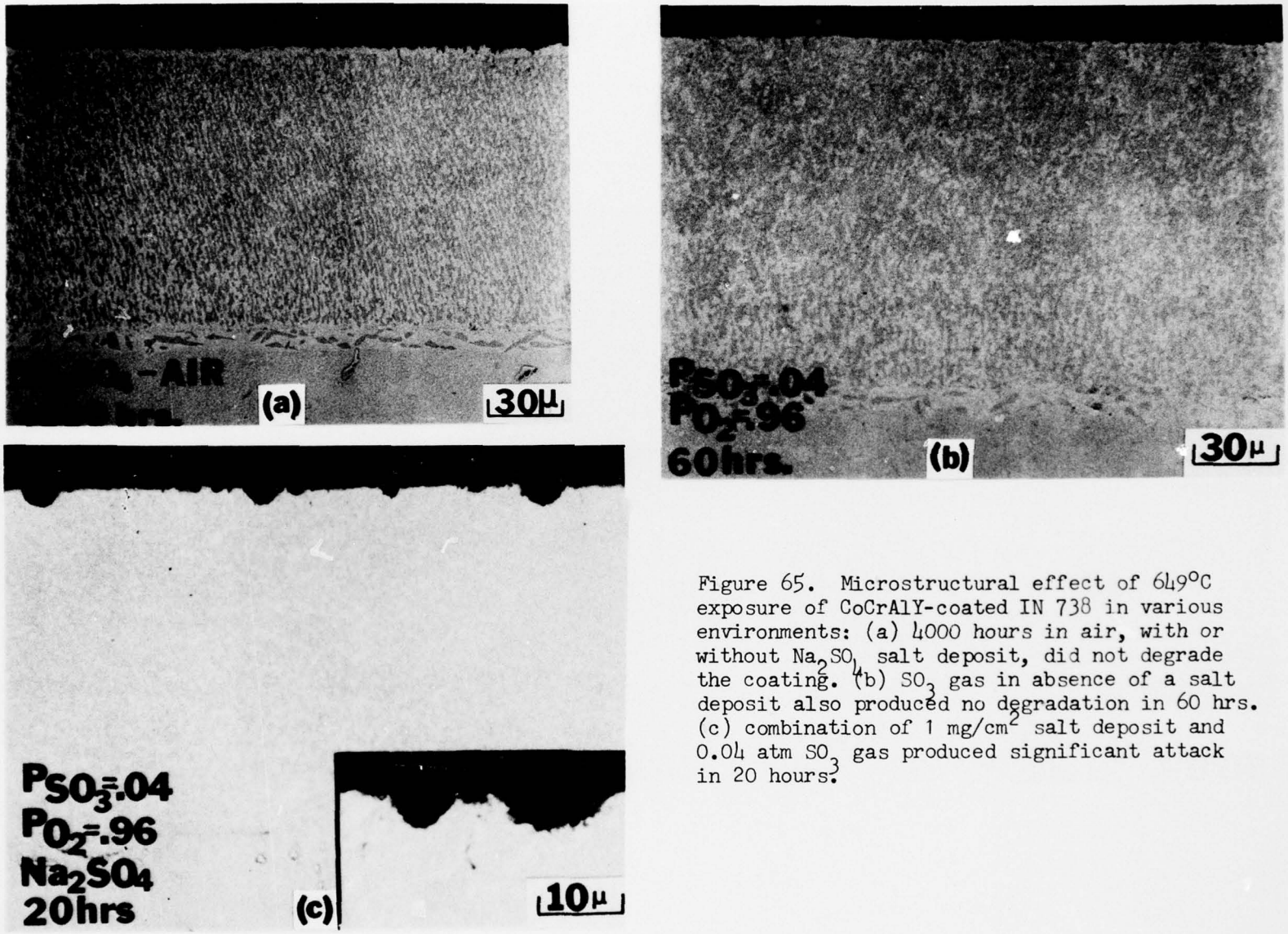


Figure 65. Microstructural effect of 649°C exposure of CoCrAlY-coated IN 738 in various environments: (a) 4000 hours in air, with or without $Na_2SO_4$ salt deposit, did not degrade the coating. (b) $SO_3$ gas in absence of a salt deposit also produced no degradation in 60 hrs. (c) combination of 1 mg/cm$^2$ salt deposit and 0.04 atm $SO_3$ gas produced significant attack in 20 hours.

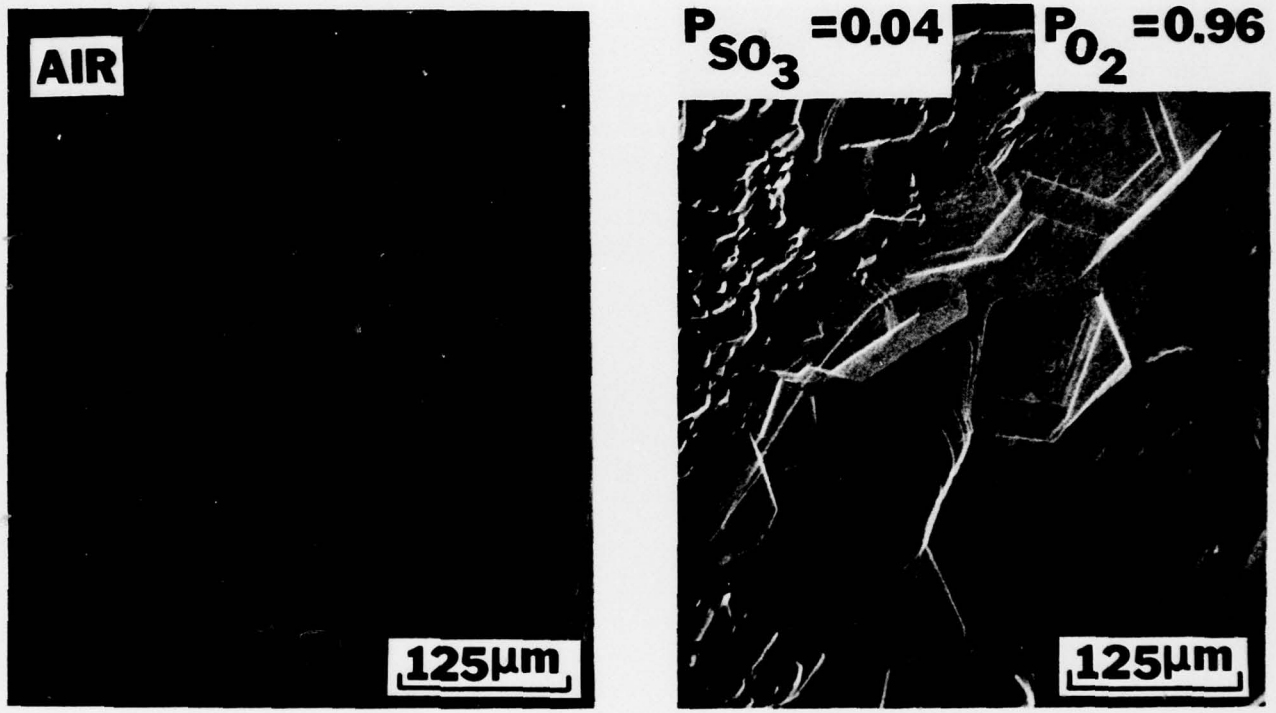


Figure 66. Surface structure of polished wafers of single-crystal $\alpha$-$Al_2O_3$ coated with 1 mg/cm$^2$ $Na_2SO_4$ and exposed for 4 hours at 649°C (1200°F). No change in weight or surface structure was observed on the sample heated in air. The sample exposed to $SO_3$ gas showed a weight loss after water washing, and Al ions were detected in the wash solution.

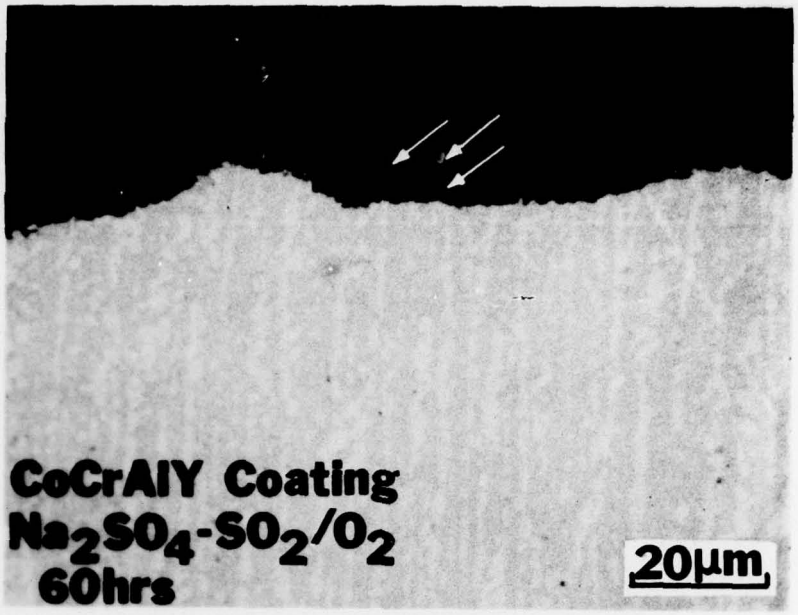


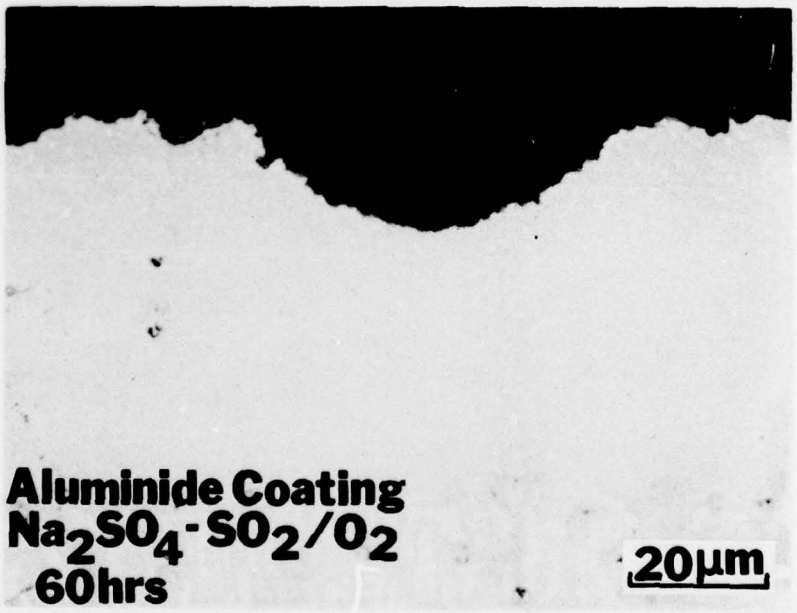


Figure 67. Attack of PWA 68 CoCrAlY and PWA 273 diffusion aluminide at 649°C produced by 1 mg/cm$^2$ $Na_2SO_4$ salt deposit and 0.04 atm $SO_3$ pressure (from equilibration of mixture of flowing $SO_2$:$O_2$ at the test temperature). White arrows mark features which appear to be small metallic globules sometimes observed in the inner layer of the scale.

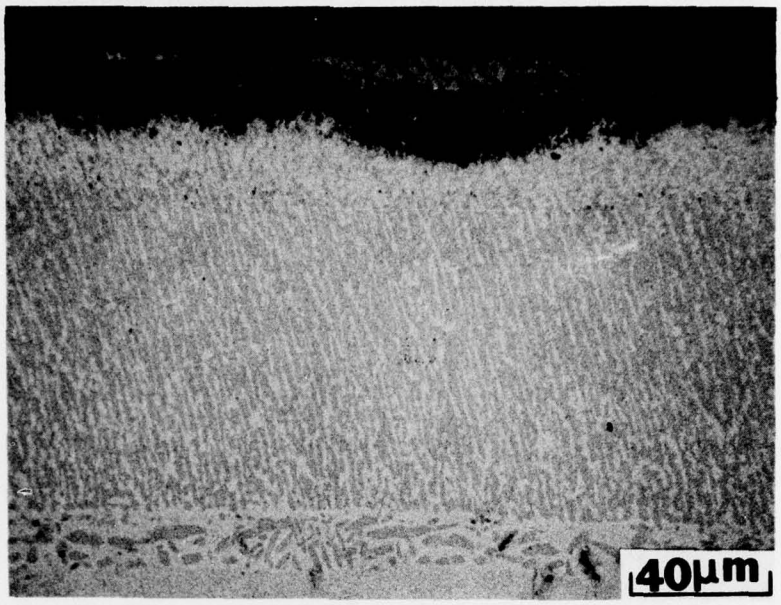


68a. typical extent of surface degradation

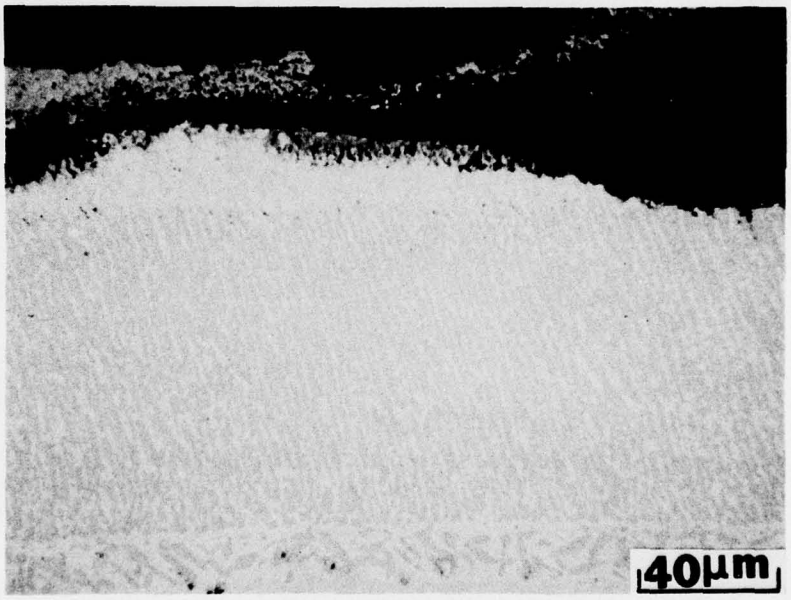


68b. spallation of oxidized overlayer

Figure 68. PWA 68 + Pt overlayer coating exposed 100 hours at 649°C (1200°F) with $Na_2SO_4$ salt deposit and $SO_3$ gas.

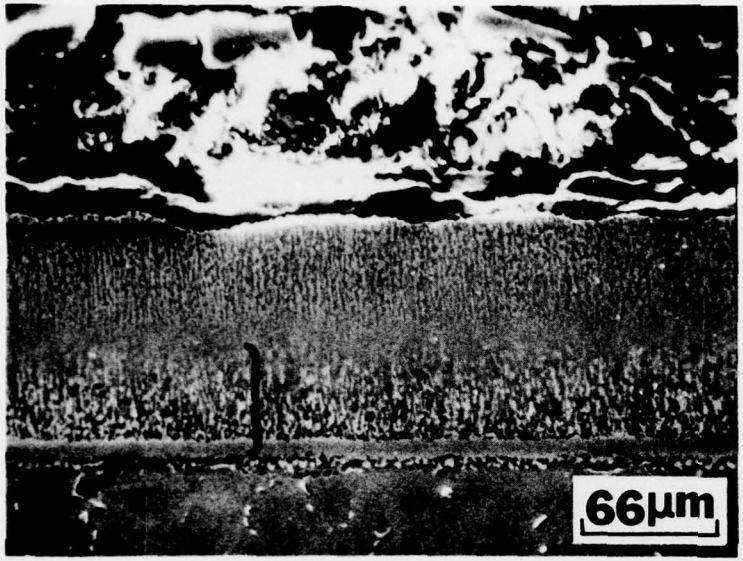



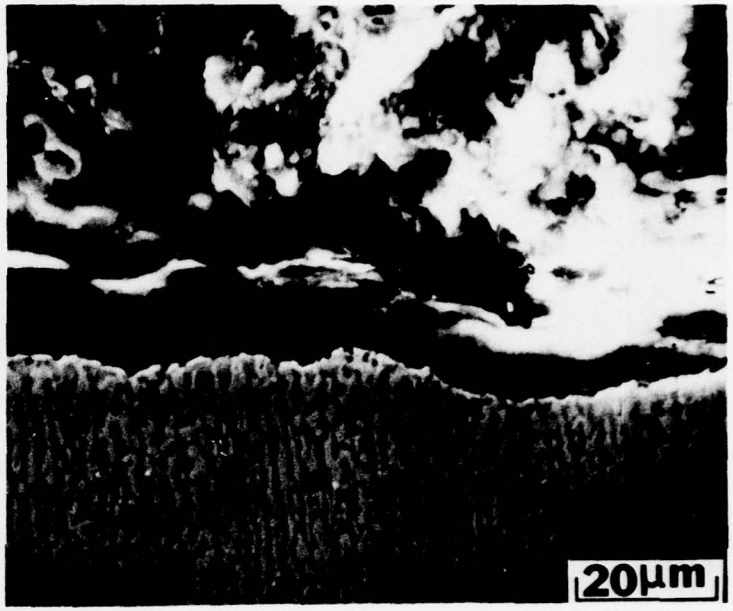


Figure 69. Secondary electron images of Pt underlayer + PWA 68 CoCrAlY coating after 100 hours at 649°C with $Na_2SO_4$ salt and $SO_3$ gas. Note complete absence of a diffusion zone at the attack front (as in Fig. 67), which has not penetrated to the underlayer (arrow) or Pt-containing diffusion zone (bracket).

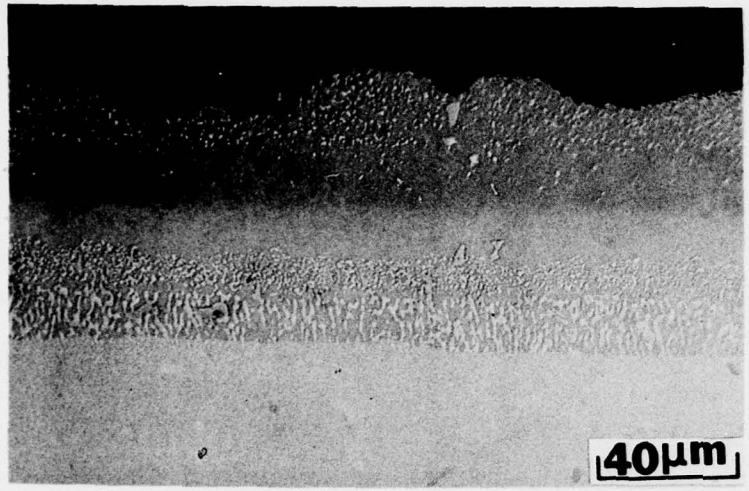


PWA 273

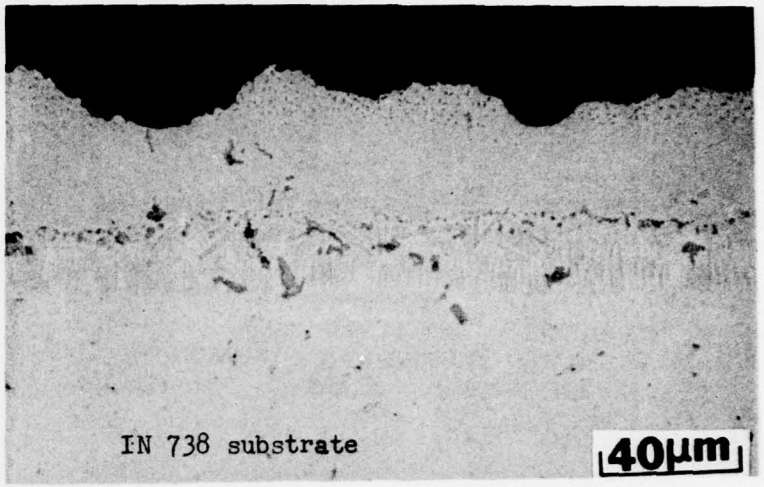


PWA 73

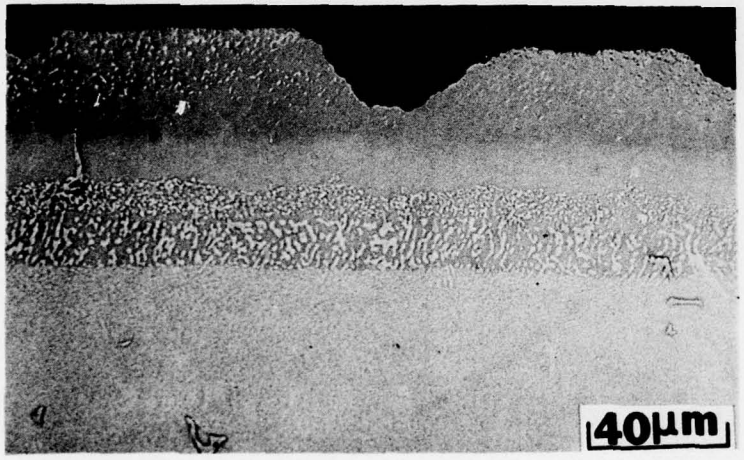


Ti + PWA 273


PWA 70 + PWA 273

Figure 70. Degradation of Ni-base diffusion aluminide coatings in 649°C hot corrosion test with $Na_2SO_4$ salt and $SO_3$ gas. Exposure time = 100 hours (5 cycles with fresh salt applied every 20 hours).

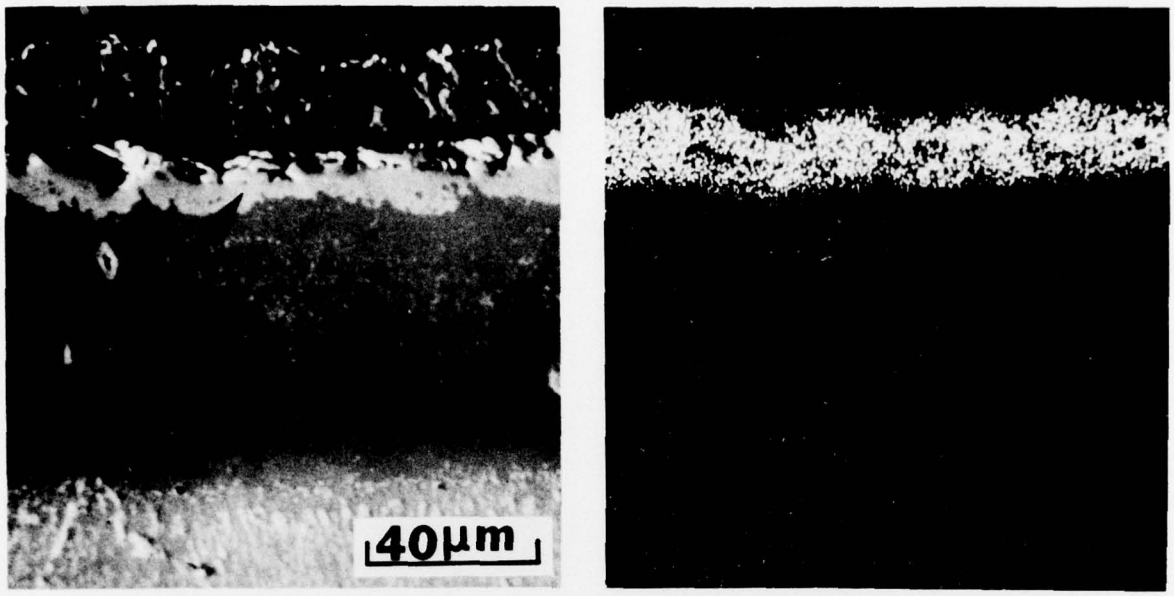


a. Secondary electrons

b. Sodium X-rays

c. Sulfur X-rays

d. Aluminum X-rays

Figure 71. SEM photomicrographs of sputtered platinum + PWA 273 diffusion aluminide coating tested concurrently with the specimens of Fig. 70. Residual salt and surface scale are evident on the dry-polished sample, but a Pt-rich surface layer (arrow) is still intact and there is minimal dealloying of the β-NiAl.

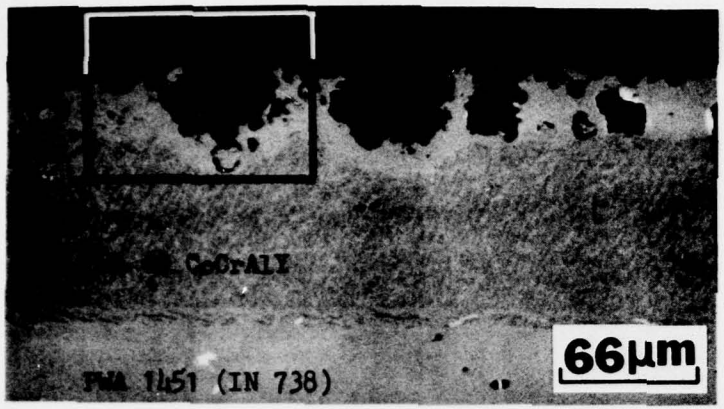


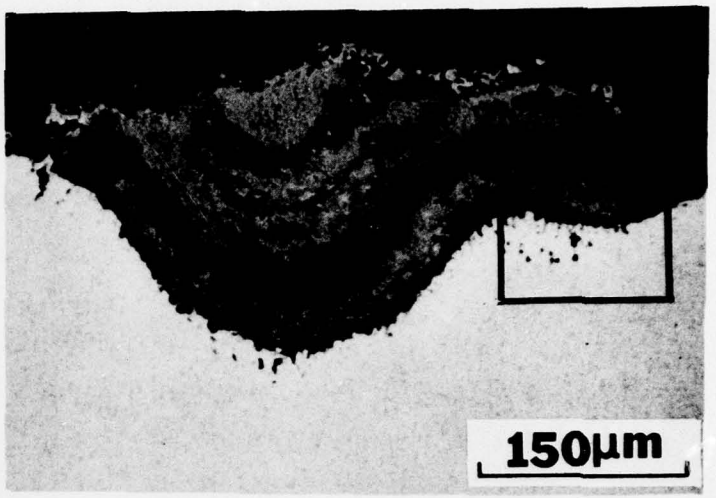


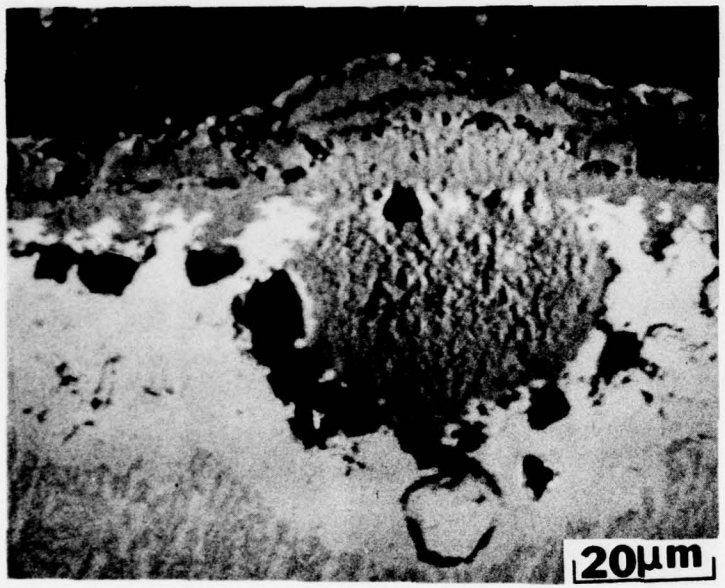


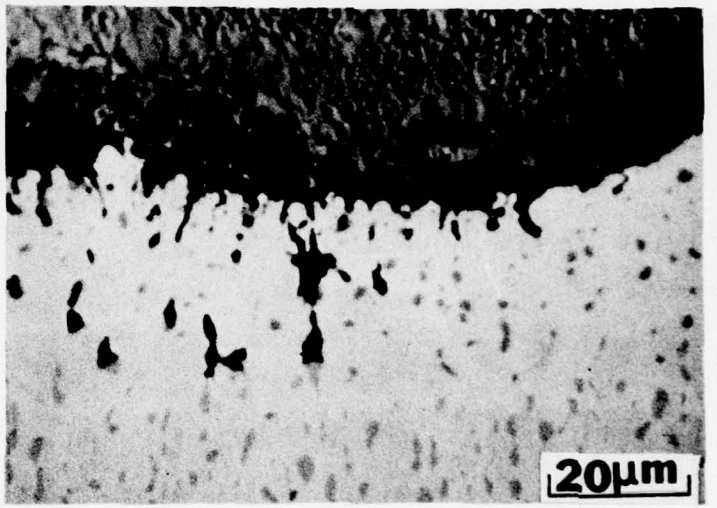


72a. PWA 68 CoCrAlY coating

72b. PVD Co-25Cr-6Al

Figure 72. Hot corrosion of CoCrAlY-coated In 738 and bulk PVD Co-25Cr-6Al in 899°C (1650°F) test with $Na_2SO_4$ salt and $SO_3$ in the gaseous environment. Exposure time = 100 hours.

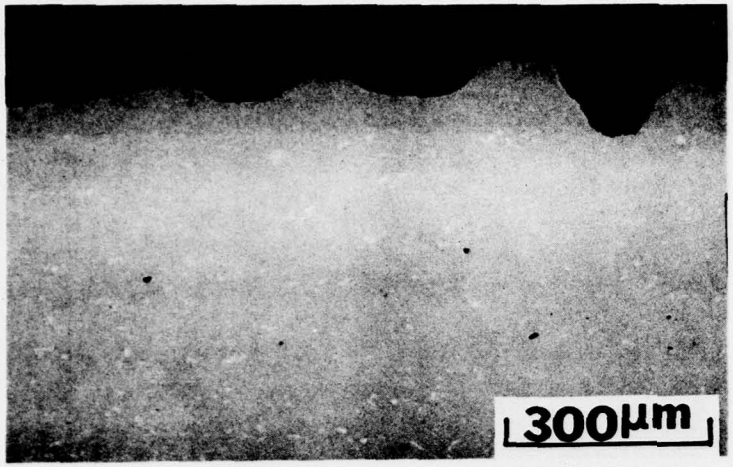


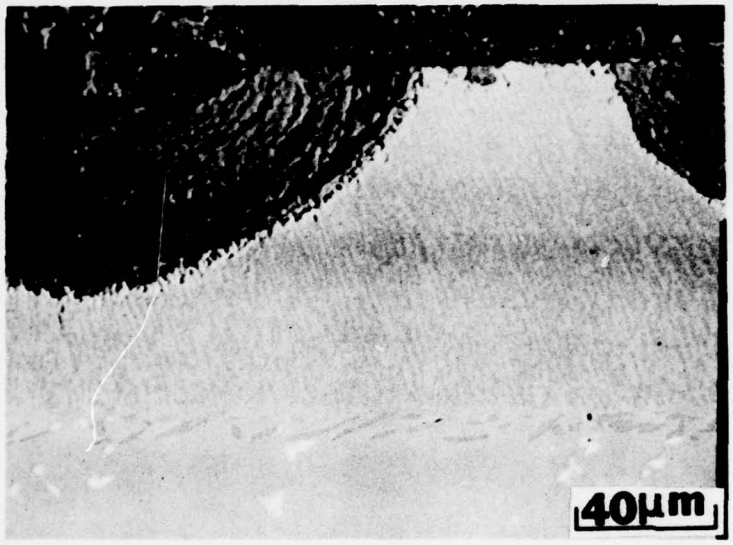


a. Typical protrusions and structure of scale/metal interface

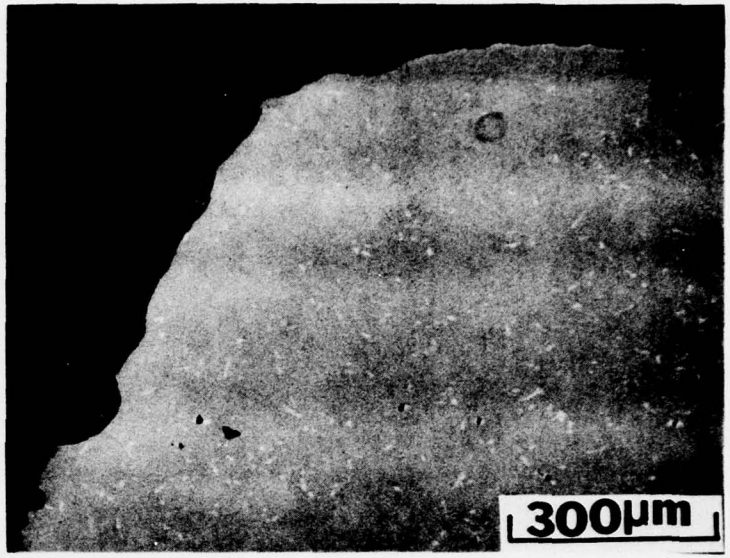


b. Failed edge

Figure 73. CoCrAlY-coated IN 738 exposed 40 hours at 760°C (1400°F) with $Na_2SO_4$ salt and $SO_3$ in the gaseous environment. Coating was penetrated in numerous areas and completely consumed on one edge of the coupon.

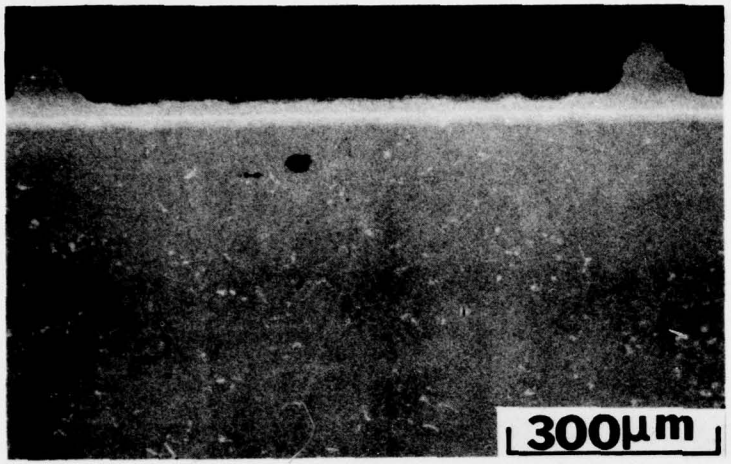


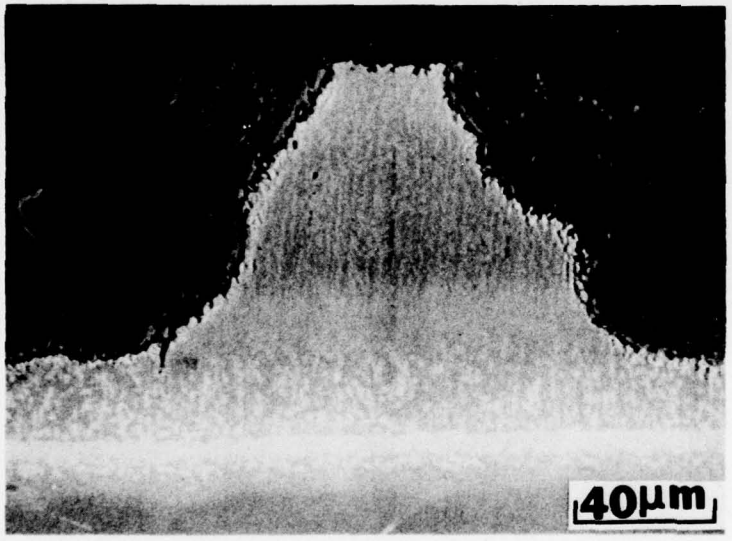


a. Typical protrusions and structure of scale/ metal interface

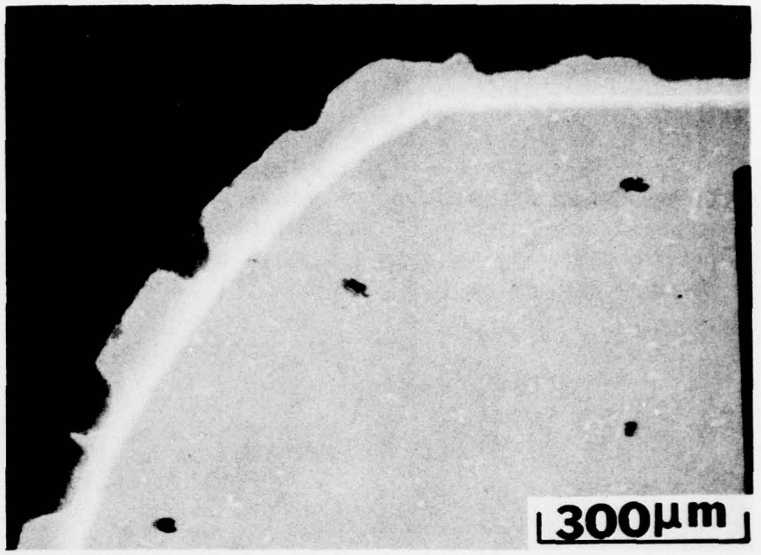


b. Coating at edge is still intact

Figure 74. Pt underlayer + PWA 68 CoCrAlY tested concurrently with the specimen of Fig. 73. General surface degradation was equally extensive, but attack front tends to stop at Pt-containing zone.

| Vane ID | Coating | Sample | Phases in Debye-Scherrer Pattern |
|---|---|---|---|
| C | IM6250A + Pt | TE salt crystals | Major: $Na_2Co(SO_4)_2$; trace possibly $Na_2SO_4$ |
| C | IM6250A + Pt | LE salt crystald | Major: $Na_2SO_4$; minor $Na_2Co(SO_4)_2$ |
| A | IM6250A + Pt | TE salt crystals | Major: $Na_2Co(SO_4)_2$; trace spinel and $Na_2SO_4$ |
| A | IM6250A + Pt | LE salt crystals | Major: $Na_2Co(SO_4)_2$; trace possibly $Na_2SO_4$ |
| A | IM6250A + Pt | LE corrosion scale | Major: spinel, $a_o$ = 8.08A; minor $Cr_2O_3$, trace CoO |
| A | IM6250A + Pt | Oxide mound on concave surface | Major: spinel, $a_o$ = 8.08A; trace $Na_2SO_4$ |
| 8-1 | PWA 268 | Concave surface scale | Spinel, $a_o$ = 8.08A, probably $Co_3O_4$ or $CoAl_2O_4$ |
| 8-1 | PWA 268 | Concave surface scale | Spinel, $a_o$ = 8.20A, trace carbon or $\alpha$-quartz |
| T | IM6250A + Pt | TE salt crystals | Major: $Na_2Co(SO_4)_2$; trace possibly $Na_2SO_4$ |
| 8-2 | PWA 268 | LE salt and oxide | Major: spinel, $a_o$ = 8.08A; minor $Na_2SO_4$ and $Na_2Co(SO_4)_2$ |

TABLE I. X-ray identification of surface deposits on nozzle guide vanes from Asiafreighter engine P-686570.

| Sample | | Na | K | Fe | Co | Pb | Ca | V | $SO_4$ | Cl | pH |
|---|---|---|---|---|---|---|---|---|---|---|---|
| WATER WASH | | | | | | | | | | | |
| C | Convex | 3125 | 118 | 12 | 510 | 30 | 151 | <25 | 4570 | <50 | 2.9 |
| | Concave | 4750 | 76 | 10 | 1023 | 11 | 496 | <25 | 7760 | 68 | 2.6 |
| 8-1 | Convex | 925 | 36 | 40 | 873 | 33 | <3 | <25 | 5100 | 75 | 1.8 |
| | Concave | 875 | 27 | 1 | 923 | <2 | 171 | <25 | 4670 | 110 | 3.4 |
| A | Convex | 3375 | 91 | 10 | 688 | 42 | 121 | <25 | 3240 | <50 | 2.9 |
| | Concave | 1350 | 63 | 4 | 293 | <2 | 151 | <25 | 4360 | 65 | 3.1 |
| T | Convex | 1650 | 51 | 28 | 414 | 32 | 66 | <25 | 7490 | <50 | 2.6 |
| | Concave | 1100 | 31 | 4 | 181 | 2 | 71 | 25 | 4890 | 115 | 3.0 |
| C8 | Convex | 2925 | 141 | 95 | 727 | 64 | 18 | 50 | 4040 | <50 | 1.9 |
| | Concave | 925 | 43 | 18 | 238 | 29 | 131 | <25 | 2820 | 80 | 4.4 |
| REWASHED WITH ACID | | | | | | | | | | | |
| A | Convex | 1469 | 59 | 240 | 729 | 600 | <3 | 175 | 2340 | <25 | --- |
| | Concave | 319 | 17 | 72 | 183 | 178 | <3 | 75 | 1170 | <25 | --- |
| 8-1 | Convex | 1394 | 73 | 132 | 1333 | 128 | 70 | 212 | 1540 | <25 | --- |
| | Concave | 144 | 8 | <2 | 162 | <2 | 52 | <25 | 640 | <25 | --- |

TABLE II. Soluble salt analysis by water and acid washing of vane surfaces. Data are total micrograms of each element in 25 ml of wash solution.

| Coating | Relative Lifetime | Remarks |
|---|---|---|
| Sputtered Ti + PWA 273 | 6 | Mechanism of titanium effect not understood; microstructural degradation slower |
| PWA 68 + Pt overlayer | 3 | Overlayer must be partially dissolved and penetrated before melten salt can dealloy the CoCrAlY coating |
| PWA 68 + Pt + PWA 273 | 3 | Performance variable; one surface looked very good, others were oxidized |
| Sputtered Pt + PWA 273 | 2 | Variable microstructural degradation; lifetime essentially the same as PWA 273 |
| PWA 273 | 2 | Ni-base coatings appear to be more resistant than Co-base to chloride-induced dealloying |
| Ti-alloyed CoCrAlY | 2 | Mechanism of Ti effect not understood; microstructural degradation slower |
| PWA 68 CoCrAlY | 1 | Chloride-containing liquid salt deposit dealloys the coating of aluminum |
| Pt underlayer + PWA 68 | 1 | Underlayer is ineffective against initiation of attack and penetration of developing protrusion |
| PWA 68 + PWA 273 | 1/4 | Susceptible to general surface oxidation and edge failure |
| Preoxidized PWA 68 | 1/4 | Oxide spalls off in cyclic hot corrosion |
| PWA 68 + Ni Overlayer | 1/4 | Overlayer oxidizes and spalls off |
| PWA 73 | <1/4 | Rapid dealloying and sulfidation |
| PWA 70 + PWA 273 | <1/4 | " " " " |
| PWA 70 + PWA 73 | <1/4 | " " " " |

TABLE III. Relative performance of various state-of-the-art and modified coatings in 899°C cyclic hot corrosion test with $Na_2SO_4$ - 50% NaCl. Estimated lifetime, in multiples of lifetime of PWA 68, is based on visual observations and post-test metallographic characterization of general surface degradation and localized attack.

## REFERENCES


1. G. W. Goward: "Proceedings of 1974 Gas Turbine Materials in the Marine Environment Conference," MCIC Report 75-27, U. S. Dept. of Commerce, NTIS, Springfield, Va., pp. 277-296.

2. P. W. Hancock: Ibid, pp. 225-236.

3. R. L. Jones and S. T. Gadomski: "Mixed Sulfate/$SO_3$ Reactions in Low Power Hot Corrosion," NRL Letter Report 6170-773a:RLJ:blr, 1 November 1977.

4. L. F. Aprigliano: "Burner Rig Simulation of Low Temperature Hot Corrosion," Report MAT-77-68, David W. Taylor Naval Ship Research and Development Center, November 1977.

5. R. L. Jones and S. T. Gadomski: "The Cut-Edge Degradation of CoCrAlY Turbine Blade Coatings: NiS Involvement." Proceedings of the Symposium on Properties of High Temperature Alloys, Z. A. Foroulis and F. S. Pettit, Eds., Proceedings Volume 77-1, The Electrochemical Society, 1976.

6. R. L. Jones: "The Sulfidation of CoCrAlY Turbine Blade Coatings by $Na_2SO_4$-NaCl," NRL Letter Report 6170-859, 1 December 1975, Naval Research Laboratory, Washington, D.C. 20375.

7. R. L. Jones and S. T. Gadomski: "The Hot Corrosion of CoCrAlY Turbine Blade Coatings by $Na_2SO_4$ and Vaporous NaCl," J. Electrochem. Soc., Vol. 124, No. 10 (Oct. 1977) pp. 1641-1648.

8. C. A. Stearns, F. J. Kohl, and G. C. Fryburg: "Interaction of NaCl(g) and HCl(g) with condensed $Na_2SO_4$," Proceedings of the Symposium on High Temperature Halide Chemistry, D. Cubicciotti, Ed., The Electrochemical Society, 1977.

9. Metals Handbook, "Volume 10, Fracture Analysis and Prevention," pp. 175-176, Selective Leaching. American Society for Metals, Metals Park, Ohio (1975).

10. A. U. Seyboldt: "Oxidation of Ni-20Cr Alloy and Stainless Steels in the Presence of Halides," Oxid. Metals, Vol. 2 (1970) pp. 161-171.

11. D. W. McKee, D. A. Shores, and K. L. Luthra: "The Effect of $SO_2$ and NaCl on High Temperature Hot Corrosion," J. Electrochem. Soc., Vol. 125, No. 3 (March 1978) pp. 411-419.